UNIVERSIDADE ESTADUAL DE CAMPINAS
Faculdade de Engenharia Mecânica

CÉSAR SILVA ROTHER

Analysis and Optimization of Rotors Supported on Hydrodynamic Bearings

Análise e Otimização de Rotores Apoiados Sobre Mancais Hidrodinâmicos

CAMPINAS
2019

CÉSAR SILVA ROTHER

Analysis and Optimization of Rotors Supported on Hydrodynamic Bearings

Análise e Otimização de Rotores Apoiados Sobre Mancais Hidrodinâmicos

Dissertation presented to the School of Mechanical Engineering of the University of Campinas in partial fulfillment of the requirements for the degree of Master in Mechanical Engineering, in the area of Mechanics of Solids and Mechanical Project.

Dissertação apresentada à Faculdade de Engenharia Mecânica da Universidade Estadual de Campinas como parte dos requisitos exigidos para a obtenção do título de Mestre em Engenharia Mecânica, na área de Mecânica dos Sólidos e Projeto Mecânico.

Orientador: Prof. Dr. Tiago Henrique Machado

ESTE EXEMPLAR CORRESPONDE À VERSÃO FINAL DA DISSERTAÇÃO DEFENDIDA PELO ALUNO CÉSAR SILVA ROTHER E ORIENTADA PELO PROF. DR TIAGO HENRIQUE MACHADO.

CAMPINAS
2019

Agência(s) de fomento e nº(s) de processo(s): CNPq, 143102/2017-6; FAPESP, 2017/07454-8
ORCID: https://orcid.org/0000-0003-4523-599X

Ficha catalográfica
Universidade Estadual de Campinas
Biblioteca da Área de Engenharia e Arquitetura
Rose Meire da Silva - CRB 8/5974

R743a

Rother, César Silva, 1993-
Analysis and optimization of rotors supported on hydrodynamic bearings / César Silva Rother. – Campinas, SP : [s.n.], 2019.

Orientador: Tiago Henrique Machado.
Dissertação (mestrado) – Universidade Estadual de Campinas, Faculdade de Engenharia Mecânica.

1. Rotores. 2. Mancais. 3. Otimização. I. Machado, Tiago Henrique, 1986-. II. Universidade Estadual de Campinas. Faculdade de Engenharia Mecânica. III. Título.

Informações para Biblioteca Digital

Título em outro idioma: Análise e otimização de rotores apoiados sobre mancais hidrodinâmicos
Palavras-chave em inglês:
Rotors
Bearings
Optimization
Área de concentração: Mecânica dos Sólidos e Projeto Mecânico
Titulação: Mestre em Engenharia Mecânica
Banca examinadora:
Tiago Henrique Machado [Orientador]
Fabio Dalmazzo Sanches
Marco Lúcio Bittencourt
Data de defesa: 31-01-2019
Programa de Pós-Graduação: Engenharia Mecânica

UNIVERSIDADE ESTADUAL DE CAMPINAS
FACULDADE DE ENGENHARIA MECÂNICA
COMISSÃO DE PÓS-GRADUAÇÃO EM ENGENHARIA MECÂNICA
DEPARTAMENTO DE SISTEMAS INTEGRADOS

DISSERTAÇÃO DE MESTRADO ACADÊMICO

Analysis and Optimization of Rotors Supported on Hydrodynamic Bearings

Análise e Otimização de Rotores Apoiados Sobre Mancais Hidrodinâmicos

Autor: César Silva Rother

Orientador: Tiago Henrique Machado

A Banca Examinadora composta pelos membros abaixo aprovou esta Dissertação:

Prof. Dr. Tiago Henrique Machado
Universidade Estadual de Campinas – UNICAMP/FEM

Dr. Fábio Dalmazzo Sanches
Universidade Federal do Rio Grande do Norte - UFRN/DEM

Prof. Dr. Marco Lúcio Bittencourt
Universidade Estadual de Campinas – UNICAMP/FEM

A Ata da defesa com as respectivas assinaturas dos membros encontra-se no processo de vida acadêmica do aluno.

Campinas, 31 de janeiro de 2019.

Acknowledgments

The author thanks CAPES, CNPq and grant # 2017/07454-8 from the São Paulo Research Foundation (FAPESP) for the financial support to this research; ABCM and Springer for licensing the papers reproduced in this dissertation.

Resumo

As máquinas rotativas são essenciais para o desenvolvimento de diversas atividades humanas. Com emprego em indústria, transporte, agricultura, entre outras áreas, é evidente a importância dessa classe de maquinário e seu grande efeito em vários setores da sociedade moderna. Dentre os tipos de mancais utilizados em máquinas rotativas, destaca-se o mancal hidrodinâmico, por sua simplicidade de fabricação e baixo custo de implementação em máquinas que já contém sistemas de lubrificação. Por este motivo, este trabalho se propõe a simular e otimizar máquinas rotativas apoiadas em mancais hidrodinâmicos. Essa dissertação apresenta a pesquisa desenvolvida durante o curso de mestrado em engenharia mecânica. O texto é escrito em um formato de coletânea de artigos precedidos por uma introdução, uma revisão bibliográfica e uma síntese da pesquisa, seguidos pelas conclusões e propostas de trabalhos futuros. Utilizando o método dos elementos finitos para as simulações, são analisadas as influências das modelagens de mancais, eixos e fundações no comportamento dinâmico dos rotores. Mostra-se incialmente o algoritmo base, e uma comparação entre os elementos de viga de Timoshenko e Euler-Bernoulli, justificando a escolha do primeiro. Analisa-se as diferenças de resposta entre rotores engastados e apoiados sobre mancais hidrodinâmicos, bem como entre fundações rígidas e flexíveis. Por fim, através das análises, obtém-se as relações entre os componentes e a resposta do sistema, que são utilizadas na proposição das otimizações demonstradas no quarto artigo.

Palavras-chave: Dinâmica de rotores; mancais hidrodinâmicos; parâmetros concentrados; otimização

Abstract

Extensively used in industry, transportation, agriculture, among other areas, it is evident that rotating machines are essential for the development of several human activities. Among the types of bearings used in rotating machines, the hydrodynamic bearings stand out because of their simplicity of manufacture and low implementation cost in machines that already have lubrication systems. For this reason, this work proposes to simulate and optimize rotating machines supported in hydrodynamic bearings. This dissertation presents the research developed during the master's degree in mechanical engineering. The text is written as a collection of articles preceded by an introduction, a bibliographical review and a research synthesis and followed by the conclusions and proposals of future works. Using the finite element method for the simulations, the influences of the modeling of bearings, shafts and foundations on the dynamic behavior of the rotors are analyzed. Initially, it shows the initial algorithm and a comparison between the beam elements of Timoshenko and Euler-Bernoulli, justifying the choice of the first one. The differences in response between clamped and supported rotors on hydrodynamic bearings, as well as between rigid and flexible foundations, are analyzed. Finally, through the analyses, the relations between the components and the response of the system are shown. These relations are used in the optimization proposed in the fourth article.

Keywords: Rotordynamics; hydrodynamic bearings; lumped parameters; optimization

List of Tables

Contents

1 INTRODUCTION

Mankind makes use of rotating machines for at least 5000 years. From the earliest potter's wheels dating back more than three millennia BC to today's modern turbines, rotating machines have been employed to increase the efficiency of tasks and processes in society (ROUX; PIERRE, 2009).

Due to the great utility and wide range of applications, these machines have been continuously improved, acquiring more and more complexity. Water wheels were common in antiquity and ways of extracting energy from nature through rotating machines were being developed and improved. One application of complex rotor with great importance today – the steam turbine - was introduced in the 1st century BC by Heron of Alexandria (POTTS, 2012). Even though the use of steam turbines to produce work was made feasible only after almost two millennia, the concept was clearly demonstrated.

Since then, the study of rotating machines has aroused the interest of many researchers of machines and structures, because of the significant number of typical phenomena that occur during their operation. This type of system represents the largest and most important class of machinery. Rotors are used for the transportation of fluid media, machining and forming of metals, power generation, naval and aeronautical propulsion, among many other applications. The existence of a rotating component supported in bearings and transmitting power creates a family of problems, found in the most diverse machines: compressors, pumps, motors, turbines of great and small size (MACHADO, 2014).

In order to reach the current state of the study of rotor dynamics, besides the strong demand of society for rotating machines, several areas of science have been explored previously so that the set of knowledge on which the rotor dynamics is structured could be established.

One of the essential fields in rotor dynamics, the study of vibrations began in the fifth century BC in ancient Greece through the experiments of Pythagoras of Samos with ropes, pipes, rocks and hammers. His experiments investigated the harmonic

movements and Pythagoras postulated on the existence of natural frequencies determined in function of the system properties.

With the period of Renaissance and the scientific revolution brought about by it, the mechanics of the solids were created that would permit an efficient study of moving bodies. In the 18th century, there was already a large knowledge base on mechanics and mathematics that would facilitate the study of rotating machines.

The industrial revolution, however, was the major boost to research and development on machines. Along with it, came the search for increasingly sophisticated machines that could increase productivity and replace manual labor in production. Machines could replace both human labor force, in activities such as weaving and mining as well as animal traction in mills and transport.

Although rotative motions are desirable as output for machines applied in various processes, reciprocative machines were dominant at the beginning of the use of steam power. Whenever rotative motion was needed, there was usually a crank mechanism for conversion. James Watt pointed out at the end of the 18th century that the technology needed to make viable steam turbines, as desired by Heron of Alexandria, still did not exist.

At the beginning of the 19th century the first viable steam turbines were produced and soon the typical phenomena that affect rotors working at high rotations were perceived. Rankine proposed in 1869 a limit of rotation speed for rotors and named it critical velocity. As it was postulated, critical velocity was a limit that could not be crossed. The advantages of operating a turbine at high speeds encouraged developments to cross this limit. Two decades later, De Laval developed a turbine presenting a slender shaft with some flexibility. This configuration, when crossing the limit proposed by Rankine, operated smoothly.

The advantages of the turbines over reciprocative engines were clear: constant torque and very low vibrations. Compared to the other engines, the turbines were considered, at the time, free of vibrations. For these reasons, more and more of these turbines were being sought. With the pressure for the development of these rotating machines, their study had to be deepened and components that were not previously evaluated had to be.

The influence of bearings and foundations on the rotors has become increasingly important and analyzes of the separate components and their interaction with other components is essential in the design refinement of rotating machines. The bearings have great influence in the dynamics of these kind of machines. They support all the applied forces to the shaft and the vibrations inherent to the operation, allowing the rotation with a low friction coefficient. Among the bearings types that can be used in rotating machines, the hydrodynamic bearing is one of the most used. It has constructive advantages such as low manufacturing cost and ease of assembly. There are also operational advantages such as low friction coefficient and ability to reduce the transmission of shaft vibrations to foundation. Due to the oil film variable pressure and thickness that is inherent to this type of bearing, its characteristics vary according to the shaft rotating speed, making complex its analysis and modeling.

Within this context, this work is focused on analysis and optimization of rotating machines supported on hydrodynamic bearings. A finite element approach is used for numerical models. The analysis of the influence of the modeling choices for shafts, bearings and foundations are previously analyzed to define the simulation parameters to be used. From these choices, optimization methods are proposed to modify the rotor response considering these elements.

1.1 Structure of the work

This work is presented in the format of a set of articles preceded by a bibliographic review and a research synthesis. The bibliographic review contains essential texts in the development of the theory used for the rotor modeling are presented, comprising both the theory about the dynamic behavior of the system and methods to obtain numerical solutions for the resulting equations of motion. This chapter is followed by the research synthesis, which gives an overview about the papers and more details about modelling and computational aspects omitted in the papers due to publication size constraints.

The first article comprises the initial stages of finite element modeling. Two of the beam elements most commonly used in the modeling of rotor shafts are compared.

A comparison is made between the elements of Euler-Bernoulli and Timoshenko, showing the situations where they differ most and when they are similar.

From the finite element studies presented in the first article, an algorithm for rotor analysis is written. This algorithm is used in the second article, for the several analyzes shown in it. The second article demonstrates several rotor phenomena through frequency, time and modal analyzes. The effects of disc decentralization on a Jeffcott rotor, as well as the influence of hydrodynamic bearings on the behavior of the system are analyzed.

In order to increase the complexity and, consequently, to approximate the theoretical model of real results, foundations were included in the model. The third article analyzes the interactions between foundations and rotors, showing the influence of the foundation parameters on the dynamic response of the rotor. Also, the anisotropy in the foundation and its effects are analyzed.

With the complete model used in the third article, a study of rotor optimization was done. In the fourth article, two methods of rotor optimization are proposed. By adding discs or modifications to the shaft, the response of a rotor with the smallest possible mass increase is sought. The case studies are rotors that, when supported on foundations other than the original one, showed unacceptable amplitudes of vibrations. Through a search method, the best compensation options are found by adding discs or reinforcements to the shafts.

After the articles, discussions involving all of them and the information they presented are described in the next section. The dissertation finishes with the conclusions regarding the articles and presents the future work being developed.

2 BIBLIOGRAPHIC REVIEW

2.1 Rotordynamics fundamentals

Even with the earliest investigations of rotors and vibrations occurring in antiquity, studies relating rotating machines and vibrations only emerged in the post-industrial revolution, as pointed out in the introduction. Rankine, in 1869, was the first to analyze rotors from the point of view of the shaft deformation as a function of the rotating speed and he stated that “the shaft is considerably bent and whirls around in this bent form".

Rankine’s analysis predicted that, at a given rotation, called critical velocity at the time, the shaft would bend considerably describing a whirling motion (RANKINE, 1869). In his model, the deflection of the shaft increases unlimitedly as the rotating speed exceeds this value, demonstrating a failure of the model that can be experimentally tested.

Although the identification of critical speeds was an important advance in the study of rotor dynamics, Rankine did not consider the Coriolis acceleration in his studies. In addition, he considered the centrifugal force to be a real force. This foundation of his studies led to erroneous conclusions that have persisted in the scientific world for half a century (TIWARI, 2010).

The creation of the first viable steam turbine by Gustaf de Laval in 1882 increased the need for further studies on the dynamics of rotors, since turbines must be operated at high speeds to achieve maximum efficiency (SMIL, 2005). Laval experimentally proved in 1895, to be able to operate a rotor above the critical speed. His arrangement consisted of a disc and a thin, flexible shaft (VANCE; ZEIDAN; MURPHY, 2010). Subsequently, Foppl and Laval presented analytical models explaining the stability achieved at supercritical velocities, contrary to Rankine predictions (DIMAROGONAS, 1995).

Parallel to these, Durkeley wrote in 1893 a work entitled '*On the Whirling and Vibration of Shafts*'. The work contained some of the most advanced concepts on the subject at the time, such as the equations for the unloaded shaft supported by ball bearings and the shaft with pulleys. It is also discussed the conditions for the shaft self-centering effect. However, the analytical solutions are limited to cases of simple geometry, with conclusions dependent on the experimental results obtained, with gaps in the theoretical development.

In 1905, Stodola published his book on steam turbines. It describes turbines of his time and takes up the studies of rotordynamics presented by De Laval and Dunkerley, in addition presenting their own. As a novelty in his work, he used the two-plane rigid rotor balancing theorem to describe the determinant method and the matrix iteration method to calculate the critical speeds of multi-disc rotors.

All models presented so far neglected the presence of damping in the bearings, which led to a forecast of sudden phase change during the critical speed. Only in 1919, the complete theory about the smooth transition through the critical velocity and the amplitudes of whirling was described – by Jeffcott (VANCE; ZEIDAN; MURPHY, 2010). Due to its pioneering study in including the damping effects and clarity of mathematical demonstrations, the simple rotor model proposed by De Laval (Figure 2.1) became known as Jeffcott Rotor.

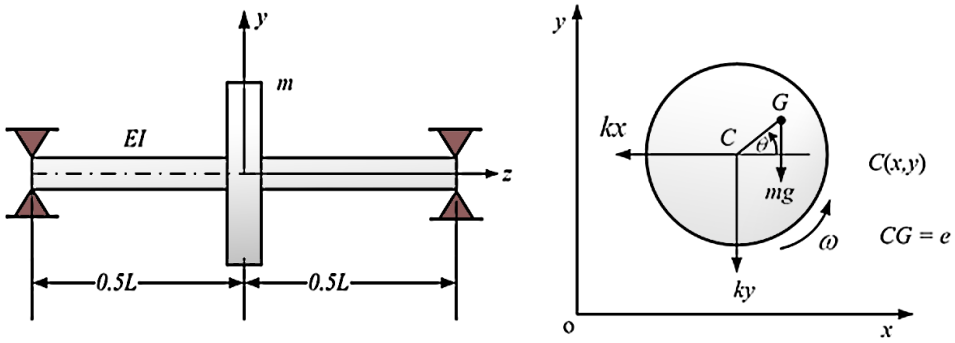

Figure 2.1 – Symmetric Jeffcott Rotor

This rotor model has been extensively modified for the analysis of different parameters and frequently used for further investigations due to its simplicity and the possibility of observing many of the phenomena present in rotordynamics. The model consists of a flexible shaft of negligible mass with a disc mounted at its center,

supported at the ends. Viscous forces in the bearing oppose its translational speed. Jeffcott (1919), neglected the effect of gravity in his analyses.

Although it is a simplified model of real rotors, it is possible to note several rotordynamic effects such as critical speeds, whirling and destabilization due to the internal damping. In rotors where the disc is not in the center of the shaft, a change in the natural whirling frequencies can be perceived.

The vibration of the non-centralized disc interacts with the angular momentum vector of the disc producing an effect that leads to an increase in the frequency of whirl in the direction of rotation (forward whirl) and a decrease in the frequency of whirl in opposite direction of rotation (backward whirl). This behavior is due to gyroscopic effect. Its action is most evident when the disc polar inertia is much greater than the shaft inertia.

When a rotor, as shown in Figure 2.1, has its center of mass displaced relative to the axis of rotation, it is considered unbalanced. An unbalanced rotor, when in operation, will undergo deformation of its shaft, which will bend.

As described by Jeffcott (1919), starting from rest, as the operation speed of an unbalanced rotor increases, it approaches a rotation in which there is a peak in the amplitude of the shaft vibration. At this speed, there is a change in the motion described by the rotor. The center of mass that was previously closer to the geometric center of the bearings than to the elastic center - where there will be less resistance to bending - will have an inverse behavior, as well as the direction of the transverse oscillation (whirl). After this transition velocity, the shaft stabilizes at a small deflection until the next speed, with a new peak in the vibration. Jeffcott was the first to name the transverse oscillation velocities as whirl velocities and the motion described by the bent shaft as a whirl.

In Jeffcott's analysis, the shaft is considered to have a restitution force proportional to the distance to the elastic center and an unbalance force caused by an eccentric mass. For a shaft simplification containing only one disc at its center and supported by bearings on its ends, with an unbalanced mass “m” at *G*.

With the studies presented so far, the analyzes proceeded based on rotors with flexible shafts operating at supercritical speeds. The industry followed this line, and supercritical rotors were mainstream, which led to frequent problems with sub

synchronous whirl. In some cases, the deflection of the shaft could be seen by naked eye, given the low frequency of this phenomenon. In studying this phenomenon, Newkirk, in 1924, concluded that it was not affected by the rotor balancing and that its occurrence was noted only above the critical velocity.

Campbell, in 1924, presented his work, which later came to be known as Campbell diagram (Figure 2.2); one of the most important tools for understanding the dynamic behavior of rotating machines. The diagram consists of a graph where the natural frequencies of the system are plotted as a function of rotating speed. Although based on complete linearity, important information about a nonlinear system can be obtained through the linearized model (DUMITRU; SECARA; MIHALCA, 2009).

Campbell Diagram allows visualization of critical velocities and whirling directions for a given speed. A critical velocity of a rotor system is the rotating speed that coincides with one of the natural whirl frequencies of the system (RADES, 1995). The usual rotor behavior can be understood by the analysis of intersections in the Figure 2.2. Starting from the rest, until the velocity where the X=Y curve intersects the backward whirl mode natural frequency (BW) the rotor whirls in the same direction of the rotation. At the intersection, a critical speed is achieved and a peak in vibrations is expected. From the BW to FW intersection speeds, the rotor whirls in the opposite direction of rotation speed, reversing its whirl direction again at the intersection with FW curve, with another peak in vibrations.

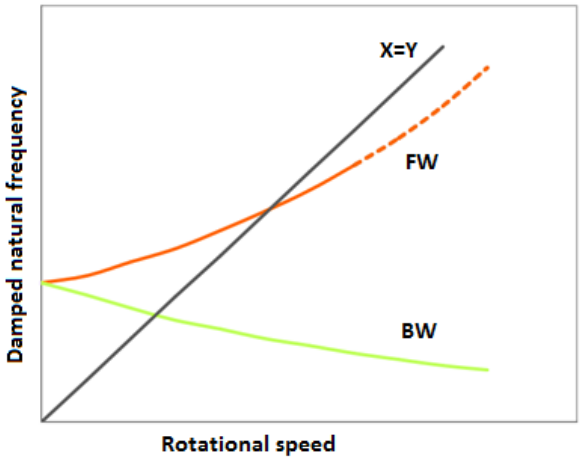

Figure 2.2 – Simplified Campbell Diagram

Working with Newkirk in 1925, Kimball postulated that internal friction and its damping would produce internal tensions at supercritical speeds that would lead to whirl. The idea of an instability condition being caused by the damping, being counter intuitive, had great resistance to being accepted, but was proved later with the experiments conducted by Kimball (1925).

In an advance that introduced the effects of the bearings on rotor behavior, Newkirk, along with Taylor, described the phenomenon of oil whip, which is an instability present in hydrodynamic bearings due to nonlinearity of the oil wedge on which the shaft rotates (NEWKIRK, TAYLOR, 1925). Smith (1933) investigated the rotor-bearing interface including in his model the flexibility of the shaft, the bearing support flexibility and internal friction. He concluded that a system without stationary damping is unstable at all speeds above critical. He also concluded that damping on bearing supports always increases the stability of the system, while damping on the rotating parts should be avoided for supercritical operation.

Expanding the understanding of the interaction between rotor and bearings, Kapitsa (1939) shown that a rotor could become unstable due to friction in its bearings. Smith's theory was expanded by analyses of Foote, Poristky, and Slade (1943) on the effects of asymmetry on rotating parts and bearings, seeking explanations for the vibrations found on rotors with asymmetry stiffness. They concluded that insufficient damping in the bearings caused whirl instabilities at a specific speed.

In most works published until then, the consequences of the gyroscopic effect were not highlighted. As rotating speeds were relatively low, the errors were small and the approximation could be considered valid. As the constructive advances allowed higher speeds, the gyroscopic effect could no longer be neglected, as well as its implications on critical speeds and whirl movement.

As the importance of the gyroscopic effect in the dynamics of rotors was being understood, the subject began to be more investigated. Green (1948) was the first to carry out these investigations, using Campbell diagram to show the influence of gyroscopic effect in critical frequencies of a given rotating system.

From the 1950s, the foundations of rotordynamics theory had been established, and the research followed two main directions. One concentrated in detailing models of the components that make up the rotating system, such as bearings, flow seals, discs and couplings. The more complex models allowed more realistic analysis of their effects on the system dynamics. At the same time, with the advent of computers, the interest in research of non-analytical methods for the solution of the equations of motion increased, leading to great advances related to numerical methods of solution.

At the time, computational effort was expensive and proposed solutions should be computationally simple to be feasible. At the same time, they must provide a good prediction of the system dynamics – a difficult compromise. Bearings response were evaluated through the solution of Reynolds equations. Having no closed solutions, the equation is difficult to be solved and numerical methods must be applied (DOWNSON, 1962).

Dubois and Ocvirk (1953), presented an approximate analytical solution for short bearings that included effects of the flow at journal extremities. In short bearings, the axial pressure gradient is much higher than the circumferential one, allowing to neglect the second one. For bearing length to diameter ratios of up to one, their approximation agreed with experimental data.

Another solution to simplify calculations was the linearization of bearings' behavior through equivalent damping and stiffness. Hagg and Sankey (1958) started investigations in 1958. Soon this type of solution was available for even more complex bearing types, such as tilting-pad bearings, as shown by Lund (1964). These models offer several computing advantages, as they allow bearings effects to be inserted

directly into damping and stiffness matrices. Because of this, even with the computational power available nowadays, linear bearing models are still relevant with refinements to the model being proposed (ZHOU et al, 2004; ZHAO et al, 2005; ZHANG et al, 2015). Linear bearings simulations results are very similar to non-linear ones in situations where the operation is kept in the linear range of the bearing - low unbalances and excitation forces. For larger perturbations, however, the linear model is less adequate (MACHADO; ALVES; CAVALCA, 2018). As this work is focused in lightly loaded rotors, with small bearing orbits, the linear model will be used with computing advantages and little prejudice to precision.

2.2 Methods of analysis

From the development of the rotor study until the 1940s, only analytical methods were used to calculate the system parameters. These methods were, however, laborious and limited in application and they did not apply to elaborate geometries or complex problems.

With the onset of World War II, there was a sudden increase in the interest for the analysis of rotating systems because of the great advantage afforded to the holders of more sophisticated machines. In this scenario with great pressure for equipment improvements, it was evident the need for methods that allow a faster analysis, boosting the development of numerical methods.

Prohl (1945) proposed a new method for obtaining the critical speeds of multi-disc rotors distributed along their length. The method became known as the transfer matrix method. Myklestad (1944) also developed studies on the subject, however, with an application focused on the calculation of natural frequencies of aircraft structures.

The method of the transfer matrix has since been developed, receiving contributions from several researchers, among them, Lund. He presented a broad approach on the subject, in four works, (LUND, 1964, 1967, 1974 and 1987). The method remains viable for industrial applications even today, after more than half a century of its first work, due to the constant updates and improvements it continues to receive.

Another approach to analyze this type of problem is the finite element method. It was first employed in the aeronautics industry by Turner while working at Boeing in 1950. He generalized and perfected the direct stiffness method, and received from Boeing sufficient budget to develop the method, while other companies in the industry used the method of forces (FELIPPA, 2004). The dissemination of the finite element method to other areas of knowledge occurred when it was first treated by Clough (1960).

In the 1960s, the finite element method received important contributions that further expanded its applications. Melosh (1963) shown that shifting conformation models are a Rayleigh-Ritz form based on the principle of minimum potential energy. This research was of great importance in unifying the three lines of research: Argyris (1960) energy methods, Turner (1959) direct stiffness method and the initial ideas of compatibility between elements as a basis for defining the limits of error and convergence.

The need for a large number of nodes to generate a precise solution through finite elements could make the analysis computationally very complex and costly to the point of not being economically feasible. To circumvent this problem, the condensation of degrees of freedom was introduced by Guyan (1965). Since then, other condensation techniques were suggested by Uhrig (1966) and Friswell and Mottershead (1996).

Concomitantly, Martin, after several studies involving structural applications of the method, introduced them to more generalized applications along with Carey (MARTIN; CAREY, 1973). With an increasing application range of the finite elements, the publication of books on the subject begins in 1967. The first published book on the subject was '*The Finite Element Method – Its Basis and Fundamentals*' by Zienkiwicz et al. A reference to the subject several decades after it was published, the book is a demonstration of the method's growth - its first edition in 1967 had 267 pages, while the sixth, published in 2005, has more than 1600 pages divided into three volumes (ZIENKIEWICZ, 2006).

During this period, the development was again being stimulated by the war, this time, the Vietnam War. Although already consolidated in several engineering strands, the finite element method had its first application in the resolution of rotating systems

by Ruhl and Booker (1972). Subsequently, Nelson and McVaugh (1976) generalized the method by adding rotational inertia, gyroscopic effect and axial forces, greatly increasing the accuracy of the method and the complexity of the systems to which it can be applied.

With the end of the incentives provided by the war, the advances are made in small increments that consolidated and improved what had been developed until then. In the 1980s, new implementations emerged, such as free formulation, orthogonal control and hybrid voltage methods, as well as their variants and derived methods. These approaches present in common the compatibility with the method of direct stiffness of Turner and the presence of simple elements, but that allow to obtain considerable precision, even in coarse meshes.

Even with the progress made, the analysis of finite elements for rotors still had great scope for improvement. Crandall (1992) analyzed several simulation software, including ANSYS, ComboRotor, DYNAMICS R4, DyRoBeS, iSTRDYN and NASTRAN. It was concluded that the software used at the analysis of rotor dynamics was still well outdated in relation to other areas.

With the latest developments, finite-element based commercial software is a well stablished engineering tool with increasing economic importance. The constant evolution in computational capacity, as provided by Moore's law, ensures that even very complex algorithms are computationally feasible, approximating simulations of real behavior (MOORE, 1965). Due to these characteristics, the finite-element method was chosen for this work.

2.3 Methods of optimization

The motivation behind the methods of analysis described before is reducing the cost of design outcome prediction through avoiding the building of models or prototypes.

Predicting the outcome was an important achievement, but a further improvement in computational design was desired, the so-called optimization.

Optimization is the search for a design that achieves the best results with minimum effort while satisfying certain constraints (HAFTKA; GURDAL, 1992).

Before the availability of computers with enough processing speed for the task of optimization, analysis of structures was done by differential equations. For simple designs, analytical methods of optimization could be used. Simple structures could be optimized even by analytical and trial and error methods as shown by (Figure 2.3 and Table 2.1). Complex structures, however, cannot be easily analyzed by the illustrated method, requiring prototypes, and their cost limited the number of iterations.

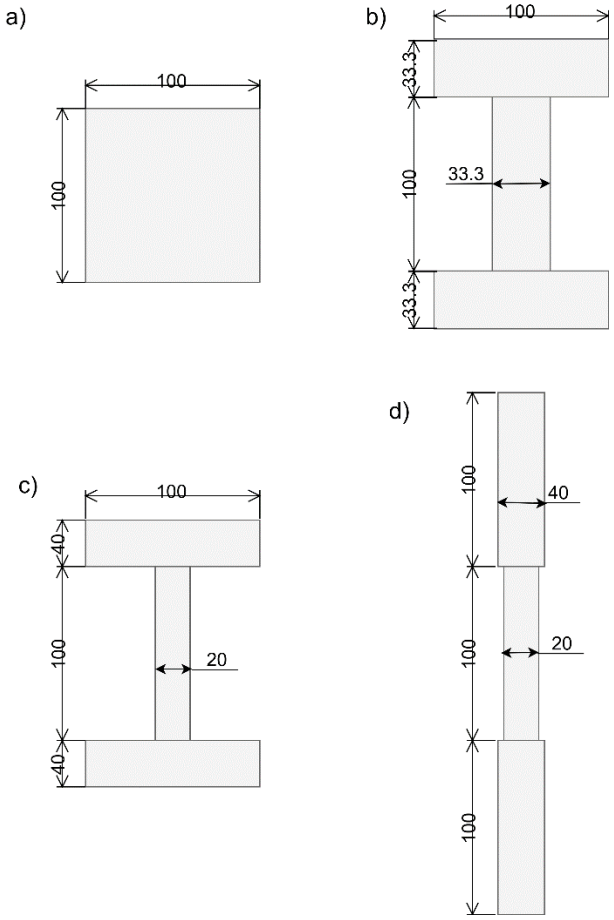

Figure 2.3 – Four beam cross sections with the same area. Adapted from Xie and Steven (1997)

Table 2.1 – Maximum load capacities for a simply supported beam for the cross sections in Figure 2.3

Cross Section	Max. load / Max. load (a)
(a)	1.00
(b)	2.38
(c)	2.80
(d)	3.53

The first step of computational optimization was the redesign of the structure critical points after finite element analysis and stress evaluation – this procedure was similar to trial and error, but without the prototype. Soon after, algorithms that generated solutions without manual interventions appeared. One of the first methods for structural optimization, named Fully Stressed Design (FSD), modifies the element cross sectional area by its ratio to allowable stress at each iteration (SOBIESZCZANSKI-SOBIESKI, 1984) Several other methods derived from the FSD, such as weight-strength methods and optimality criteria.

When applying a stress-based method like FSD, the criterion for element modification is easily assessed – its stress. In this case, the entire structure can be analyzed in a single FEA iteration, and the elements to be modified will be found. For complex objectives, however, it is difficult to mathematically define the objective function. In these cases, search methods can be employed with advantages in convergence and implementation difficulty. Search methods can be successfully employed in rotor optimization as shown by El-Shafei and Yakoub (2001). Their advantages were decisive in the employment of the method in the fourth paper; with small changes, the algorithm could be adapted for two distinct optimizations -stiffness and mass placement.

Despite of their advantages, search methods have a high computational cost. Some techniques can be used to offset this cost. Model reduction and heuristics are two of the most common. As shown in the first paper, once the number of nodes in the model is sufficient to describe rotor features, there is a negligible difference in increasing model discretization. This finding pointed out that the problem was suitable to the model reduction employed later in the fourth paper.

3 RESEARCH SYNTHESIS

3.1 Introduction

This chapter synthesizes the steps that led to the articles, as well as shows some details omitted by size limits in the publications. The articles are described in chronological order of research, which does not coincide with the chronological order of publication.

The main objective of the master research is to model and analyze rotating machines and propose an optimization method applied to the studied model. To achieve this objective, the research has gone through several steps, many of which are discussed in this chapter and in the articles presented in the following chapters, as well as in their results.

3.2 Research timeline

The timeline in Figure 3.1 shows the steps taken to achieve the desired objectives. The research started with an extensive review of rotordynamics, finite element method and optimization literature. This review is synthetized in the previous chapter, showing the main works used to provide theoretical support to the algorithm development.

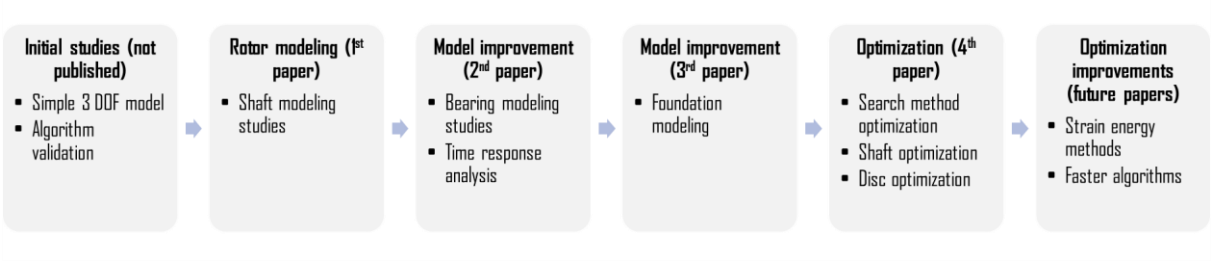

Figure 3.1 – Research timeline

Algorithm implementation started by simple three degrees-of-freedom models to validate results and evaluate computational aspects of the code and developing environment. Once a good base algorithm was established, the process of model study and refinement was started.

Being the main source of compliance in the rotor and the component of largest size in a rotor, the shaft was the first component to be modeled. Two of the most common beam models were tested and their differences analyzed for different shaft dimensions. These studies were published in the first paper. An overview of this paper is presented in section 3.5 and the full paper is in Chapter 4.

In order to improve the model, the effects of hydrodynamic bearings were included in the algorithm. Response of rotors supported by hydrodynamic bearings was compared to rigid bearings rotors. Time response was included in the analysis. The results of this steps, published in the second paper, are overviewed in section 3.6 and the full paper is in Chapter 5.

Continuing with model improvements, foundations were included and their influence in the system's response evaluated in the third paper (section 3.7 and Chapter 6).

After the foundations were included, a good model was achieved to support the optimizations that would be tested. Using this model, the fourth paper (section 3.8 and Chapter 7) shows results of modifications in shaft and also disc placement to optimize rotor response. A search method is employed for the optimizations.

The search algorithm used in the fourth paper, although with implementation advantages, showed a high computational cost. Another method, based on strain energy will be presented in future works to optimize shaft shape using a fraction of the

computational effort of the search method. A preview of the results is shown in section 3.9.

3.3 Modeling

3.3.1 Shaft

The first component modeled in the rotating system was the shaft. Timoshenko beam elements were first implemented because they could be easily adapted to behave as Euler-Bernoulli elements by neglecting shearing coefficients. All elements employed were cylindrical, with nodes on both extremities. Translation in X direction and rotation in Z axis are constrained (Figure 3.2), resulting in four degrees of freedom per node and an 8x8 matrix for each shaft element.

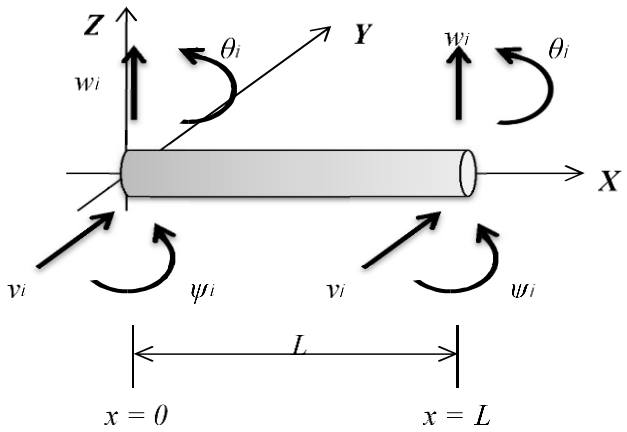

Figure 3.2 – Shaft element

Shaft elements were modeled with rotational inertia, translational inertia, bending stiffness and gyroscopic effect according to the matrices below (NELSON; MCVAUGH, 1976):

Translation inertia matrix is given by:

$$[M_T] = \begin{bmatrix} ct_1 & 0 & 0 & ct_2 & ct_4 & 0 & 0 & -ct_5 \\ 0 & ct_1 & -ct_2 & 0 & 0 & ct_4 & ct_5 & 0 \\ 0 & -ct_2 & ct_3 & 0 & 0 & -ct_5 & -ct_6 & 0 \\ ct_2 & 0 & 0 & ct_3 & ct_5 & 0 & 0 & -ct_6 \\ ct_4 & 0 & 0 & ct_5 & ct_1 & 0 & 0 & -ct_2 \\ 0 & ct_4 & -ct_5 & 0 & 0 & ct_1 & ct_2 & 0 \\ 0 & ct_5 & -ct_6 & 0 & 0 & ct_2 & ct_3 & 0 \\ -ct_5 & 0 & 0 & -ct_6 & -ct_2 & 0 & 0 & ct_3 \end{bmatrix}$$

Where:

$$ct_1 = (156 + 294\emptyset + 140\emptyset^2)\alpha_T$$

$$ct_2 = (22 + 38.5\emptyset + 17.5\emptyset^2)L\ \alpha_T$$

$$ct_3 = (4 + 7\emptyset + 3.5\emptyset^2)L^2\ \alpha_T$$

$$ct_4 = (54 + 126\emptyset + 70\emptyset^2)\ \alpha_T$$

$$ct_5 = (13 + 31.5\emptyset + 17.5\emptyset^2)L\ \alpha_T$$

$$ct_6 = (3 + 7\emptyset + 3.5\emptyset^2)L^2\ \alpha_T$$

$$\alpha_T = \frac{\rho AL}{420(1+\emptyset)^2}$$

Rotational inertia matrix is given by:

$$[M_R] = \begin{bmatrix} cr_1 & 0 & 0 & cr_2 & -cr_1 & 0 & 0 & cr_2 \\ 0 & cr_1 & -cr_2 & 0 & 0 & -cr_1 & -cr_2 & 0 \\ 0 & -cr_2 & cr_3 & 0 & 0 & cr_2 & -cr_4 & 0 \\ cr_2 & 0 & 0 & cr_3 & -cr_2 & 0 & 0 & -cr_4 \\ -cr_1 & 0 & 0 & -cr_2 & cr_1 & 0 & 0 & -cr_2 \\ 0 & -cr_1 & cr_2 & 0 & 0 & cr_1 & cr_2 & 0 \\ 0 & -cr_2 & -cr_4 & 0 & 0 & cr_2 & cr_3 & 0 \\ cr_2 & 0 & 0 & -cr_4 & -cr_2 & 0 & 0 & cr_3 \end{bmatrix}$$

Where:

$$cr_1 = (36)\alpha_R$$

$$cr_2 = (3 - 15\emptyset)L\ \alpha_R$$

$$cr_3 = (4 + 5\emptyset + 10\emptyset^2)L^2\ \alpha_R$$

$$cr_4 = (1 + 5\emptyset - 5\emptyset^2)L^2\ \alpha_R$$

$$\alpha_R = \frac{\rho A(R^2 + r^2)}{120L(1+\emptyset)^2}$$

Gyroscopic matrix is given by:

$$[G] = \begin{bmatrix} 0 & -cg_1 & cg_2 & 0 & 0 & cg_1 & cg_2 & 0 \\ cg_1 & 0 & 0 & cg_2 & -cg_1 & 0 & 0 & cg_2 \\ -cg_2 & 0 & 0 & -cg_3 & cg_2 & 0 & 0 & cg_4 \\ 0 & -cg_2 & cg_3 & 0 & 0 & cg_2 & -cg_4 & 0 \\ 0 & cg_1 & -cg_2 & 0 & 0 & -cg_1 & -cg_2 & 0 \\ -cg_1 & 0 & 0 & -cg_2 & cg_1 & 0 & 0 & -cg_2 \\ -cg_2 & 0 & 0 & cg_4 & cg_2 & 0 & 0 & -cg_3 \\ 0 & -cg_2 & -cg_4 & 0 & 0 & cg_2 & cg_3 & 0 \end{bmatrix}$$

Where:

$$cg_1 = (36)\alpha_G$$

$$cg_2 = (3 - 15\emptyset)L\ \alpha_G$$

$$cg_3 = (4 + 5\emptyset + 10\emptyset^2)L^2\ \alpha_G$$

$$cg_4 = (1 + 5\emptyset - 5\emptyset^2)L^2\ \alpha_G$$

$$\alpha_G = \frac{2\rho A(R^2 + r^2)}{120L(1 + \emptyset)^2}$$

Bending stiffness matrix is given by:

$$[K_B] = \begin{bmatrix} cb_1 & 0 & 0 & cb_2 & -cb_1 & 0 & 0 & cb_2 \\ 0 & cb_1 & -cb_2 & 0 & 0 & -cb_1 & -cb_2 & 0 \\ 0 & -cb_2 & cb_3 & 0 & 0 & cb_2 & cb_4 & 0 \\ cb_2 & 0 & 0 & cb_3 & -cb_2 & 0 & 0 & cb_4 \\ -cb_1 & 0 & 0 & -cb_2 & cb_1 & 0 & 0 & -cb_2 \\ 0 & -cb_1 & cb_2 & 0 & 0 & cb_1 & cb_2 & 0 \\ 0 & -cb_2 & cb_4 & 0 & 0 & cb_2 & cb_3 & 0 \\ cb_2 & 0 & 0 & cb_4 & -cb_2 & 0 & 0 & cb_3 \end{bmatrix}$$

Where:

$$cb_1 = (12)\alpha_B$$

$$cb_2 = (6)L\ \alpha_B$$

$$cb_3 = (4 + 1\emptyset)L^2\ \alpha_B$$

$$cb_4 = (2 - 1\emptyset)L^2\ \alpha_B$$

$$\alpha_B = \frac{EI}{L^3(1 + \emptyset)^2}$$

In the previous matrices, '*L*' is the element length, '*r*' is the element internal radius (used only for hollow elements), '*R*' is the external radius, '*ρ*' is the density, '*E*' is the Young Modulus and '*G*' is the shear modulus. '*A*' is the element area, obtained by Equation (3.1) and area moment of inertia '*I*' is in Equation (3.2). In addition, '*∅*' is

the shear coefficient, obtained by Equation (3.3), and the coefficient '*k*', that is used to obtain the shear coefficient, is shown in Equation (3.4).

$$A = \pi (R^2 - r^2) \tag{3.1}$$

$$I = \pi/4 \ (R^2 - r^2) \ (R^2 + r^2) \tag{3.2}$$

$$\emptyset = \frac{12EI}{kAGL^2} \tag{3.3}$$

$$k = \frac{6(1+v)(1+m^2)^2}{(7+6v)(1+m^2)^2+(20+12v)m^2} \tag{3.4}$$

Since Euler-Bernoulli beam is a case of Timoshenko beam without shear, that model can be employed by simply defining the shear coefficient '∅' as zero. The decrease in computational cost achieved by using Euler-Bernoulli beam, therefore, is obtaining shear coefficient through Equations (3.3) and (3.4).

Shaft elements also have internal damping. Steel shafts damping can be approximated to a fraction of stiffness with good precision, therefore, shaft damping is given by Equation 3.5 for the purposes of this work. A value of β = 1.5. 10^{-4} was adopted, except in simulations where it is explicit indicated otherwise, since is a good approximation frequently used in literature.

$$[C] = \beta[K] \tag{3.5}$$

3.3.2 – Disc

The disc is modelled as rigid and uniform, using a single node element. Spanning only one node, the disc model cannot affect stiffness, therefore its effects are only in inertia and gyroscopic matrices. Because of the one-node-element approach, discs must have a large diameter to thickness ratio to ensure good precision in simulations.

As with shaft elements, discs are constrained in axial direction (X in Figure 3.3). For unbalance analysis, an arbitrary unbalanced mass is assumed to be placed at disc node.

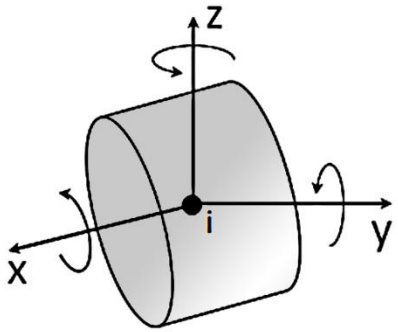

Figure 3.3 Disc element

The inertia and gyroscopic effects of the disc are obtained through the matrices below (NELSON; MCVAUGH, 1976).

Considering the coordinates vector:

$$\begin{bmatrix} Y \\ Z \\ \theta \\ \psi \end{bmatrix}$$

Where Y and Z are the translational degrees of freedom and θ and ψ the angular ones.

Translational inertia matrix is given by:

$$\begin{bmatrix} M_d & 0 & 0 & 0 \\ 0 & M_d & 0 & 0 \\ 0 & 0 & 0 & 0 \\ 0 & 0 & 0 & 0 \end{bmatrix}$$

Rotational inertia matrix is given by:

$$\begin{bmatrix} 0 & 0 & 0 & 0 \\ 0 & 0 & 0 & 0 \\ 0 & 0 & J_d & 0 \\ 0 & 0 & 0 & J_d \end{bmatrix}$$

Gyroscopic matrix is given by:

$$\begin{bmatrix} 0 & 0 & 0 & 0 \\ 0 & 0 & 0 & 0 \\ 0 & 0 & 0 & -J_P \\ 0 & 0 & J_P & 0 \end{bmatrix}$$

Where M_d is the disc's mass, obtained through Equation 3.6, J_d is the disc's transversal inertia moment, Equation 3.7, and J_p is the polar inertia moment, Equation 3.8.

$$M_d = \pi R^2 L \rho \qquad (3.6)$$

$$J_d = \frac{1}{12} M_d (\frac{3}{4} D^2 + L^2) \quad (3.7)$$

$$J_p = \frac{1}{8} M_d D^2 \quad (3.8)$$

3.3.3 – Bearings

The first bearing model used in this work was the simple rigid bearing model, where the degrees of freedom constrained by bearings are eliminated from the problem through removal of their rows and columns in system main matrices. Two types of rigid bearings were tested. The first one constraints all degrees of freedom except rotation in X axis in the node and the second one only constraints the translational movements.

In addition to the rigid bearing model, a hydrodynamic bearing model was also used in the simulations. The bearing behavior was obtained through the Reynolds equations. Since these complete equations do not present an analytical solution, and even the complete numerical solution presents a high computational cost, the use of simplifying hypotheses was necessary to make a solution feasible, albeit to the detriment of the precision of the results.

The two simplifications commonly used are those of infinitely long bearing (where the oil flow at bearing ends is neglected) and infinitely short bearing (where the oil flow in the circumferential direction is neglected). Due to the characteristics of the formulation used, by finite elements, where the bearing is positioned in a node of infinitesimal dimensions, it is natural that a bearing consideration of negligible length be more appropriate.

Being coherent with the infinitesimal axial dimensions imposed by the resolution method, the hypothesis also represents more closely the actual dimensions of bearings that are used in real machines, and, therefore, was used in this work. Moreover, short bearings are best suited for slender shafts that suffer from large deflections, since a long bearing is prone to the reduction of clearance to zero at the ends of the bearing under large deflections, leading to shaft contact with the bearing surface and invalidating the model.

For the bearing characterization and determination of its influence on the dynamics of the system, the following entries is necessary: radial clearance (δ), lubricant viscosity (η), bearing length (L) and shaft diameter (R). Bearing's equations

also use the rotational speed of the shaft, which is already given by other inputs (pre-established in the time domain and varied by a loop with fixed step for the frequency and modal domains).

The type of bearing chosen for the model is the cylindrical bearing, so the thickness of the oil film varies according to the eccentricity of the shaft inside the bearing. The lubricant was considered an incompressible Newtonian fluid with constant viscosity throughout the film adhering to the surfaces of the bearing, and also perfectly smooth and rigid.

The oil film in the bearing had its mass ignored due to the small thickness. The pressure variations in the radial direction and, consequently, the flow velocity in the same direction were also neglected. Due to the small ratio between the thickness of the oil film and the radius of curvature, the effects of this curvature were overlooked. With these characterizations, the flow is approximated to laminar between two flat surfaces, easing the modeling.

The bearing behavior is obtained from the Reynolds equation (Equation 3.9), as presented in Krämer (1993):

$$\frac{\partial}{\partial x}\left(h^3\frac{\partial p}{\partial x}\right)+\frac{\partial}{\partial z}\left(h^3\frac{\partial p}{\partial z}\right)=6\mu U\frac{\partial h}{\partial x}+12\mu\frac{\partial h}{\partial t} \quad (3.9)$$

Where *p* is the pressure developed on the oil film and *h* is the thickness of the lubricant film.

Since the rotors are analyzed in steady state and constant load, the height of the lubricant film will be constant in time, eliminating the term ∂h/dt and simplifying Equation 3.9 to:

$$\frac{\partial}{\partial x}\left(h^3\frac{\partial p}{\partial x}\right)+\frac{\partial}{\partial z}\left(h^3\frac{\partial p}{\partial z}\right)=6\mu U\frac{\partial h}{\partial x} \quad (3.10)$$

Assuming that the bearing is short, in *Z* direction pressure must fall at a very small interval (bearing length) from the peak pressure to the atmospheric pressure. This leads to a large axial pressure gradient (*∂p/∂z)*, which is several orders larger than the circumferential gradient (*∂p/∂x).* Therefore*, ∂p/∂x* can be neglected. A further simplification of the Reynolds equation with these new ponderings leads to:

$$\frac{\partial}{\partial z}\left(h^3\frac{\partial p}{\partial z}\right)=6\mu U\frac{\partial h}{\partial x} \quad (3.11)$$

The solution of Equation (3.11), according to Krämer, leads to:

$$\frac{F0}{Fn} = S^* = \frac{\pi}{2} \frac{\varepsilon}{1-\varepsilon^2}^2 \left(1 - \varepsilon^2 + \left(\frac{4}{\pi}\varepsilon\right)^2\right)^{0.5} \quad (3.12)$$

where *Fn* is the frictional force on the bearing, F_0 the bearing equivalent static load and ε is the eccentricity ratio of the shaft inside the bearing. Due to oil film small thickness, *Fn* can be given by:

$$Fn = \eta \; L^3 \; \omega \; \frac{\frac{R}{2}}{\delta^2} \quad (3.13)$$

where η is the lubricant viscosity, is L is the bearing length, ω is the shaft angular speed and δ is the radial clearance. Rearranging Equation 3.12 leads to:

$$F_0 = S^* Fn$$

S* is the modified Sommerfeld number, the relation between radial and frictional forces on the bearing. Therefore, by joining Equations 3.12 and 3.13, the relation between eccentricity and applied load is given by:

$$F_0 = \eta \; L^3 \; \omega \; \frac{\frac{R}{2}}{\delta^2} \frac{\pi}{2} \frac{\varepsilon}{1-\varepsilon^2}^2 \left(1 - \varepsilon^2 + \left(\frac{4}{\pi}\varepsilon\right)^2\right)^{0.5} \quad (3.14)$$

The load on the bearing is obtained through a static analysis of the rotor. Equation 3.14 is then solved for ε numerically for each rotating speed.

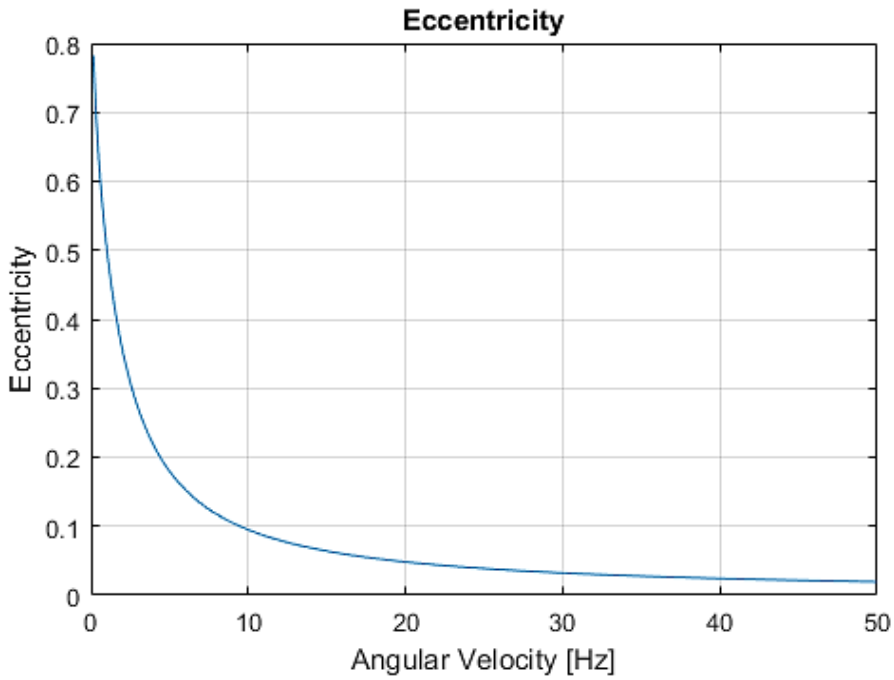

Figure 3.4 – Eccentricity of shaft inside the bearing as a function of shaft angular velocity

Values of eccentricity for a Jeffcott rotor similar to the one used in the Chapter 5 are shown in Figure 3.4. The curve relating eccentricity to angular velocity is very

steep at the lowest velocities, but tends to almost flat as the rotor operates at higher speeds.

From the values obtained for ε, the coefficients of stiffness and damping of the bearing can be calculated.

An auxiliary variable, $A(\varepsilon)$, is used for both stiffness and damping and given by Equation 3.15:

$$A(\varepsilon) = \frac{4}{(\pi^2+(16-\pi^2)\varepsilon^2)^{\frac{3}{2}}} \tag{3.15}$$

With $A(\varepsilon)$ known, the auxiliary γ coefficients are obtained by the set of Equations 3.16:

$$\gamma(1,1) = (2\pi^2 + (16-\pi^2)\ \varepsilon^2)\ A(\varepsilon);$$

$$\gamma(1,2) = \pi(\pi^2 - 2\ \pi^2\ \varepsilon^2 - (16-\pi^2)\ \varepsilon^4) \times \left(\frac{A(\varepsilon)}{4\varepsilon\ (((1-\varepsilon^2)^{0.5}))}\right); \tag{3.16}$$

$$\gamma(2,1) = -\pi(\pi^2 + (32+\pi^2)\ \varepsilon^2 + (32-2\pi^2)\ \varepsilon^4)\ \left(\frac{A(\varepsilon)}{4\varepsilon\ (((1-\varepsilon^2)^{0.5}))}\right);$$

$$\gamma(2,2) = (\pi^2 + (32+\pi^2)\ \varepsilon^2 + (32-2\pi^2)\ \varepsilon^4)\ \left(\frac{A(\varepsilon)}{1-\varepsilon^2}\right);$$

And the stiffness coefficients can be related to the γ coefficients through Equation 3.17:

$$K_{ik} = \gamma_{ik}\frac{F_0}{\partial} \tag{3.17}$$

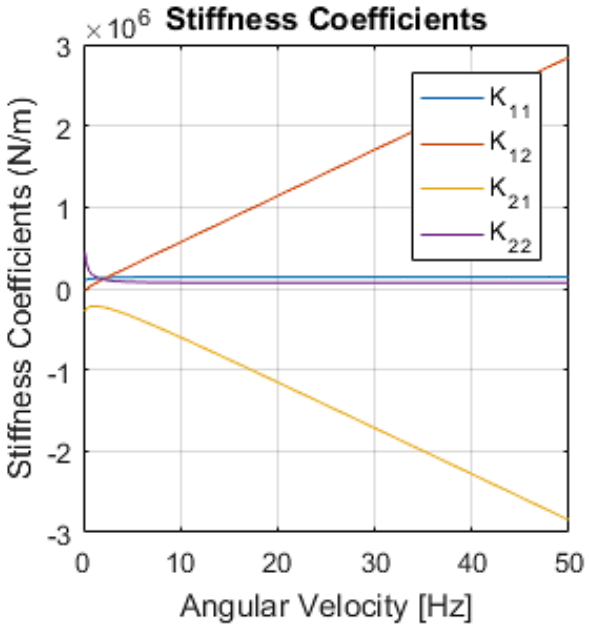

Figure 3.5 – Bearing stiffness coefficients as a function of shaft angular speed

The overall behavior of stiffness coefficients calculated by the method can be seen in Figure 3.5. The direct stiffness coefficients curve resembles the one seen in the eccentricity - with a steep slope at lowest frequencies, while the cross-coupled coefficients increase at a steady rate.

The same procedure used to obtain stiffness coefficients is applied to the damping coefficients. The auxiliary β coefficients are given by the set of Equations 3.18:

$$\beta(1,1) = \left(\frac{\pi}{2}\right)\left(\frac{(1-\varepsilon^2)^{0.5}}{\varepsilon}\right)(\pi^2 + (2\pi^2 - 16)\,\varepsilon)\,A(\varepsilon);$$

$$\beta(1,2) = -2\ (\pi^2 + (2\pi^2 - 16)\,\varepsilon)\,A(\varepsilon); \qquad (3.18)$$

$$\beta(2,1) = -2\ (\pi^2 + (2\pi^2 - 16)\,\varepsilon)\,A(\varepsilon);$$

$$\beta(2,2) = \pi\ (\pi^2 + (48 - 2\pi^2)\,\varepsilon^2 + \pi^2\,\varepsilon^4)\frac{A(\varepsilon)}{2\varepsilon\ (1-\varepsilon^2)^{0.5}};$$

Finally, damping coefficients are related to β coefficients by Equation 3.19:

$$D_{ik} = \beta_{ik}\frac{F_0}{\partial.\omega} \qquad (3.19)$$

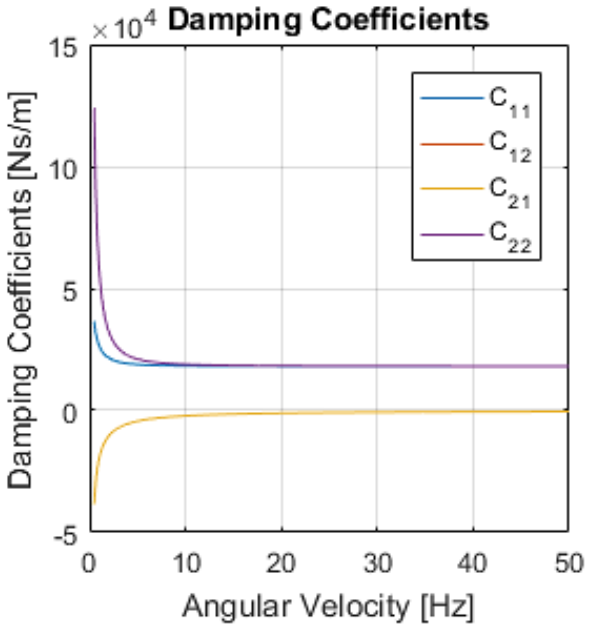

Figure 3.6 - Bearing damping coefficients as a function of shaft angular speed

Contrary to the stiffness coefficients, cross-coupled and direct damping curves have similar shapes, differing only in sign, as can be seen in Figure 3.6. It is noteworthy that cross-coupled damping coefficients tends to negligible values as angular velocity increases.

Through this characterization of the hydrodynamic effects by means of springs and dampers equivalent to stiffness and damping, the coefficients found can be inserted directly into the position of the appropriate elements of the respective matrices for both time domain and frequency domain analyzes. This approximation is equivalent to an equivalent model of shaft supported on springs and dampers, as shown in Figure 3.7.

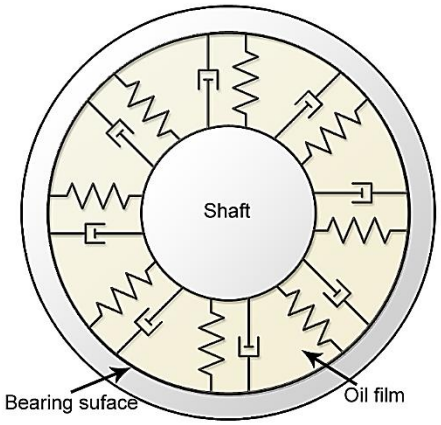

Figure 3.7- Equivalent spring and damper bearings

3.3.4 – Foundations

Foundations are an important component of the rotating systems, which connects the entire rotating assembly to the ground. In order to avoid excessive computational cost while still having foundations in the model, a lumped parameter approach was used. As shown by Kang et al (2000), this approach presents good correlation between experimental results and simulations.

The use of lumped parameter foundations is especially effective when associated to the bearing model described, because the overall system can be represented only by mass, stiffness and damping, precluding the need of additional external forces when analyzing system response.

As seen in Figure 3.8, a one degree of freedom mass-spring-damper system was used at each node containing a bearing. The lumped parameter foundation is series coupled to the main rotating system by the bearings matrices, as shown in the sparse matrix below, where [*B*] contain the bearing information, [*R*] contain the rotor information and [*F*] contain the foundation information (more details of this is presented in section 3.8 and in Chapter 7):

$$\begin{pmatrix} [B] & \cdots & [-B] \\ \vdots & [R] & \vdots \\ [-B] & \cdots & [F] \end{pmatrix}$$

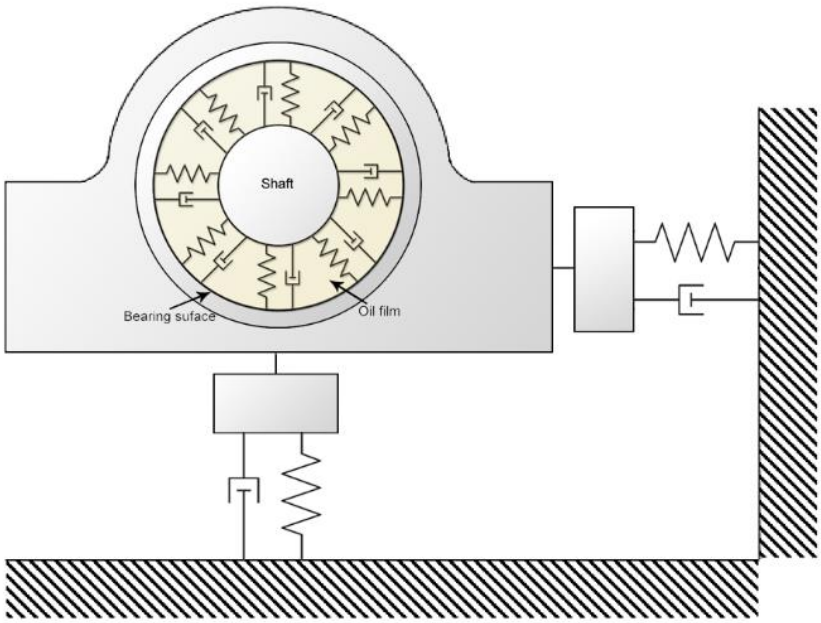

Figure 3.8 – Foundation model by lumped parameters coupled to bearing model by lumped parameters

3.4 Computational aspects

The algorithm used in this work was constructed in MATLAB™ (MATrix LABoratory), a programming environment developed by MathWorks for numerical computation. While many of the languages commonly used for numerical problem solving require an element-by-element approach to operations with arrays and matrices, MATLAB™ provides optimized functions to work with entire arrays.

Since it is an environment developed for numerical computation, it has functions already implemented for common routines in this field and a user-friendly graphical interface for result analysis as well as routines for numerical integration. The algorithm was created making use of some functions already present in the environment. Due to MATLAB™ compatibility with C and Fortran functions, it is possible to test and compare the performance of other functions when necessary.

The algorithm segments were designed with the least possible dependence between the blocks. The functions were written to use few results from each other, taking advantage of previous results only where recalculation is computationally costly.

This approach, while causing a certain overhead, leads to improved execution in independent threads. This independence is essential to ensure that two MATLAB™ tools could be widely used: parallel processing and the use of GPU processing.

The general functioning of the algorithm is shown in the diagram of Figure 3.9. The block of inputs and initial calculations is the least complex and is executed in a very short time. The block of arrays presents the most complex calculations of the code, but since they are performed only once, they take only a fraction of a second. The following blocks are already independent and can be executed in parallel.

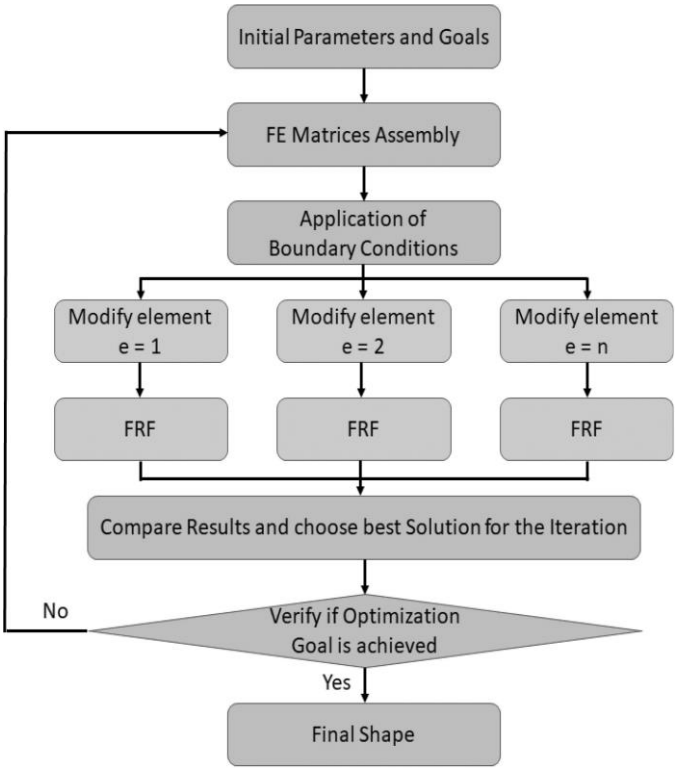

Figure 3.9 – Algorithm diagram, adapted from Rother, Alencar and Machado (2018a)

The most computationally costly step – results obtention – is divided into three main blocks: modal response, time response and frequency response. From these three blocks, the longest computing time is spent in time response, the time it takes is three orders of magnitude above the required for the other responses.

The high computational effort of the time response is consequence of three main factors: the difficulty represented by integration, sweeping of two variables (time and frequency) and the impossibility of employing out of order execution for time steps in integration. Although a reduced number of frequencies have been used in time-domain

analyzes, the tiny time step required for integration convergence results in a large number of function evaluations to complete the analysis.

3.4.1 - Time response

Suppressing the other calculations and auxiliary functions required to prepare inputs and adjust outputs, this block solves the system of state space equations shown in Equation 3.20:

$$\begin{cases} \{\dot{x}\} = [A_S]\{x\} + [B_S]\{u\} \\ \{y\} = [C_S]\{x\} + [D_S]\{u\} \end{cases} \tag{3.20}$$

In Equation 3.20, x is the state vector, A is the state matrix and B is the input matrix. C is the output matrix and D is the direct transition matrix. The output is represented by y. Matrices A to D are constant and a direct function of system parameters. This equation results in a 2n X 2n system, where n is the number of system's degrees of freedom, as shown in Equation 3.21.

$$\begin{Bmatrix} \{\dot{x}\} \\ \{\ddot{x}\} \end{Bmatrix} = \begin{bmatrix} [0] & [I] \\ -[M]^{-1}[K] & -[M]^{-1}([C] + \Omega \cdot [G]) \end{bmatrix} \cdot \begin{Bmatrix} \{x\} \\ \{\dot{x}\} \end{Bmatrix} + \begin{bmatrix} [0] & [0] \\ [0] & [M]^{-1} \end{bmatrix} \cdot \begin{Bmatrix} \{0\} \\ \{F\} \end{Bmatrix} \tag{3.21}$$

The external forces are represented by the last vector in Equation 3.21. All forces exerted on the rotor are included in this vector, such as weight and unbalanced mass of the system. The linearization of hydrodynamic bearings and, consequently, their inclusion in the constant part of equation severely reduces computational efforts. If bearings' force were obtained, a second integration loop would be nested inside equation loop.

For the solution of the system of equations, it is necessary to use numerical integration techniques. Numerical integration methods use specific iterative algorithms for differential equations. Among the numerical integrators available in MATLAB™ the main integrators indicated for non-stiff problems were tested: 'ode45', 'ode23' and 'ode113'.

The 'ode45' function is based on the Runge-Kutta algorithm, using the Dormand -Prince method and uses six function evaluations per step. The 'ode23 ' function is also an explicit implementation of the Runge-Kutta algorithm, using the Bogacki-Shampine pair. It uses only three function-by-step evaluations. The 'ode113' function, unlike the

previous functions, has no fixed order, varying between the first and twelfth order. After tests of computational performance, it was verified that the use of the 'ode23' function leads to a reduction of more than 50% in computational time, for the cases of interest in this work, in relation to the other two, with minimal reduction in accuracy.

As the time domain analyzes were less used during the research, and their results are only shown in the second paper, a customized algorithm for these solutions was not implemented and the best option among the integrators present in MATLAB™ was chosen.

3.4.2 - Frequency response

One of the most used analyzes in the research was the analysis of frequency response in permanent regime. With great importance, by identifying the amplitude of vibration in each node for a given frequency, it is obtained through the solution of Equation 3.22. For this analysis, only forces due to unbalance and gravity are included.

$$[H]^{-1} = \{q\}\{F\}^{-1} = \left[-\omega^2[M] + j\omega([C] + \Omega[G]) + [K]\right]^{-1} \quad (3.22)$$

In Equation 3.22, {F} is a force vector of gravity and unbalance force. While gravity forces are the same through the entire frequency range ($F_g = Mg$), unbalance forces are proportional to rotating speed squared ($F_U = M_U e_U \omega^2$). Matrices M, C, G and K represent mass, damping, gyroscopic and stiffness matrices respectively.

It can be noted that Equation 3.22 must be solved for each frequency value ω, in order to obtain response in the analyzed spectrum. During frequency sweeping, each analysis at a different frequency value can be assigned to a different thread, since the values are not dependent on each other. This particularity of the problem facilitates parallel execution.

For this situation, there is great advantage in using GPU. In addition to the matrix problem being suitable for a GPU architecture, it is possible to use a much larger number of concomitant threads in relation to CPU usage.

3.4.3 - Modal response

Like the frequency analysis, modal analysis is widely used during the research. The Campbell diagram and the damping coefficient of each mode are important tools

to determine system stability. A free-body analysis is performed, so unbalance and gravity have no influence in modal response. Natural frequency of vibration modes is obtained through solving the eigenvalue problem for the state space matrix of the rotor. The construction of state space matrix can be seen in Equations (3.23) and (3.24) below:

$$[A] = \begin{bmatrix} [0] & [I] \\ -[M]^{-1}[K] & -[M]^{-1}[C_C] \end{bmatrix} \tag{3.23}$$

$$[C_C] = [C] + \omega[G] \tag{3.24}$$

The gyroscopic effect influence in frequency change of vibration modes is clear when Equations (3.23) and (3.24) are analyzed. In fact, it is easily perceived that the gyroscopic effect is the only reason to have a Campbell diagram. A hypothetical rotor unaffected by gyroscopic effect would exhibit only straight parallel lines in Campbell diagram.

3.4.4 – Parallelism and GPU processing

The analyses described in Sections 3.4.1 through 3.4.3 are the major computational load of the algorithm. While time response is less suited to parallel processing due to the dependence between consecutive time steps, the other two analyses characteristics favor the use of parallel processing.

Time response analysis of a single rotor with dozens of nodes will require several hours since very small time-steps are required to ensure integration convergence. Because of this, time response analysis was withdrawn in the last works. Especially when combined with the costly search method employed, time response analysis is not viable for the current algorithm and hardware used.

The remaining results, modal and frequency response, are obtained through matrix operations, independent between frequency steps and combined to the search method optimization, an even larger number of independent matrix operations can be done concomitantly, as seen in Figure 3.10.

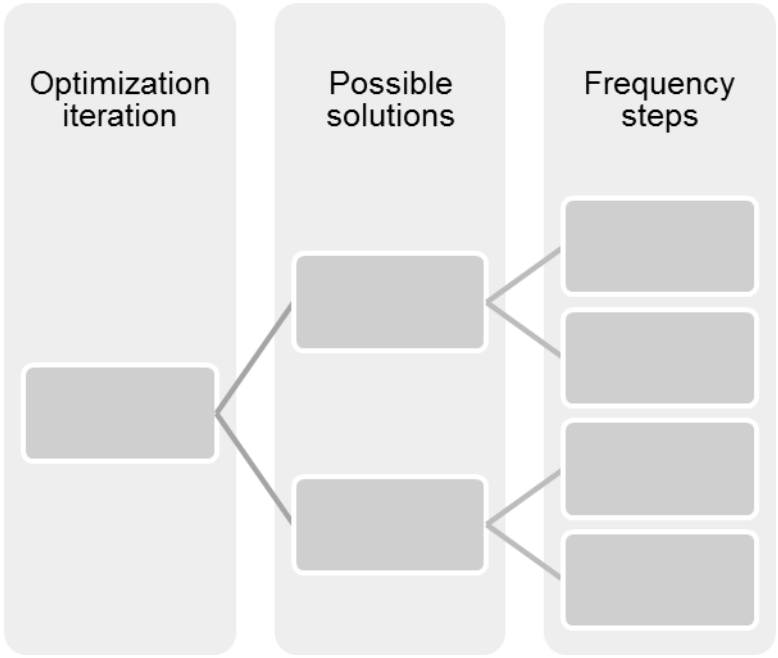

Figure 3.10 – Parallelization of workload for modal and frequency response analyses

The number of independent threads for each analysis can be calculated through Equation 3.25

$$T_{max} = (N - 2).S \tag{3.25}$$

The hardware used in most computations was a Core i7 4770K CPU and a GTX 1060 GPU. The GPU is composed by 10 streaming multiprocessors (SM), with 128 CUDA™ cores each, giving an upper bound of 20480 concurrent threads. The CPU have 4 cores with simultaneous multithreading enabled, allowing 2 threads per core, for a total of 8 simultaneous threads.

Although GPU have more computational power, as seen in Table 3.1, the large number of cores dictates that a high number of threads is essential to achieve full performance. The optimization method used provides this required number of threads. For very discretized models, the Equation 3.25 shows that the algorithm will provide full core occupancy even for multi-GPU arrays.

Table 3.1 – Comparison of hardware theoretical peak float point performance

Hardware	GFLOPS (single precision)	GFLOPS (double precision)
i7 4770	101	70
GTX 1060	3855	120

Table 3.1 compares GPU and CPU performance in number of float point operations per second (FLOPS). The higher (70%) GPU double precision capabilities results in significant performance advantages. The code uses the faster hardware (GPU) for suitable operations, as matrix multiplication, increasing speed of these operations and reducing CPU workload.

Reducing the load in CPU allow its core frequency to be higher due to Intel® Turbo Boost, which increases processor clock when there is thermal headroom. This boost on CPU clock will increase single threaded operations performance, therefore, the use of GPU will have a positive effect even in the operations executed only in the CPU.

Another noteworthy fact in Table 3.1 is the large difference in single precision capabilities between GPU an CPU. While the code employs double precision for its math operations, a major rework for single precision would result in substantial performance increases and will be worked on for future works.

3.5 Paper 1 overview

The first paper, "*Comparação Entre Modelagens de Elementos de Eixo em Sistemas Rotativos*", is adapted as the Chapter 4. This article can be found in the Proceedings of the X National Congress of Mechanical Engineering – CONEM, published in the first half of 2018. Although not the first in chronological publication order, it contains the initial studies of modeling, comparing Euler-Bernoulli and Timoshenko beam models in shaft modeling.

From the analyzes, it could be noted that the difference between the models was relevant in only two conditions: vibration modes with higher number of nodes and shafts with low slenderness ratio, as can be seen in the graph of Figure 3.10 and Table 3.1. For most of the studied rotors, none of these conditions are common, since they usually have slender shafts and operate, at most, in speeds around the second critical frequency.

Through these results, it can be concluded that even the simplest model, the Euler-Bernoulli beam, can represent a good approximation of a shaft model for the

study of rotors. However, the additional computational cost due to the use of the Timoshenko model is small and justifies its use, since the two models have already had to be implemented for the comparison. Thus, subsequent studies were performed using the Timoshenko model.

Table 3.2 – Simulations' results, adapted from Rother, Alencar and Machado (2018*b*)

Case	$\frac{L}{D}_{shaft}$	$\frac{L}{D}_{elem}$	ω_{n1} Timoshenko [Hz]	ω_{n1} Euler-Bernoulli [Hz]	$100\% - \frac{\omega_{n1T}}{\omega_{n1E}}$
1	80	40	13,76	13,79	0,22%
2	80	20	13,76	13,79	0,22%
3	80	10	13,76	13,79	0,22%
4	80	1	13,76	13,79	0,22%
5	40	10	43,39	43,70	0,71%
6	20	10	108,6	110,70	1,90%

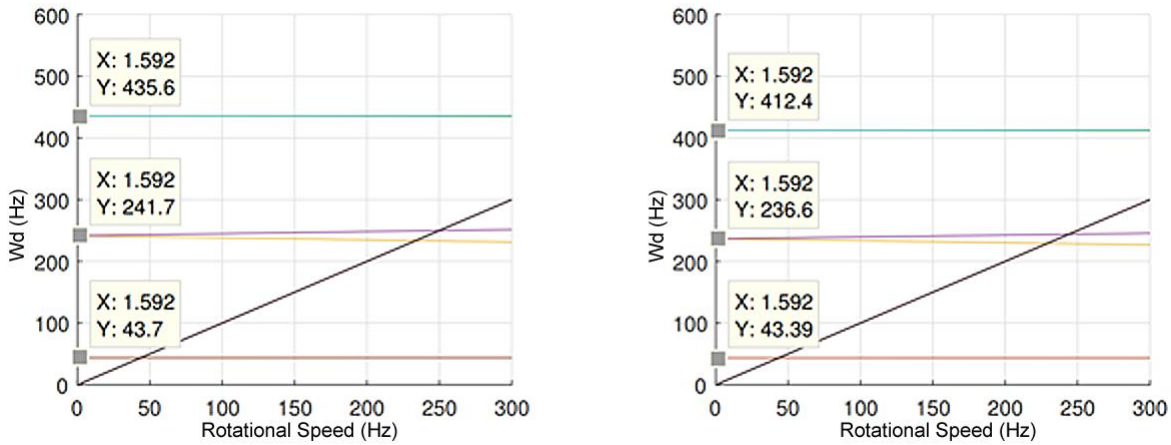

Figure 3.11 – Campbell diagram for case 5. Euler-Bernoulli model (left) and Timoshenko (right), adapted from Rother, Alencar and Machado (2018b)

3.6 Paper 2 overview

The second paper, "Analysis of the bearings' influence on the dynamic behavior of a rotating machine", is adapted as the Chapter 5. This article can be found in the Proceedings 24th ABCM International Congress of Mechanical Engineering - COBEM published in the second half of 2017.

Through comparisons between rotors supported on rigid bearings and hydrodynamic bearings, the oil film influence on rotor dynamics is assessed. Reduced system stiffness as result of employing hydrodynamic bearings causes the rotor to have lower natural frequencies and their damping and compliance reduced vibration peaks as seen in Figures 3.11 and 3.12.

The shaft is modeled by Timoshenko beam elements, as their use is advantageous as shown in 3.5. The modeling of hydrodynamic bearings is done as described in subsection 3.3.3. Frequency response, modal analysis and time response is evaluated for both centralized and decentralized Jeffcott rotors, as can be seen in Chapter 5.

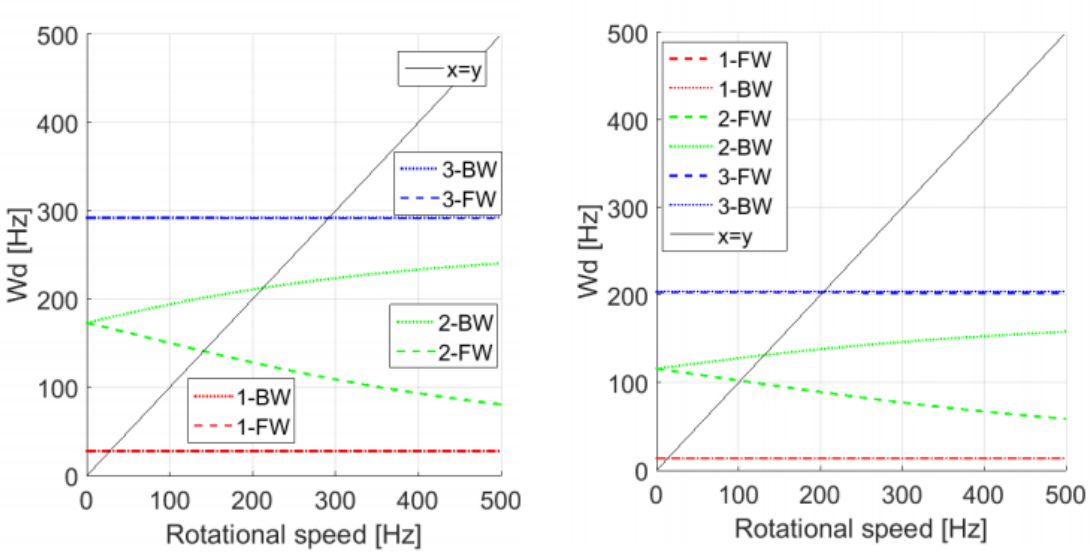

Figure 3.12 – Campbell diagram of rotor supported on rigid bearings (left) and hydrodynamic bearings (right) – adapted from Rother and Machado (2017)

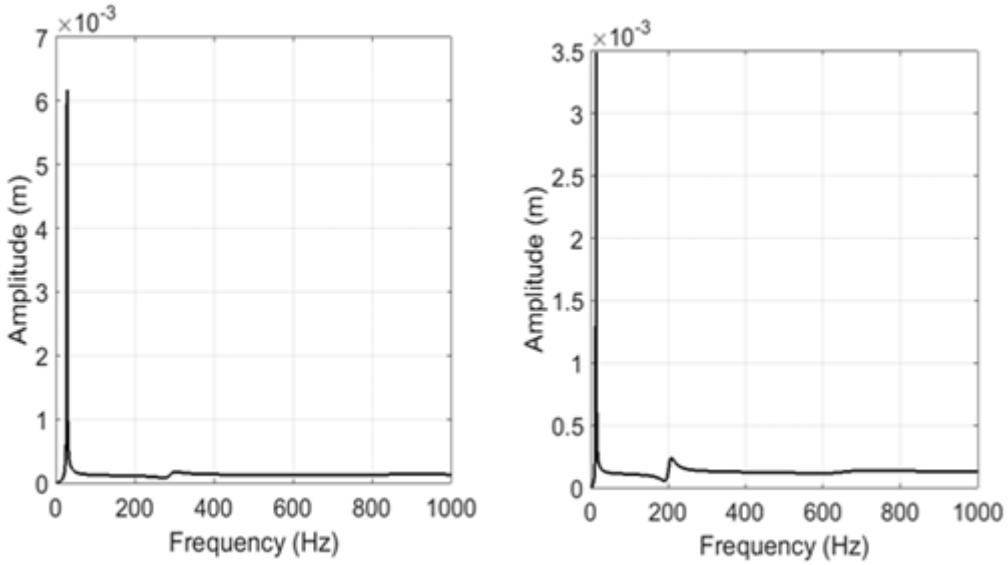

Figure 3.13 – Frequency response function of rotor supported on rigid bearings (left) and hydrodynamic bearings (right) – adapted from Rother and Machado (2017)

3.7 Paper 3 overview

The third paper, “Estudo da Influência da Fundação na Resposta de Sistemas Rotativos”, is adapted as the Chapter 6. This article, was published in the same congress of the first paper, appearing in the Proceedings of the X National Congress of Mechanical Engineering - CONEM published in the first half of 2018.

In this paper, the effects of foundations on rotor response is evaluated. Comparison between response in rigid and compliant direction of foundations show their influence in rotor response, as seen in Figure 3.13.

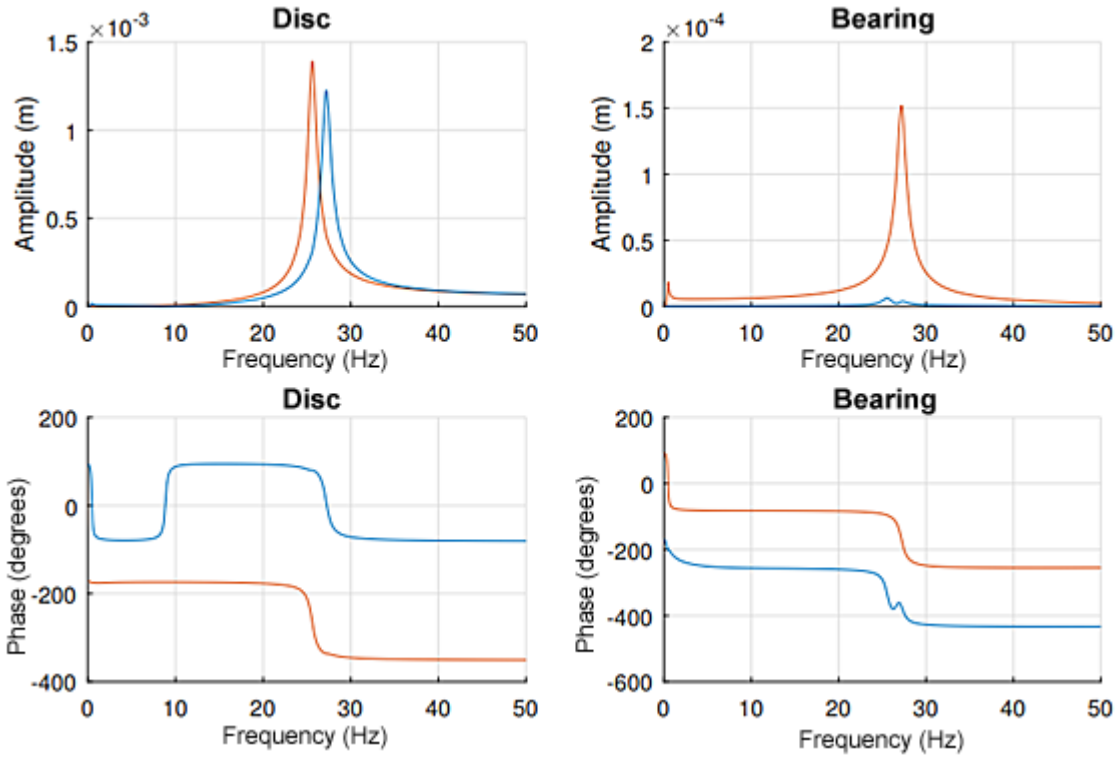

Figure 3.14 – FRF of rotor supported in anisotropic foundations. Response in the rigid direction (blue) and in the compliant direction (red). Adapted from Rother, Alencar and Machado (2018b)

Foundation compliance had limited effects on disc's node where the unbalance was placed; amplitude and frequency of peak vibrations changed 15% at most, even in a very compliant 100N/m foundation. In bearings' nodes however, an increase of magnitude is observed in vibration amplitude; this can be attributed to much higher initial stiffness in these nodes. Whereas disc's node is affected by entire shaft compliance plus oil film compliance, bearing's nodes are affected only by oil film, which is very stiff, therefore the increase in compliance is much more significant at these nodes.

3.8 Paper 4 overview

The fourth paper, "A Compensation Method for Foundation Effects in Rotating Systems through Shape Optimization", is adapted as Chapter 7. This article was presented in the 10th IFToMM International Conference on Rotordynamics held in the

second half of 2018 and published as a chapter by Springer International Publishing in a special volume of Mechanisms and Machine Science.

Using the algorithm and modelling of the previous works to evaluate rotor response, this paper adds an optimization block to the algorithm. Based on a search method, the algorithm modifies the element with most influence in the rotor response at each iteration. Parallel and GPU computing are used to enhance the performance of the costly operations associated with testing several elements at each iteration.

The method was employed for two kind of rotor modifications: shaft elements modification and disc placement. While changes in shaft shape have the advantage of allowing mass and stiffness rearrangement, placing discs is a less costly option and more feasible to employ in a rotor already manufactured.

For a same rotor, both methods were compared in the task of restoring system's amplitude of vibration. In the case shown in Figures 3.14 and 3.15, a rotor which operated at 215 Hz is placed in another foundation, which was more compliant than the original one. The new foundation produced unacceptable levels of vibration at operating speed. It can be noted that both methods produced similar responses after the iterations needed to revert the amplitude at 215 Hz. In situations like this, modifications of rotor through disc placement are preferred due to their lower cost and easier implementation.

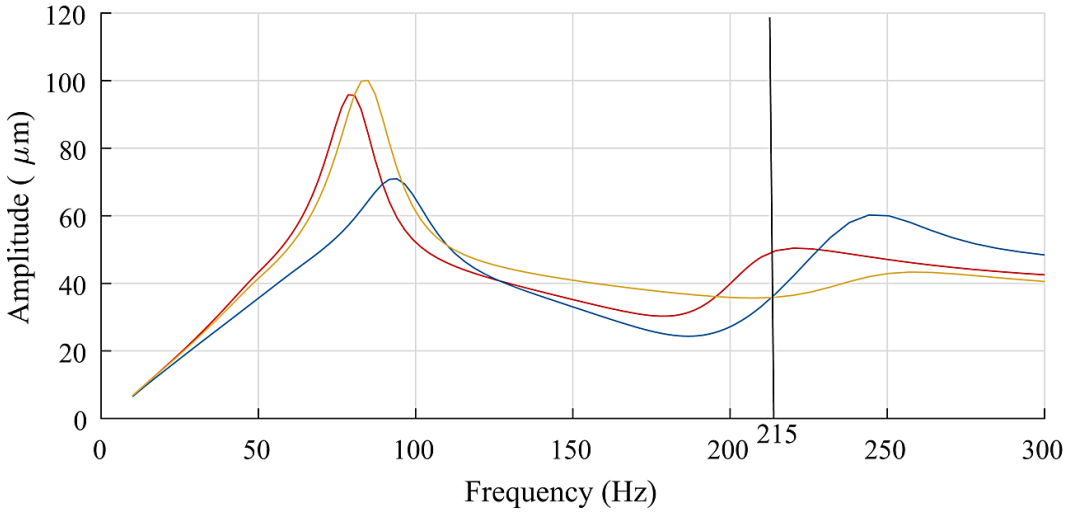

Figure 3.15 – FRF comparison between the initial response (blue) and the response in the more compliant foundation before (red) and after (yellow) the shaft optimization adapted from Rother, Alencar and Machado (2018a)

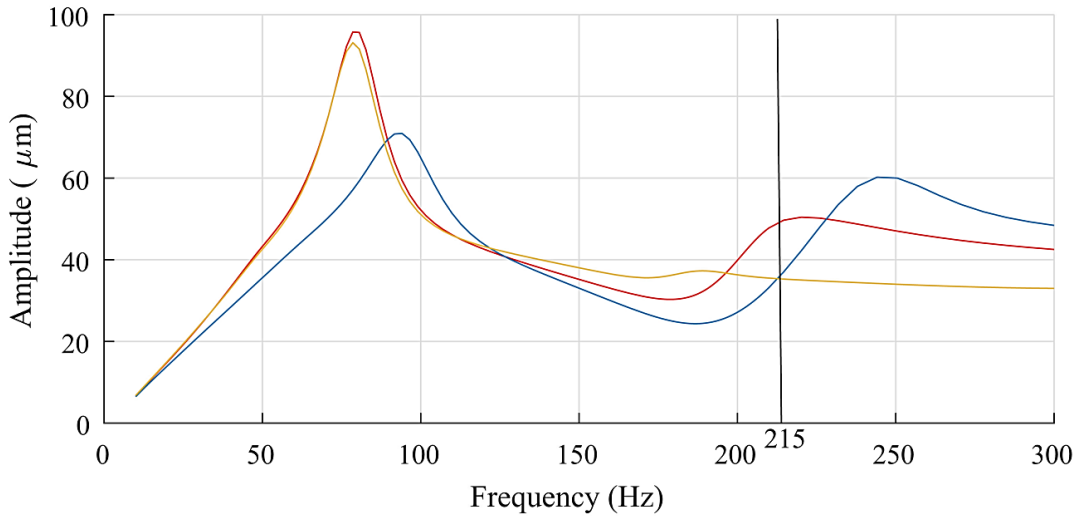

Figure 3.16 – FRF comparison between the initial response (blue) and the response in the more compliant foundation before (red) and after (yellow) the disc optimization adapted from Rother, Alencar and Machado (2018a)

3.9 Future works preview

In order to continue the studies in rotor optimization, a future work intend to propose a method to increase the operating stability margins of rotors supported on hydrodynamic bearings by increasing the shaft stiffness. The sensitivity of the system to changes in the elements is evaluated through the strain energy of the elements. Modification of the elements throughout iterations is accomplished through a bi-directional evolutionary method.

A simple case is used to demonstrate preliminary optimization results. The classic Jeffcott rotor is used, discretized with 16 nodes (Figure 3.16). The optimization runs at 18 iterations per second in a middle-end desktop, highlighting the low computational cost of the algorithm.

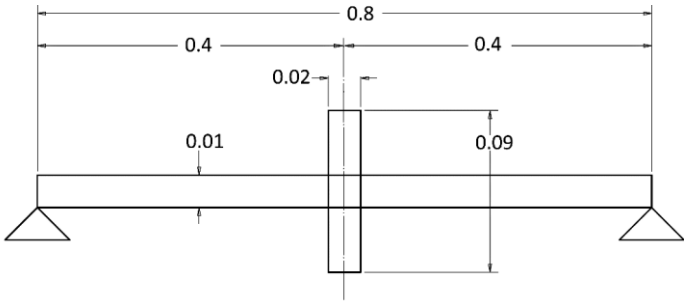

Figure 3.17 - Classical Jeffcott rotor used for the first case

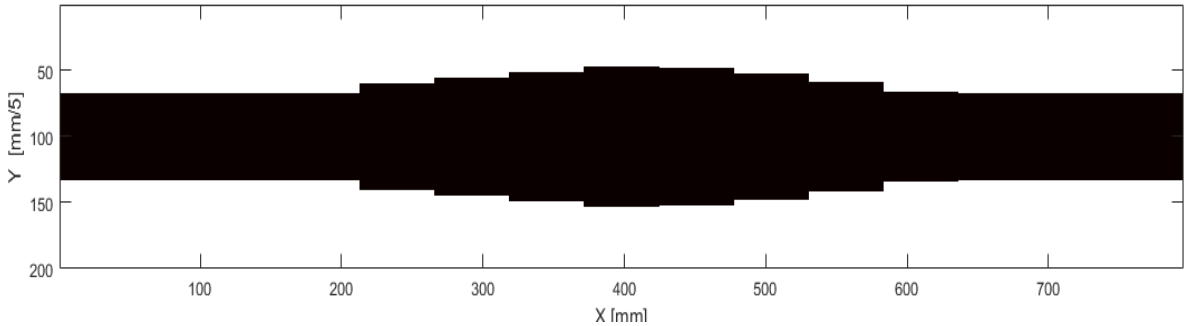

Figure 3.18 – Final shaft shape

The final shape of the shaft is shown in Figure 3.17. Response improvements can be seen by comparing initial and final Campbell diagrams (Figures 3.18 and 3.19) and damping ratios (Figures 3.20 and 3.21).

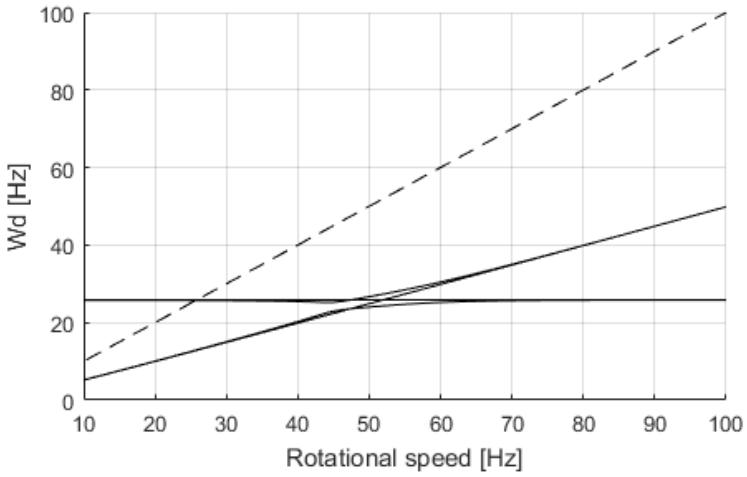

Figure 3.19 – Initial Campbell Diagram; eigenfrequencies (solid lines) and x=y (dashed line)

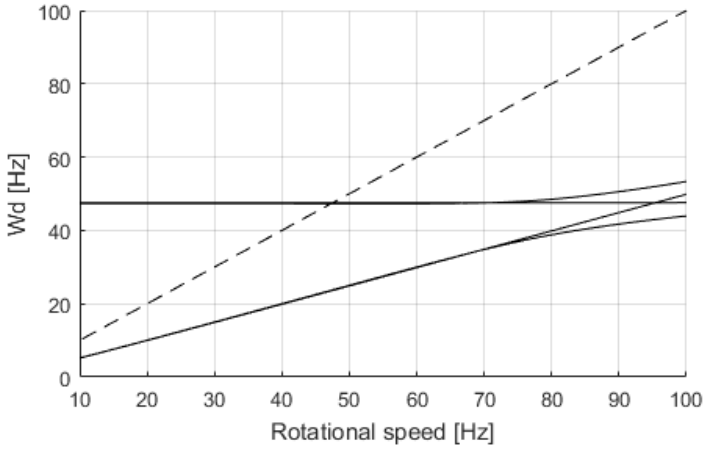

Figure 3.20 – Optimized shaft Campbell Diagram; eigenfrequencies (solid lines) and x=y (dashed line)

An important assessment of stability is the damping ratio. Whenever the damping ratio for a given mode of vibration is less than zero, instability is achieved and damping forces will increase system's energy instead of dissipating it. In Figure 3.20, negative damping will be achieved at 48 Hz. Operating near or above this speed will cause crescent vibrations until metal-to-metal rubbing occurs inside the bearings, damaging the rotor. After the optimization, this speed limit is raised to 70 Hz, as seen in Figure 3.21, providing an increase of 45% in maximum stable speed for the rotor.

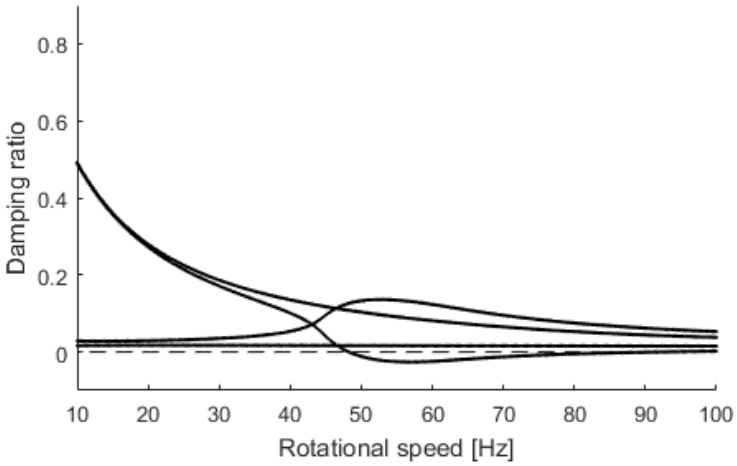

Figure 3.21 – Initial damping ratios; damping ratio for relevant modes (solid lines) and zero damping line (dashed line)

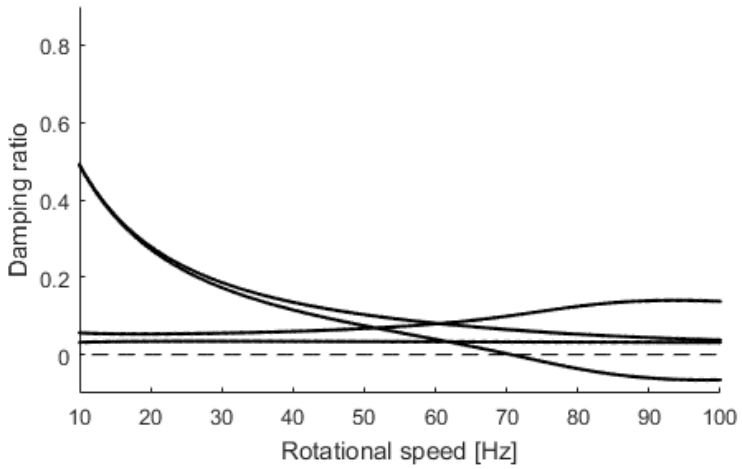

Figure 3.22 – Optimized shaft damping ratios; damping ratio for relevant modes (solid lines) and zero damping line (dashed line)

4 PAPER 1 – COMPARISON OF SHAFT MODELS IN ROTATING SYSTEMS

4.1 Introduction

To be valid, a computational simulation must present results correlating to empirical evidence and, for this, an adequate modeling is indispensable. MacNeal (1993), regarded modeling and discretization as the most important considerations in a finite element analysis.

Among the elements of a rotating machine, the shaft is one of the most significant. A good shaft model, containing the most significant effects of this component, is essential in a rotor simulation.

This chapter contains an adaptation of the paper overviewed in section 3.5. The objective is to quantify the differences between the two most used shaft models: Euler-Bernoulli and Timoshenko beam in steady-state response of a rotating system. A simple rotor geometry, like the one proposed by Jeffcott (1919), is used. Although simple, this rotor is prone to common phenomena in rotordynamics, as explained by Nelson (2007), hence, adequate for this study.

4.2 Methodology

For the foundations, rigid couplings were used between bearings and the inertial reference. The bearings modeled as rigid for translational movements and unconstrained for angular movements. In this way, the ends are supported in relation to the inertial frame. The disc is modeled as an equivalent concentrated inertia. Thus, the influence of the disc on the natural frequencies will occur only through its contribution in inertia and gyroscopic effect.

With this modeling, it is possible to minimize the interference of other components in system dynamic response, resulting in a better visualization of effects of the shaft and its modeling.

The two models of beam elements differ in the treatment of shear between planes. In Euler-Bernoulli model, the transverse planes are assumed to be perpendicular to the neutral axis, therefore, there is no shear between the planes. The Timoshenko model, however, contemplates the angle between the transverse planes and the neutral axis (Figure 4.1).

Since there is a difference between the two models in the shear considerations, it is expected that the greatest difference between the results obtained by each model is in situations where shear is of significant importance. This effect is expected in beams having a small ratio between length and diameter. For this shape of shaft, bending will be small due to the stiffness of the beam and shear effect will be pronounced due to the distance between the longitudinal planes.

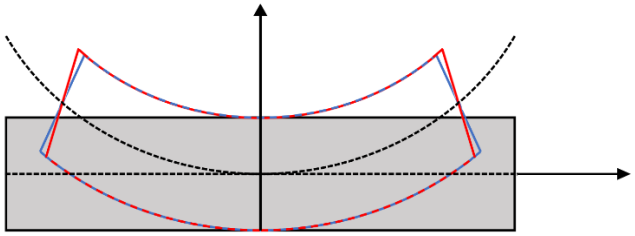

Figure 4.1 – Comparison between models; Euler-Bernoulli (blue), Timoshenko (red) compared to neutral axis (dashed)

To identify the length to diameter ratios that lead to differences between the two approaches, computational simulations were performed. Variations in the length and diameter ratio were tested both for the shaft as a whole and for each element, through variations in diameter and the number of nodes of the finite element model.

The mass matrix [M] is obtained through the geometric analysis of the components, as proposed by Nelson (1980) considering concentrated parameters where necessary. The damping matrix uses only the internal damping of the shaft, which can be represented by the Equation 4.1:

$$[C] = \alpha[M] + \beta[K] \tag{4.1}$$

As shown in Tuckmantel (2010), for steel shafts, a good estimate is that the alpha coefficient is zero and the beta coefficient should be adjusted according to the characteristics of the material and the system.

For the stiffness matrices, both beam models were used, so that they could be compared. The overall stiffness matrix [K] includes the bending stiffness matrix for each of the elements, superimposed according to the distribution of the nodes and elements. For the Timoshenko model, the stiffness matrix of each element (K_B) is given by:

$$[K_B] = \frac{E\,J_t}{l^3(1+12\phi)} \begin{bmatrix} 12 & 0 & 0 & 6l & -12 & 0 & 0 & 6l \\ 0 & 12 & -6l & 0 & 0 & -12 & -6l & 0 \\ 0 & -6l & 4l^2(1+3\phi) & 0 & 0 & 6l & 2l^2(1-6\phi) & 0 \\ 6l & 0 & 0 & 4l^2(1+3\phi) & -6l & 0 & 0 & 2l^2(1-6\phi) \\ -12 & 0 & 0 & -6l & 12 & 0 & 0 & -6l \\ 0 & -12 & 6l & 0 & 0 & 12 & 6l & 0 \\ 0 & -6l & 2l^2(1-6\phi) & 0 & 0 & 6l & 4l^2(1+3\phi) & 0 \\ 6l & 0 & 0 & 2l^2(1-6\phi) & -6l & 0 & 0 & 4l^2(1+3\phi) \end{bmatrix} \quad (4.2)$$

Where *E* is the Young's modulus of the material, *l* is the length of the element and J_t is the transverse moment of inertia.

The difference between the Euler-Bernoulli model is the absence of the shear coefficient Φ in the matrix presented in Equation 4.2. The analysis was therefore simplified using the same matrix and only rendering the coefficients of the shear terms null when the Euler-Bernoulli was used and calculating it for the model of Timoshenko according to Equation 4.3

$$\phi = \frac{(12\,E\,J_t\,\chi)}{G\,A\,l^2} \quad (4.3)$$

Where χ is the shear factor, *G* transversal elasticity modulus and *A* element transverse cross section.

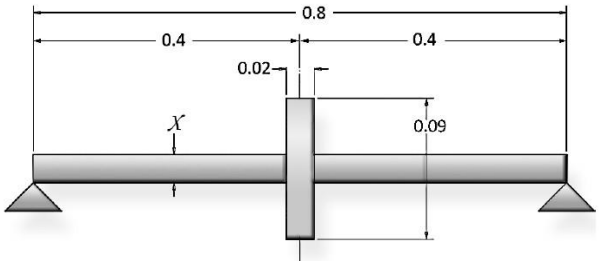

Figure 4.2 – Rotor model used in simulations

Shaft element matrices were assembled using the Timoshenko model, as presented in Equation 4.2 and when the Euler model was used, it was only necessary to nullify shear coefficient.

The rotor simulation was assembled with the remaining parameters and methods as described by Tuckmantel (2010). In the modal analysis, only the vibration modes below 400 Hz were considered for the first 4 cases. For the latter two cases, however, the higher stiffness of the spindle made it necessary to analyze higher frequencies so that it was possible to assess other modes of vibration.

Rotor dimensions can be seen in Figure 4.2. The base configuration, in which simulations 1 to 4 are performed, uses a shaft 800 mm long and 10 mm of diameter. This configuration is similar to the rotor test rig at LAMAR - UNICAMP, which allows future experimental verification of the data of these simulations. For simulations 5 and 6, the shaft diameter was changed to assess the effects of variations in shaft slenderness.

4.3 Results and discussion

Simulations were chosen to cover a range of usual ratio ratios between length and diameter. The number of nodes was kept low in most simulations so that the slenderness of elements was kept close to shaft slenderness. Case 4 is an exception and was chosen to investigate the effects of a large discretization and a very low L / D value for the element. Table 4.1 shows the characteristics of the 6 cases simulated in this study.

Table 4.1 – Simulated cases

Case	Shaft length (mm)	Shaft diameter (mm)	Elements	$\frac{L}{D_{shaft}}$	$\frac{L}{D_{elem}}$
1	800	10	2	80	40
2	800	10	4	80	20
3	800	10	8	80	10
4	800	10	80	80	1
5	800	20	4	40	10
6	800	40	2	20	10

Simulations were started by 800mm length and 10mm shaft diameter. Case 1 presents the smallest discretization possible for the algorithm used: 3 nodes, which allows the placement of the contour conditions at the ends and the effects of the disc in the center. Figure 4.3 shows the amplitude and phase of the FRF obtained using each of the different axis.

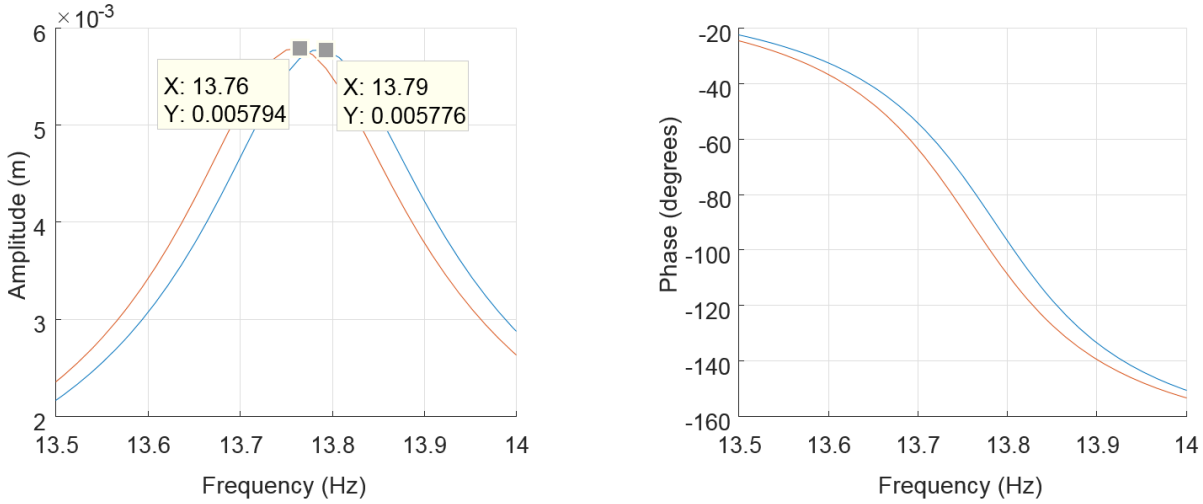

Figure 4.3 – FRF and phase, magnified around response peak for Euler-Bernoulli (blue) and Timoshenko (red) - Case 1

Analyzing Figure 4.3, it is noticeable that the differences between the results obtained with each of the models is small. Both the peak amplitude values and the critical speeds values are very close. For the phase graph, the behavior is also similar.

Figure 4.4 shows the comparison of the Campbell diagram of the system for each of the models used. By analyzing these Campbell diagrams one can confirm the frequencies already observed in the graphs of Figure 4.3 for the first mode, as well as

to note that for the third mode there is a greater difference between results obtained with each of the models.

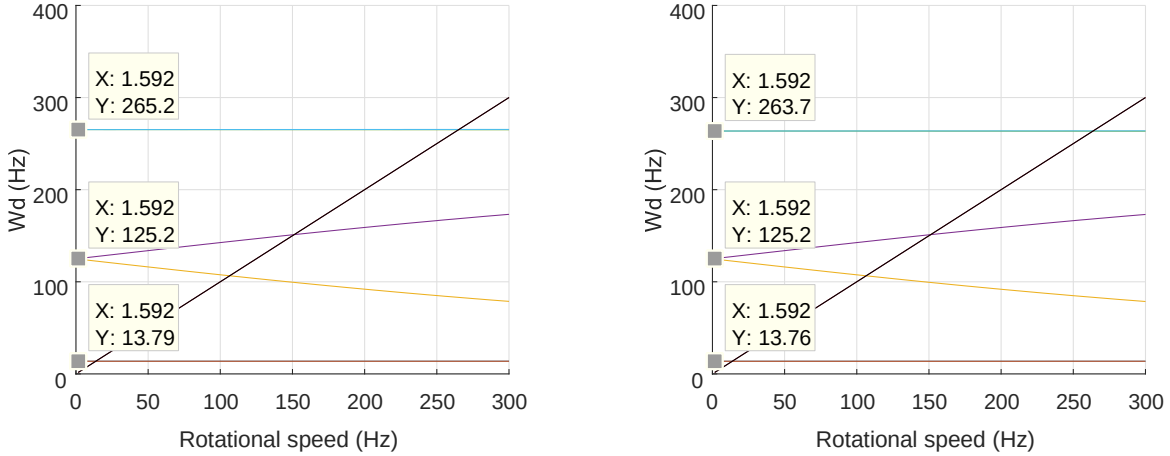

Figure 4.4 – Campbell diagram for both models: Euler-Bernoulli (left) and Timoshenko (right) - Case 1

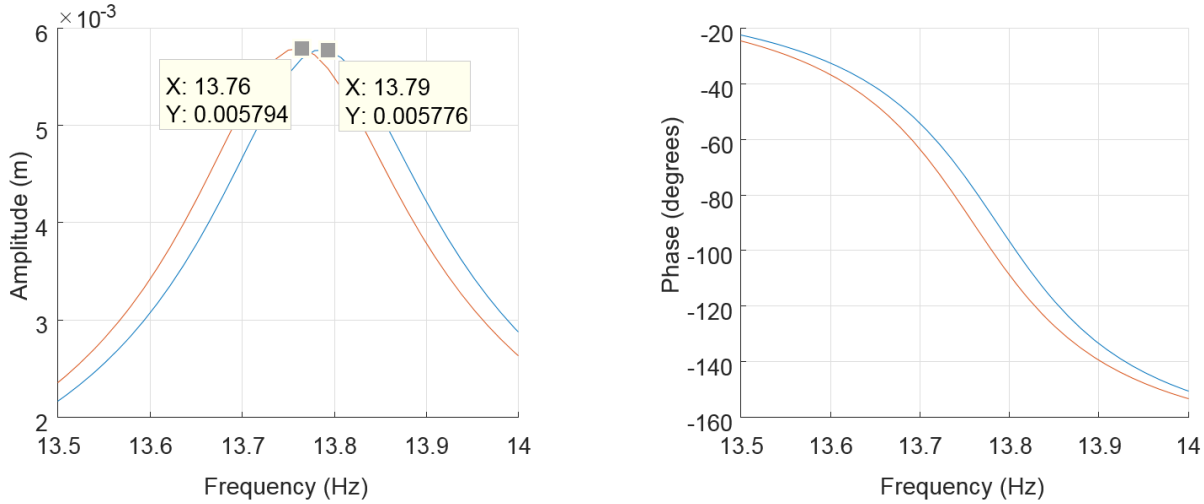

Figure 4.5 – FRF and phase, magnified around response peak for Euler-Bernoulli (blue) and Timoshenko (red) - Case 2

For case 2, the discretization was increased to 5 nodes, that is, 4 elements. Two different comparisons can be made for this case: between the models and between the results obtained for case 1 and 2. The frequency response is indistinguishable between case 1 and 2. Regarding the Campbell diagram, there is slightly more difference between the models for the second and third modes. This shows that in higher modes there is greater influence of discretization of the system. Figures 4.5 and 4.6 show the results of the FRF of the Campbell diagram, respectively, for case 2 presented in Table 4.1.

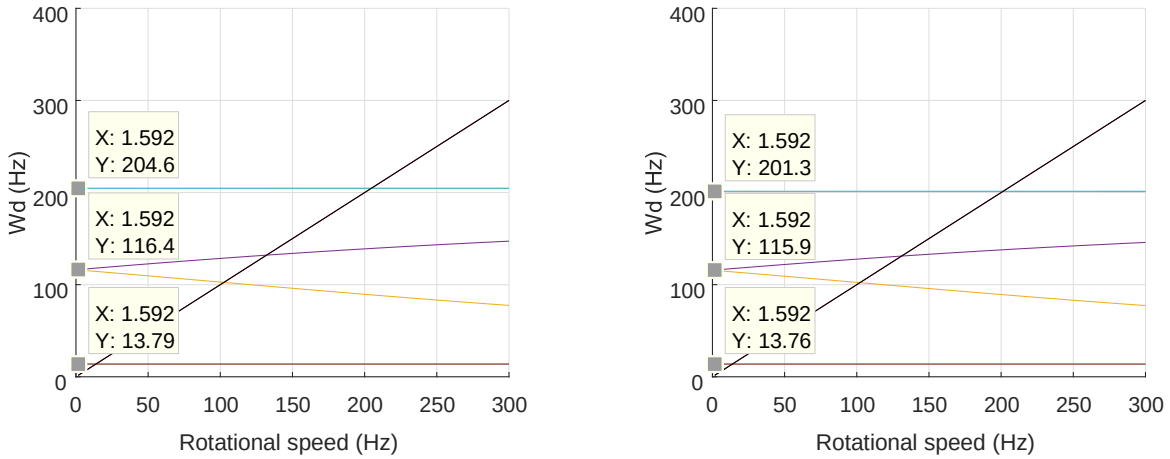

Figure 4.6 – Campbell diagram for both models: Euler-Bernoulli (left) and Timoshenko (right) - Case 2

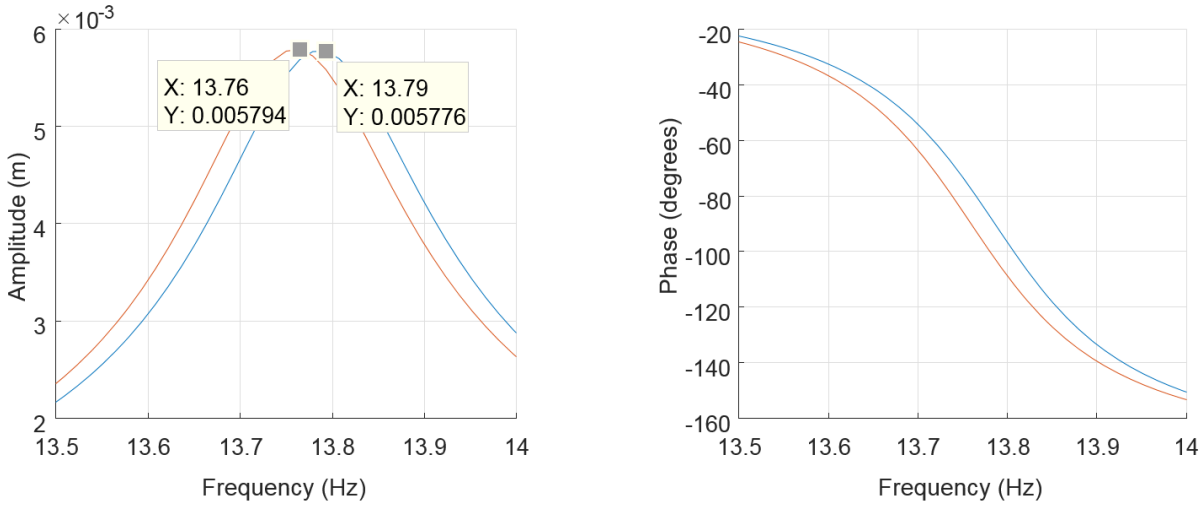

Figure 4.7 – FRF and phase, magnified around response peak for Euler-Bernoulli (blue) and Timoshenko (red) - Case 3

The following Figures 4.7 and 4.8 show the results for the third case. In this case 3, the trend already observed is repeated and the FRF is indistinguishable from the first ones. The difference between this case's Campbell diagram and the previous one is much smaller than between the first and the second, indicating that for the modes being analyzed the increase from 5 to 9 nodes had a much smaller impact than 3 to 5.

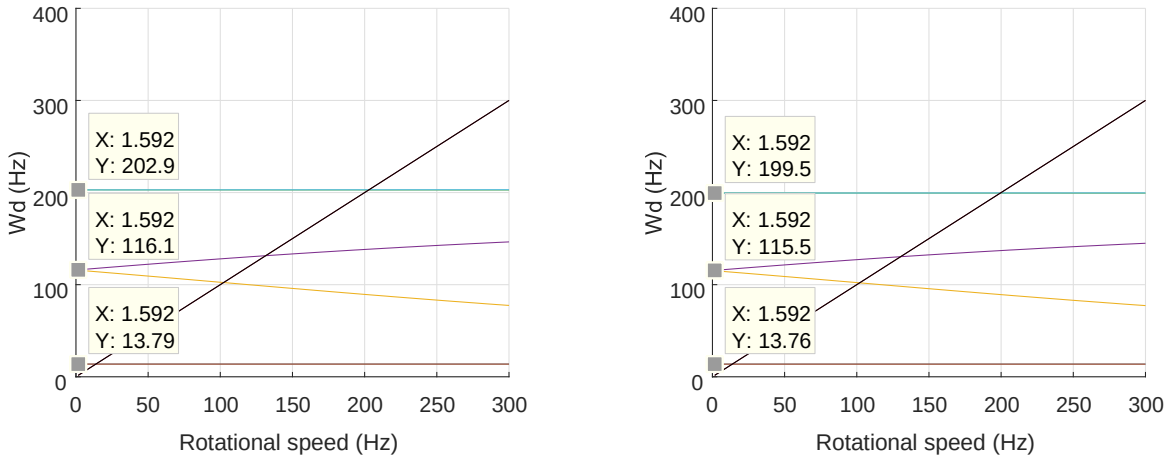

Figure 4.8 – Campbell diagram for both models: Euler-Bernoulli (left) and Timoshenko (right) - Case 3

The last simulation performed with the 10 mm diameter shaft was done with a discretization of 81 nodes to obtain 80 elements. With this discretization L/D = 1 is obtained for the element. The goal is assessing differences between the models for this level of discretization. The results for this simulation are shown in Figures 4.9 and 4.10. It can be noted that the differences are the same observed in previous simulations, indicating that this level of discretization does not bring differences when comparing the two models of shaft analyzed in this work.

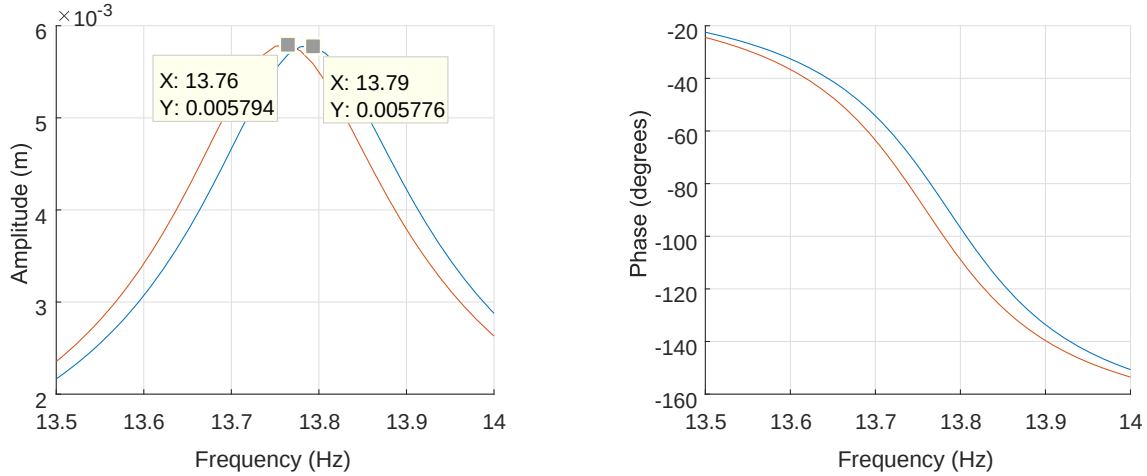

Figure 4.9 – FRF and phase, magnified around response peak for Euler-Bernoulli (blue) and Timoshenko (red) - Case 4

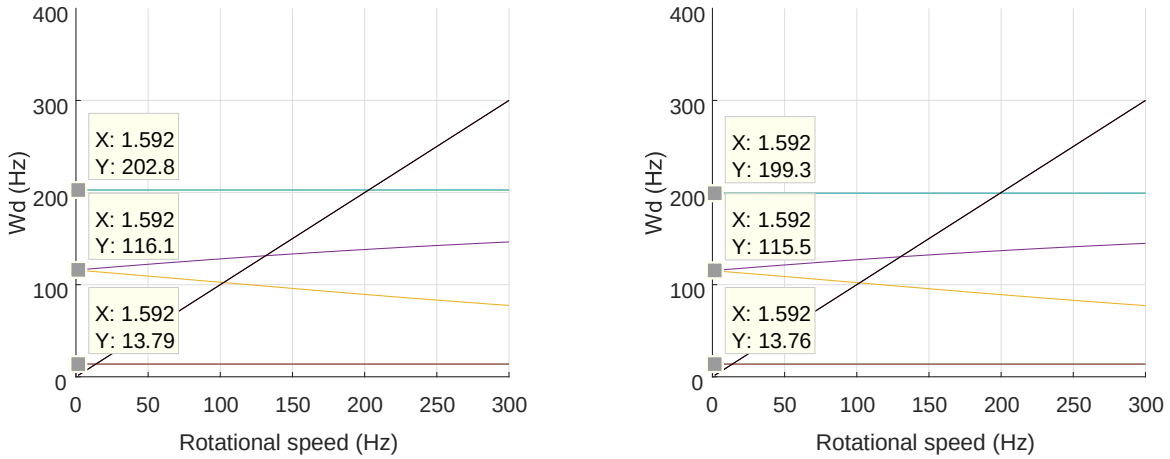

Figure 4.10 – Campbell diagram for Euler-Bernoulli (left) and Timoshenko (right) - Case 4

After the simulations were carried out with variations in the discretization, which maintained shaft proportion and varied the proportion of the element, simulations with varying proportions of shaft were run. The results of the first simulation of this new test block, case 5, are presented in Figures 4.11 and 4.12. Although the difference between the models is still small, it can be noted that it is larger than that presented in previous simulations.

Figure 4.11 shows that the variation in the first critical speed is somewhat greater than the variations observed in the previous cases. In Figure 4.12, there is an increase in the difference of the frequencies of the second and third modes. It is worth mentioning that, for this case, the simulated frequency range for obtaining the Campbell diagram had to be changed. Frequency was swept between 0 to 600 Hz, since the stiffer shaft presented higher critical speeds.

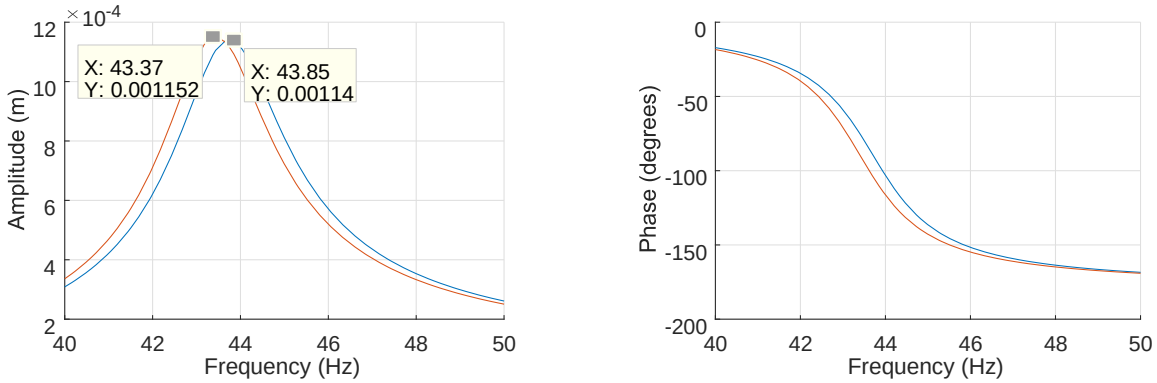

Figure 4.11 – FRF and phase, magnified around response peak for Euler-Bernoulli (blue) and Timoshenko (red) - Case 5

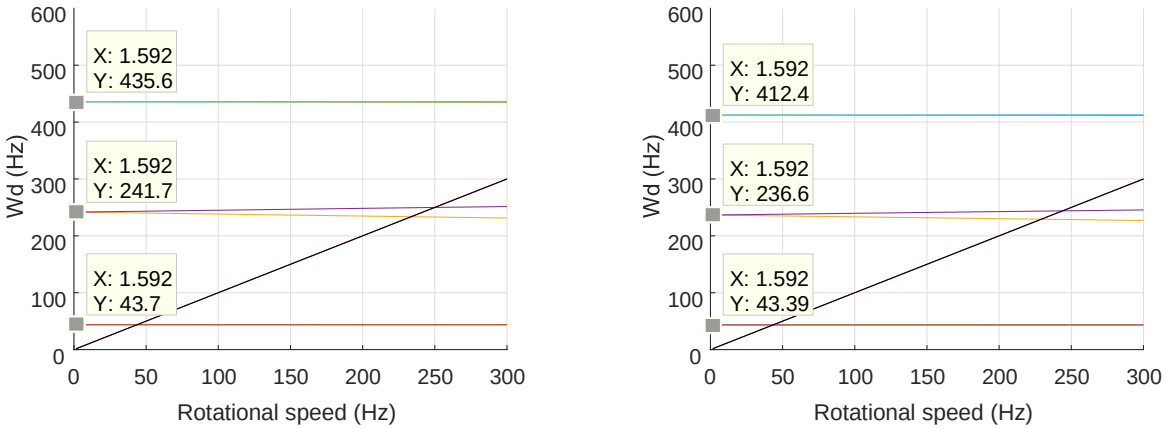

Figure 4.12– Campbell diagram for Euler-Bernoulli (left) and Timoshenko (right) - Case 5

Finally, the results in Figures 4.13 and 4.14, referring to case 6. A further decrease in shaft slenderness makes the difference between models evident. For this simulation the effects are more pronounced and it is not necessary to enlarge the FRF charts, as done in all previous cases, so that the differences can be perceived.

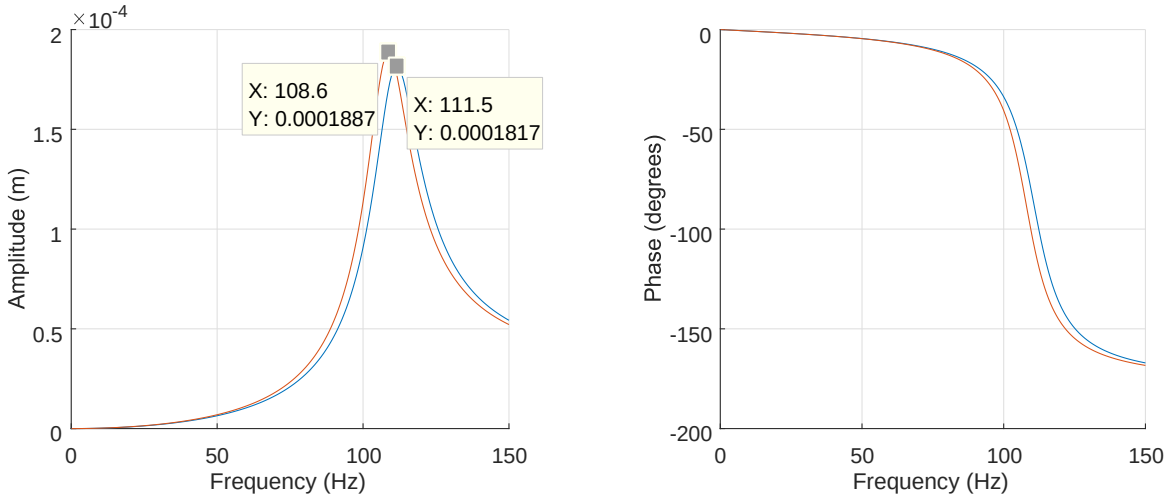

Figure 4.13: FRF and phase, magnified around response peak for Euler-Bernoulli (blue) and Timoshenko (red) - Case 6

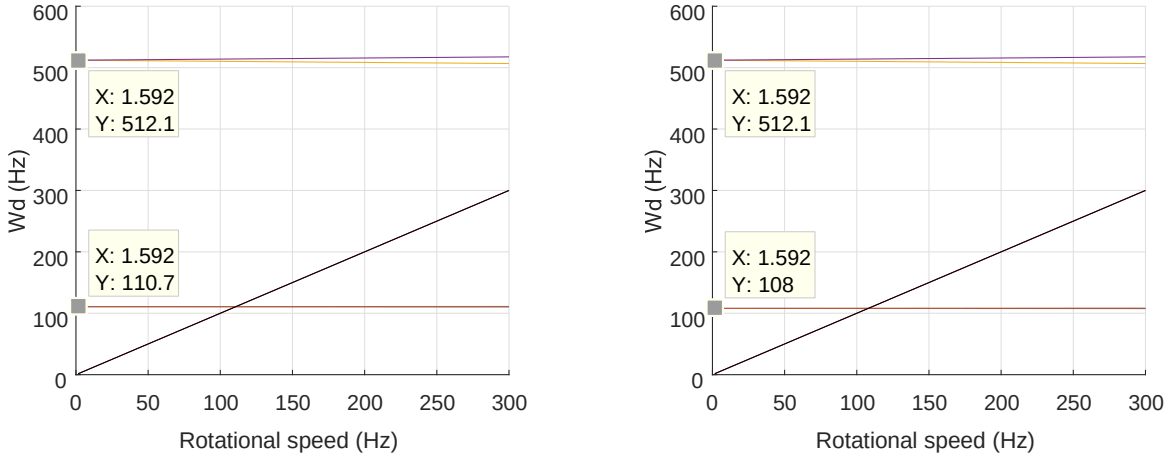

Figure 4.14 – Campbell diagram for Euler-Bernoulli (left) and Timoshenko (right) - Case 6

Summarizing some of the results found, Table 4.2 presents first critical speed variation in each of the six simulated cases, comparing the two shaft models analyzed in the study.

Table 4.2: Results summary for the first natural frequency

Case	$\frac{L}{D_{shaft}}$	$\frac{L}{D_{elem}}$	ω_{n1} Timoshenko [Hz]	ω_{n1} Euler-Bernoulli [Hz]	$100\% - \frac{\omega_{n1T}}{\omega_{n1E}}$
1	80	40	13.76	13.79	0.22%
2	80	20	13.76	13.79	0.22%
3	80	10	13.76	13.79	0.22%
4	80	1	1376	13.79	0.22%
5	40	10	43.39	43.70	0.71%
6	20	10	108.6	110.70	1.90%

4.4 Conclusion

Two classic models were tested, Euler-Bernoulli and Timoshenko. The influence of this modeling was analyzed in the frequency response (FRF) function and the Campbell diagram of the system. Analyzing the data in Table 4.2, it can be seen that the determinant factor in the difference between the models is shaft slenderness. Even the large change in L / D ratio of the element between Case 1 and Case 4 was not sufficient to modify the results between the models, while changes in the shaft proportions caused perceptible changes. In addition to the factors that affect the difference between the models, it was also possible to evaluate the influence of discretization on the response of the simulations. For the analyzes performed there are no noticeable gains in the increase of the discretization above 9 nodes. If only the first mode is relevant, even the use of only 3 nodes generates appropriate results for a simple rotor.

4.5 Acknowledgments

The author thanks CAPES, CNPq and grant # 2017/07454-8 from the São Paulo Research Foundation (FAPESP) for the financial support to this research and ABCM for licensing the use of the paper in this dissertation.

5 PAPER 2 – ANALYSIS OF THE BEARINGS' INFLUENCE ON THE DYNAMIC BEHAVIOR OF A ROTATING MACHINE

5.1 Introduction

Dynamic analysis of rotating machines involves many parameters and therefore must consider the interaction between components, such as bearings. Consequently, a critical issue in rotor dynamics is the modeling of the bearings, which directly affects the dynamic behavior and stability of the rotating system.

In order to obtain the characteristics of a rotating system, there are several approaches. Among these, is noteworthy the finite element method, since it presents relative ease of implementation and has good scalability, allowing increase of algorithms' complexity according to the need of precision.

In this context, this chapter is an adaptation of the paper presenting an analysis of the effect of the characteristics of the bearings on the dynamic behavior of rotors, being the computational part developed through the finite element method in an algorithm implemented in MATLAB®.

5.2 Methodology

Modeling a rotating system involves the analysis of its components such as shafts, bearings, discs, foundation, and their interaction with each other. The numeric analysis of the rotor model, in this work, uses the finite element method (FEM). Therefore, each component, and its respective dynamic response, must be discretized considering the interaction with the adjacent nodes.

Finite Element Method

Analytical solutions for complex equations are computationally costly and often not even possible with currently available algorithms. The impossibility of solving a system through mathematical manipulation may require a simplification of the model to make an analytical solution possible. However, simplification will lead to loss of accuracy. Since the accuracy of the answer constitutes a great advantage of the analytical method, the simplification of a problem to solve it analytically is contradictory. Thus, the most feasible way to perform the analysis of systems with several coupled equations is through numerical methods.

In order to solve engineering problems, several discretization methods can be used, such as the Finite Element Method, Finite Differences Method, Finite Volume Method, among many others. In the analysis of rotors, the most used method is the finite element method (FEM). Due to its dissemination in this area, this method was chosen to be used in this work.

The main assumption of the method is dividing the continuum into a finite number of elements, which can be characterized by a finite number of parameters. The solution of the complete system as a set formed by its elements follows the same impositions applied to general discretized problems.

The model used in the simulations of this work consists of a rotating system with typical elements such as discs, shaft elements and bearings, as shown in Figure 5.1, along with the coordinate systems used to describe the movement of the system (local and Inertial).

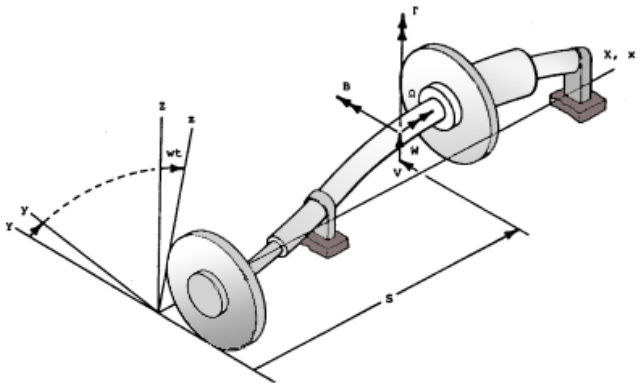

Figure 5.1 – Typical rotor configuration, Adapted from Nelson and McVaugh (1976)

The equation of motion of the complete system, according to Krämer (1993), is:

$$[M]\{\ddot{q}(t)\}+[C]\{\dot{q}(t)\}+[K]\{q(t)\}=\{F(t)\} \quad (5.1)$$

Where [M], [C] and [K] are the global mass, damping and stiffness matrices, respectively; {F (t)} is the excitation vector and {q (t)} is the displacement vector relative to the inertial coordinate system.

The complete rotor model includes the modeling of the rotor shaft, the bearings that connect it to the foundation structure and the foundation itself. For this work, the foundation is considered rigid; the shaft is modeled by Timoshenko's beam and disc elements, as presented in Nelson and McVaugh (1976); and the bearings is modeled in two ways: either simulating a bi-clamped shaft and a shaft supported by hydrodynamic bearings.

Thus, it is possible to obtain the global equations of the system with each modeled component. The matrices of each element are grouped in a global matrix and their positions in the global matrices are related to degrees of freedom, as shown in Figure 5.2.

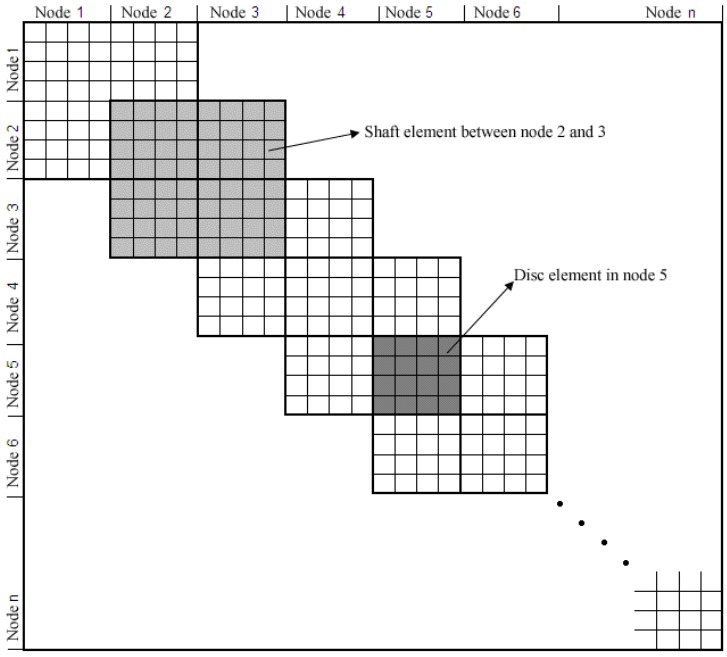

Figure 5.2 – Elements' matrices superposition (MACHADO, 2014)

Bearings Modeling

The bearing is responsible for restricting the displacement of the shaft in certain directions, as well as reducing friction in the directions in which the movement is free.

Among the various types of bearings, the most used are: ball bearings, magnetic, dry friction and hydrodynamic. Since hydrodynamic bearings is widely used in rotating machinery, this work is concentrated in type of bearing.

For the purposes of comparison with the hydrodynamic bearing, and due to the simplicity offered by the model, the idealized bi-clamped bearing is also used in the simulations. It offers infinite stiffness in all directions, allowing only the rotation in the axis parallel to the rotor.

For the hydrodynamic bearing, its behavior is obtained through the Reynolds equation. Since this complete equation does not present an analytical solution, and even the complete numerical solution presents high computational cost, the use of simplifying hypothesis is necessary to make a solution feasible, albeit it lowers the precision of the results (DANIEL; MACHADO; CAVALCA, 2016).

Equivalent springs and dampers characterize the hydrodynamic bearings. Their equivalent coefficients of stiffness and damping can be inserted directly into the appropriate elements (nodes) of the respective matrices for both the time domain and the frequency domain analyzes. This approximation is equivalent to a model of shaft supported on springs and dampers, as shown in Figure 5.3. For this work, the expressions for the coefficients of stiffness and damping are those given in Krämer (1993).

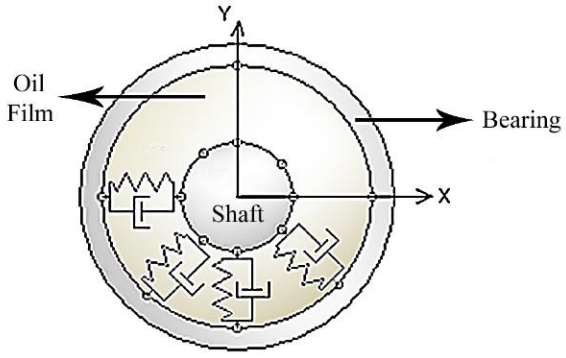

Figure 5.3 – Hydrodynamic bearing, with oil film modeled as springs and dampers, adapted from Machado and Cavalca (2009)

Computational Algorithm

The computational algorithm was written in the form of a main program divided into blocks and auxiliary functions. The use of blocks is encouraged by the recognition of blocks by MATLAB® as parts of the code that can be executed one-*by*-one easily. In addition, independent block construction favors parallel processing of the blocks, taking advantage of the increasingly common processing parallelism. The general functioning of the algorithm is shown in the diagram of Figure 5.4. The block of inputs and initial calculations is the least complex and runs in a very short time. The block of matrix assembly presents the most complex calculations of the code, but since they are performed only once, they take only a fraction of a second. The following blocks are already independent and can be executed in parallel.

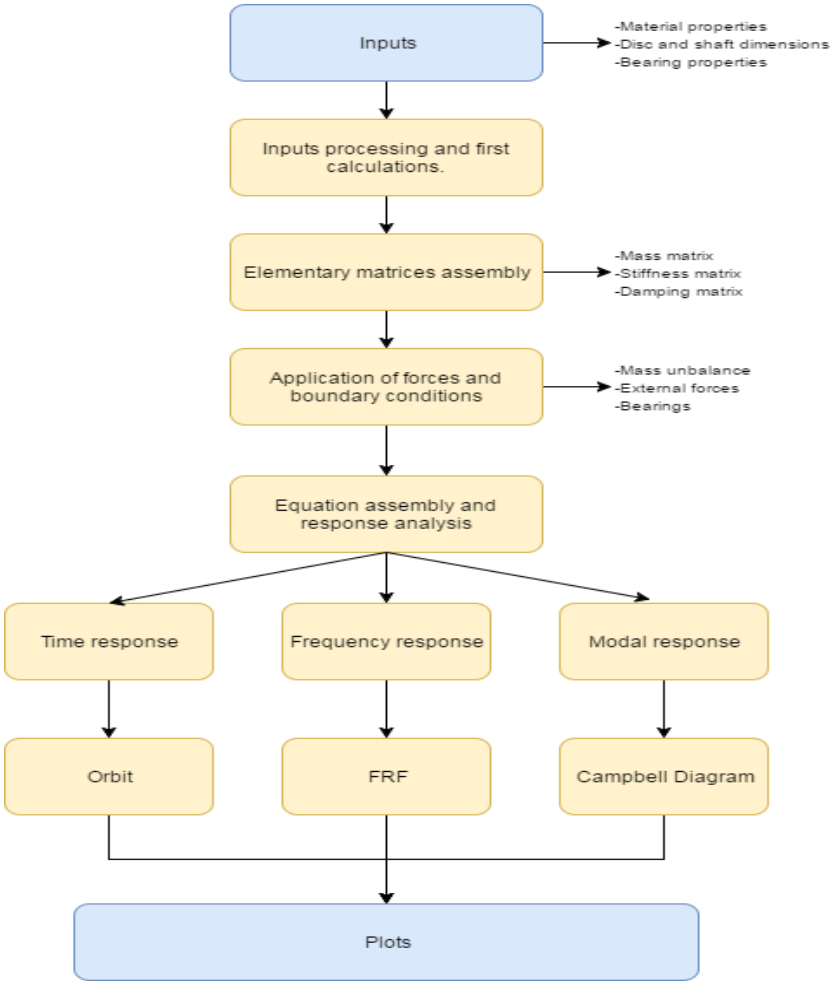

Figure 5.4 – Algorithm's workflow chart

5.3 Results and discussion

For the simulations, a model with the dimensions similar to the real rotor present in the Laboratory of Rotary Machinery (LAMAR-FEM-UNICAMP) was used, in order to provide an experimental verification of the results in the future. The dimensions of the real rotor are similar to those of Figure 5.5, while the model of Figure 5.6 is used to simulate the condition with the decentralized disc.

For each of the cases will be presented and analyzed results in time domain - disc node orbits; in frequency domain - disc node FRF due to mass eccentricity and in modal domain – Campbell's diagram. For the time domain analysis, two frequencies will be shown: one before and the other after the crossing of the forward whirling line in Campbell's diagram. This way it is possible to visualize the change in whirling direction.

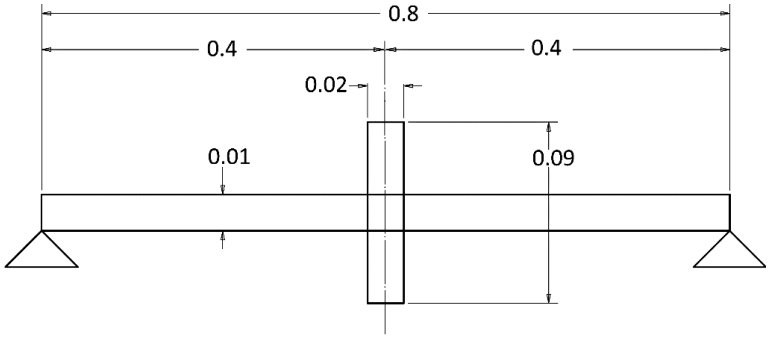

Figure 5.5 – Centralized disc rotor (dimensions in meters, out of scale for best visualization)

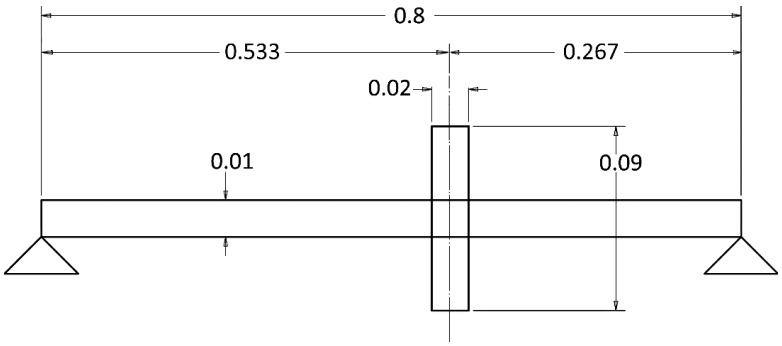

Figure 5.6 – Decentralized disc rotor (dimensions in meters, out of scale for best visualization)

Bi-Clamped Rotor

Centralized Disc

Analysis starts with the centralized disc bi-clamped rotor. It can be seen in Figure 7 that the first three modes of vibration - corresponding to the first three natural frequencies of the system – can be seen in the Campbell diagram. There is only distinction in forward and backward whirl frequencies in the second natural frequency. This behavior is due to disc in the center of the shaft. Therefore, for the odd modes, the movement is restricted to translation in a plane perpendicular to the z-axis and there is no influence of the gyroscopic effect. In the even modes, there is an inverse behavior - there is no translation movement, only rotation in an axis perpendicular to the z-axis, which explains the absence of the peak of the second natural frequency in the FRF and the frequencies of whirling are distinguishable for forward and backward whirl. In Figure 8 is visible the change of whirling direction as the rotor frequency crosses the forward whirl frequency of the second mode.

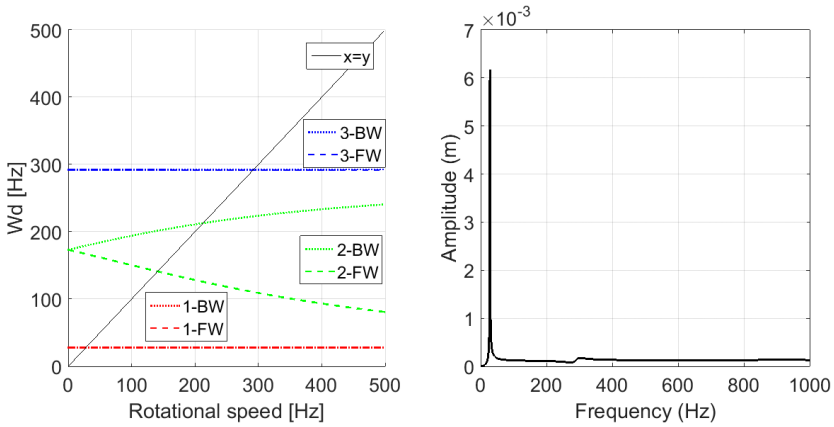

Figure 5.7 – Campbell diagram (left) and FRF (right) for centralized disc clamped rotor

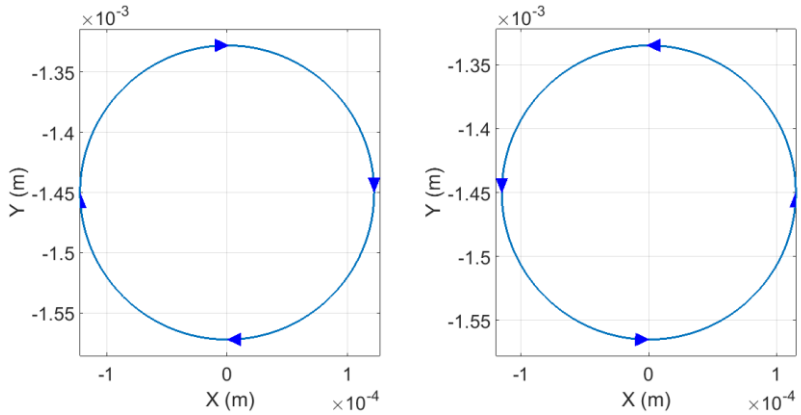

Figure 5.8 – Rotor orbits for 110 Hz (left) and 160 Hz (right)

Decentralized Disc

Differing from the centralized disc rotor, where the forward and backward whirling frequencies are the same for the odd modes, the decentralized rotor, because of its geometry, exhibits distinguishable whirling frequencies for both odd and even modes of vibration. In spite of this separation cannot be seen in the first natural frequency, because of the algorithm's low frequency resolution, starting from the third natural frequency its effect is clear. Because for the decentralized rotor forward and backward whirling frequencies are distinguishable, Figure 5.10 shows the reversion of whirling direction as the system crosses the third mode forward whirling frequency.

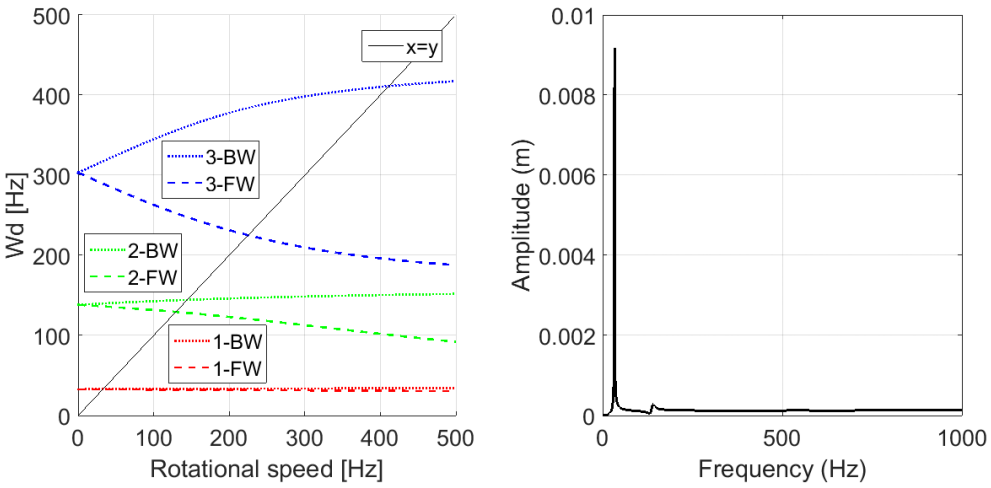

Figure 5.9 – Campbell diagram (left) and FRF (right) for decentralized disc clamped rotor

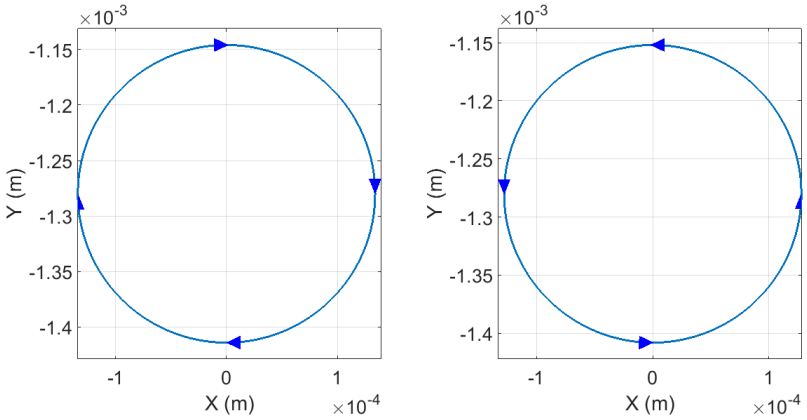

Figure 5.10 – Rotor orbits for 200 Hz (left) and 240 Hz (right)

Rotor with Hydrodynamic Bearings

Centralized Disc

Through analysis of the results shown in Figure 11, adding hydrodynamic bearings to the model lowered the natural frequency, as expected, since the oil film reduces the overall stiffness of the system without changing its mass, resulting in a lower natural frequency.

Besides the reduction in the natural frequency, is noteworthy the reduction in the peak amplitude to less than a half of the peak encountered in the clamped rotor for the centralized configuration. There is now a peak in response related to the second mode of vibration that was negligible in the clamped rotor configuration, but can affect the behavior of the rotor supported by hydrodynamic bearings. Comparing Figure 12 with Figure 8 it can be noticed that orbits' dimensions were reduced due to part of vibration energy being dissipated on the bearings.

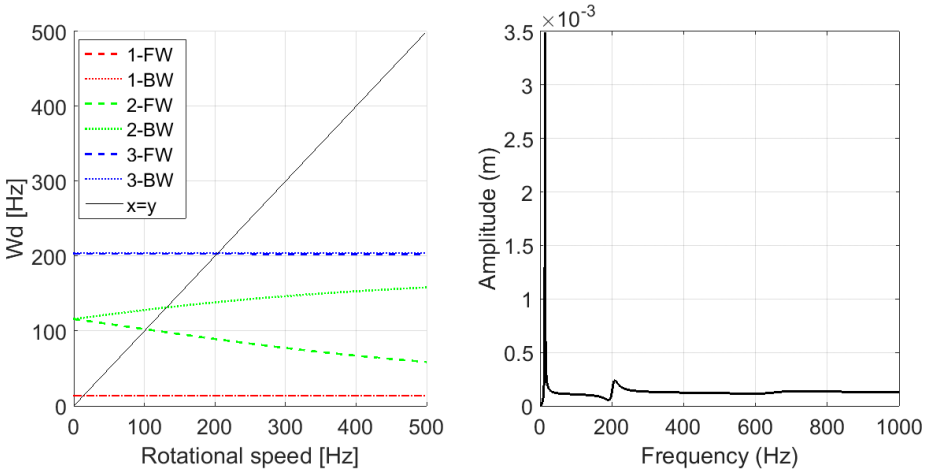

Figure 5.11 – Campbell diagram (left) and FRF (right) for centralized disc rotor supported on hydrodynamic bearings

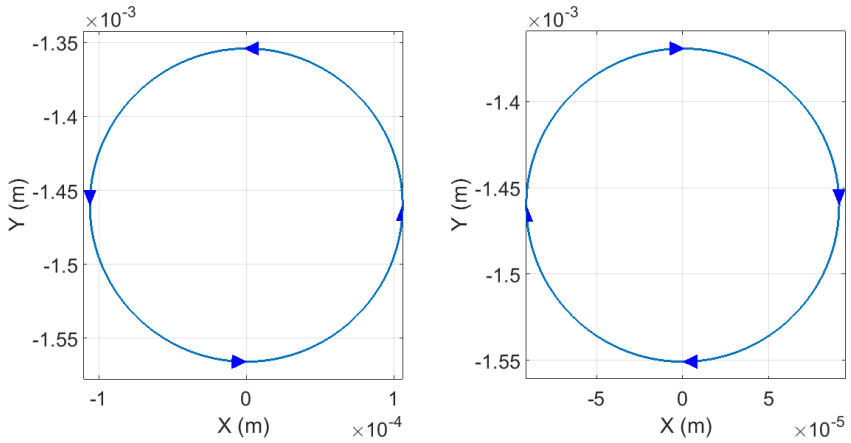

Figure 5.12 – Rotor orbits for 110 Hz (left) and 160 Hz (right)

Decentralized Disc

The decentralized disc showed a similar behavior to the centralized disc when hydrodynamic bearing was added to the model. The peak of amplitude in the first mode, shown in Figure 13, was reduced to half, compared to the peak in Figure 9. However, unlike was observed in the centralized disc rotor, the higher modes of vibration have no increase in vibration amplitudes. It is noteworthy the reduced split between the forward and backward whirling frequency for the third mode of vibration compared to the bi-clamped rotor. Because of this, the orbits on Figure 14 could not be obtained in the same frequencies of the Figure 10 and still show the reversion of whirling direction.

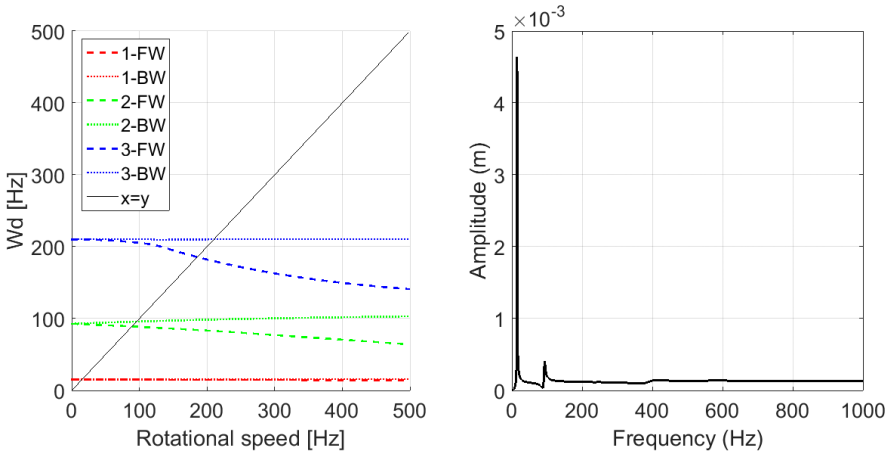

Figure 5.13 – Campbell diagram (left) and FRF (right) for decentralized disc rotor supported on hydrodynamic bearings

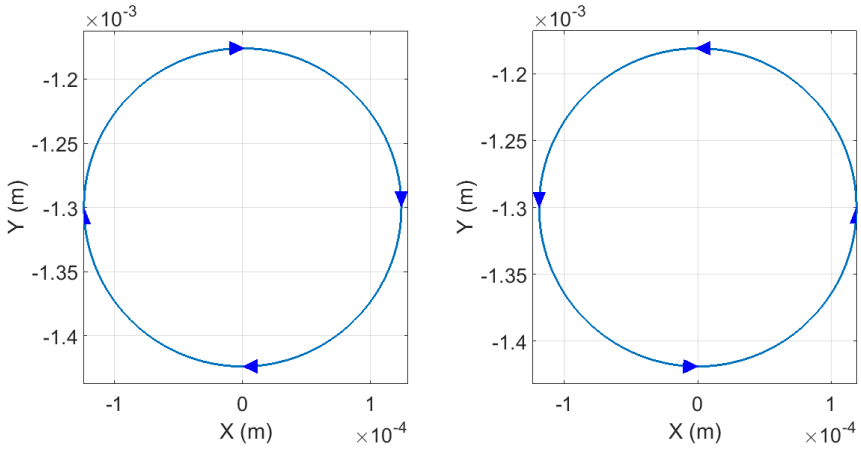

Figure 5.14 – Rotor orbits for 160 Hz (left) and 200 Hz (right)

5.4 Conclusion

For the analyzed rotor configurations, the replacement of the rigid bearing (bi-clamped rotor) by the hydrodynamic bearing presented an effect of reduction in the natural frequencies, since it reduced the stiffness of the system without any change of mass. The main change occurred in the first natural frequency, which was reduced to approximately half with the addition of hydrodynamic bearings. It is notable that the presence of hydrodynamic bearings causes a reduction in maximum amplitude of the FRF peaks while widening them. In the Campbell diagrams, besides of the reduction in natural frequencies, the rotors with hydrodynamic bearings displayed less spread between the whirl frequencies of the same mode. This behavior can be explained by the decrease of vibration of the rotor with the inclusion of the hydrodynamic bearings. As the bearings dissipate part of this vibration, the rotor, in particular in the disc position, has a lower vibration, and consequently, there is a decrease in the gyroscopic effect, causing the backward and forward frequencies to be less dispersed.

With what was presented, it can be inferred that there is a great influence of the bearings in the total damping of the system, showing the considerable effect of bearing modeling on the dynamic behavior of the rotor and justifying the need for a careful analysis of this component of the rotating system.

5.5 Acknowledgments

The author thanks CAPES, CNPq and grant # 2017/07454-8 from the São Paulo Research Foundation (FAPESP) for the financial support to this research and ABCM for licensing the use of the paper in this dissertation.

6 PAPER 3 – INFLUENCE OF FOUNDATIONS IN ROTATING SYSTEMS' RESPONSE

6.1 Introduction

The relationship between the bearings and the rotor presented in the previous chapter was studied by several authors and among recent works published in this area can be mentioned Zhao, Dai and Zhu (2005); Yang, Kim and Lee (2006); Machado, Cavalca and Arima (2010); Alves, Daniel and Cavalca (2015). The inclusion of the phenomenology caused by the foundation as described in this chapter intends to make the model more robust. The use of an improved model allows identifying natural frequencies from the foundation and influence structure parameters in these frequencies and on the overall behavior of the equipment in the operating range.

Ways to include the effects of the foundation in the system response, as well as to evaluate the impact of the foundation on the dynamic rotor behavior were analyzed by many authors, among which we can mention Stephenson and Rouch (1992), Feng and Hahn (1995), Kang et al (2000) and Cavalca, Cavalcante and Okabe (2005), improving the quality of rotor simulations. In this context, the paper adapted in this chapter presents an analysis of foundation modelling in rotative machinery and its effects in dynamic response.

6.2 Methodology

This section presents the models used for the calculations: shaft, disc, bearing and foundation models. For foundation modeling, more than one model was used to evaluate the influence of different models on system response.

Shaft Model

The shaft is modeled with four degrees of freedom per node, with two translation coordinates and two rotation coordinates, as shown in Figure 6.1, where W and V are the translations and B and Γ are the rotations. For this work, a cylindrical shaft was chosen in order to also obtain cylindrical elements. Nelson (1980), presents an equation for the motion of a rotating shaft element that has been modified in this work to include proportional structural damping, as shown in Equation 6.1.

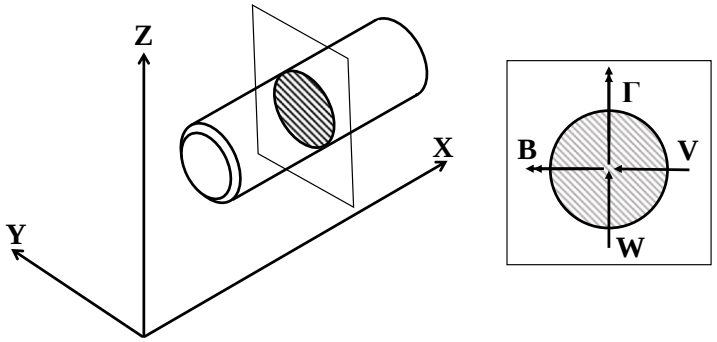

Figure 6.1 – Coordinates of degrees of freedom at each node of shaft

$$[M]\{\ddot{q}\} + ([C] - \Omega[G])\{\dot{q}\} + [K]\{q\} = \{F\}$$
$$\{q\}T = \{V_i, W_i, B_i, \Gamma_i, V_j, W_j, B_j, \Gamma_j\} \quad (6.1)$$

Each element is formed by two adjacent nodes and therefore has eight degrees of freedom. Shaft elements have mass, stiffness, damping and gyroscopic matrices that are calculated from the geometric and physical properties of the elements (NELSON, 1980).

Figure 6.2 shows the assembly of the global matrix for the shaft, the elements in dark gray represent elements obtained from the superposition of matrices, that is, the sum of matrices of different elements. For a discretization of 5 nodes, for example, the elements are represented by an 8x8 matrix and the global matrix is a 20x20 matrix.

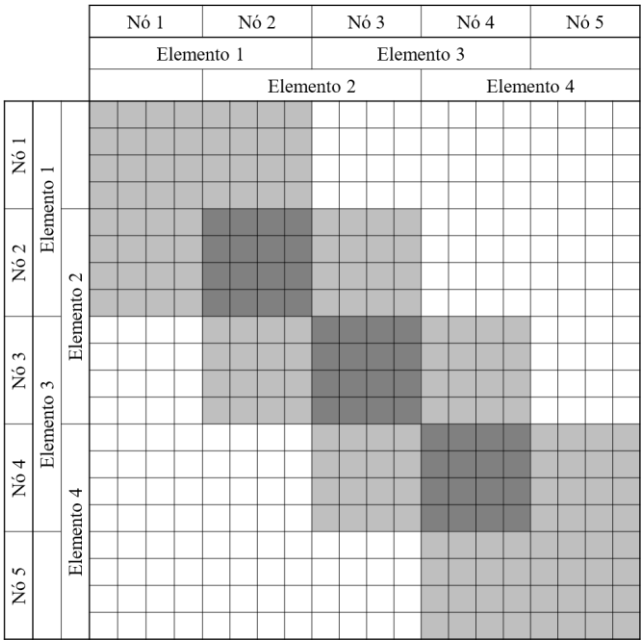

Figure 6.2 – Finite element global matrices assembly scheme

Disc model

The disc is modeled with a center of mass coincident with rotor elastic line. It has the same degrees of freedom of shaft nodes, however, this type of element does not present flexibility. The disc element matrices are shown in Equation 6.2.

$$I_{disc} = \begin{bmatrix} m & 0 & 0 & 0 \\ 0 & m & 0 & 0 \\ 0 & 0 & J_t & 0 \\ 0 & 0 & 0 & J_t \end{bmatrix}, G_{disc} = \begin{bmatrix} 0 & 0 & 0 & 0 \\ 0 & 0 & 0 & 0 \\ 0 & 0 & 0 & -J_p \\ 0 & 0 & J_p & 0 \end{bmatrix} \quad (6.2)$$

Where m is disc's mass, J_t is disc's transversal inertia moment and J_p the polar inertia moment

Bearing model

The bearing is responsible for allowing relative movement between the rotor (moving part) and the stator (fixed part), represented by the foundation. It is an important component for limiting or guiding degrees of freedom and also influences the oscillatory response of the system. The bearing must dissipate as little energy as possible (TUCKMANTEL, 2010). There are several types of bearings, using, for example, balls, oil or electromagnetism, and geometry, such as cylindrical, elliptical or

segmented. Figure 6.3 shows a representation of the bearing used in this work, hydrodynamic, short and cylindrical.

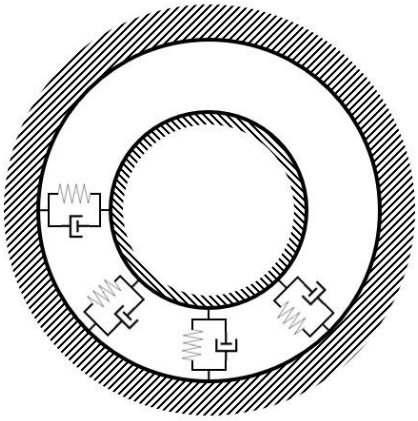

Figure 6.3 – Hydrodynamic bearing represented by equivalent springs and dampers

For this work, the oil film is modeled as several spring-damper assemblies. Krämer (1993) describes the parameters and coefficients of stiffness and damping as a function of the eccentricity, which in turn is a function of the speed of rotation of the rotor. The bearing matrices are 2x2, due to corresponding translation coordinates of the bearing node, V and W. The stiffness and damping parameters are shown in Equations 6.3 and 6.4:

$$K_{bearing} = \begin{bmatrix} K_{11} & K_{12} \\ K_{21} & K_{22} \end{bmatrix},\ K_{ik} = \frac{\gamma_{ik} F_0}{\delta} \tag{6.3}$$

$$C_{bearing} = \begin{bmatrix} C_{11} & C_{12} \\ C_{21} & C_{22} \end{bmatrix},\ C_{ik} = \frac{\beta_{ik} F_0}{\Omega \delta} \tag{6.4}$$

where Ω is the angular speed, F_0 the static loading in the bearing, δ the radial clearance. Equations 6.5, are used to obtain the coefficients of Equation 6.3:

$$\gamma(1,1) = (2\ \pi^2 + (16 - \pi^2)\ \varepsilon^2)\ A(\varepsilon);$$

$$\gamma(1,2) = \pi(\pi^2 - 2\,\pi^2\,\varepsilon^2 - (16 - \pi^2)\,\varepsilon^4)\left(\frac{A(\varepsilon)}{4\,\varepsilon\ (((1-\varepsilon^2)^{0.5}))}\right); \tag{6.5}$$

$$\gamma(2,1) = -\pi(\pi^2 + (32 + \pi^2)\,\varepsilon^2 + (32 - 2\,\pi^2)\,\varepsilon^4)\left(\frac{A(\varepsilon)}{4\varepsilon\ (((1-\varepsilon^2)^{0.5}))}\right);$$

$$\gamma(2,2) = (\pi^2 + (32 + \pi^2)\varepsilon^2 + (32 - 2\,\pi^2)\,\varepsilon^4)\left(\frac{A(\varepsilon)}{1-\varepsilon^2}\right)$$

Equations 6.6, are used to obtain the coefficients of Equation 6.4:

$$\beta(1,1) = \left(\frac{\pi}{2}\right)\left(\frac{(1-\varepsilon^2)^{0.5}}{\varepsilon}\right)(\pi^2 + (2\,\pi^2 - 16)\,\varepsilon)\,A(\varepsilon);$$

$$\beta(1,2) = -2\,(\pi^2 + (2\ \pi^2 - 16)\,\varepsilon)\,A(\varepsilon); \tag{6.6}$$

$$\beta(2,1) = -2\,(\pi^2 + (2\ \pi^2 - 16)\,\varepsilon)\,A(\varepsilon);$$

$$\beta(2,2) = \pi\ (\pi^2 + (48 - 2\,\pi^2)\ \varepsilon^2 + \pi^2\ \varepsilon^4)\frac{A(\varepsilon)}{2\ \varepsilon\ (1-\varepsilon^2)^{0.5}}$$

Equation 6.7, determines A(ε) coefficient of Equations 6.6 and 6.7, where ε is the eccentricity of shaft orbit inside the bearing.

$$A(\varepsilon) = \frac{4}{(\pi^2+(16-\pi^2)*\varepsilon^2)^{\frac{3}{2}}} \tag{6.7}$$

These stiffness and damping matrices of the bearings are inserted into the global matrices of the system at the nodes relative to each of the bearings so as to include the inherent flexibility and damping of the oil film.

Foundation model

The foundation is responsible for the interaction between the bearing and the inertial frame and can be modeled as a mass-spring-damping system in the translational degrees of freedom, as shown in Figure 6.4. There are three main approaches that allow coupling of the foundation in the system's equation of motion: lumped parameters, mechanical impedance and mixed coordinates. In this work the behavior of the first two formulations in relation to a rigid foundation will be studied.

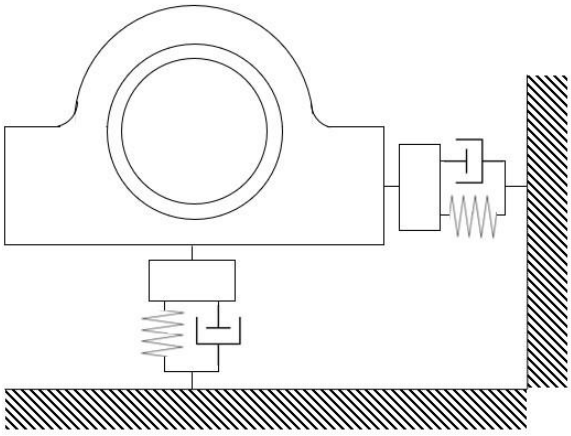

Figure 6.4 – Foundations represented by equivalent springs and dampers

The formulation by lumped parameters consists of finding foundation's matrices of mass [M_f], stiffness [K_f] and damping [R_f] using the same discretization of the shaft, the movement equation of the foundation in physical coordinates is shown in Equation 6.8:

$$[M_f]\{\ddot{x}_f\} + [R_f]\{\dot{x}_f\} + [K_f]\{x_f\} = F_f(t) \tag{6.8}$$

where x_f is the coordinate vector for nodes where rotor and foundation are coupled.

Equation 6.9 is the equation of the complete system. The main disadvantage of this method is the effort required to find parameter values that results in a correct representation of the studied foundation.

$$\begin{bmatrix} M_{rr} & 0 \\ 0 & M_{ff}+M_f \end{bmatrix}\begin{bmatrix} \ddot{x_r} \\ \ddot{x_f} \end{bmatrix}+\begin{bmatrix} R_{rr} & R_{rf} \\ R_{fr} & R_{ff}+R_f \end{bmatrix}\begin{bmatrix} \dot{x_r} \\ \dot{x_f} \end{bmatrix}+\begin{bmatrix} K_{rr} & K_{rf} \\ K_{fr} & K_{ff}+K_f \end{bmatrix}\begin{bmatrix} x_r \\ x_f \end{bmatrix}=\begin{bmatrix} F_r \\ 0 \end{bmatrix} \quad (6.9)$$

Where x_r contain rotor coordinates

The mechanical impedance method consists in obtaining the flexibility matrix and, later, the mechanical impedance matrix. The flexibility matrix can be obtained from both the lumped and experimentally formulated parameters. The flexibility matrix with lumped parameters is given by Equation 6.11, from the substitution of relations shown in Equation 6.10 in Equation 6.8. The flexibility matrix obtained experimentally is given by Equation 6.12. The main advantage of this formulation is the possibility of including empirical data (obtained through a modal analysis of the structure) in the computational model.

$$x_f = \{x_{f0}\}e^{i\Omega_e t}, F_f = \{F_{f0}\}e^{i\Omega_e t} \quad (6.10)$$

$$[H(\Omega_e,p)]_{an} = -\left(-\Omega_2^e[M_f]+ i\Omega_e[R_f]+ [K_f]\right)^{-1} \quad (6.11)$$

$$[H(\Omega_e,p)]_{exp} = -[\Phi]^t[\Phi]\left(-\Omega_2^e[M_f]+ i\Omega_e[R_f]+ [K_f]\right)^{-1} \quad (6.12)$$

Where Ω_e is the excitation frequency, $[\Phi]$ is the modal matrix of foundation and $[m_f]$,$[r_f]$,$[k_f]$ are foundation matrices in modal coordinates.

The mechanical impedance matrix is obtained from the inversion of Equation 6.11 or 6.12, as shown in Equation 6.13:

$$[\mathrm{I}(\Omega\mathrm{e},\mathrm{p})] = [\mathrm{H}(\Omega\mathrm{e},\mathrm{p})] - 1 \quad (6.13)$$

The equation of motion of the foundation with the flexibility and mechanical impedance matrices is shown in Equation 6.14

$$xf0 = -[H(\Omega e,p)]Ff0 \rightarrow -Ff0 = -[H(\Omega e,p)]-1xf0 = [I(\Omega e,p)]xf0 \quad (6.14)$$

6.3 Computational procedures

The simulated rotor is shown in Figure 6.5. It is a Jeffcott rotor with hydrodynamic bearings. Foundation parameters (mass, stiffness and damping) will be changed to evaluate their influence on response.

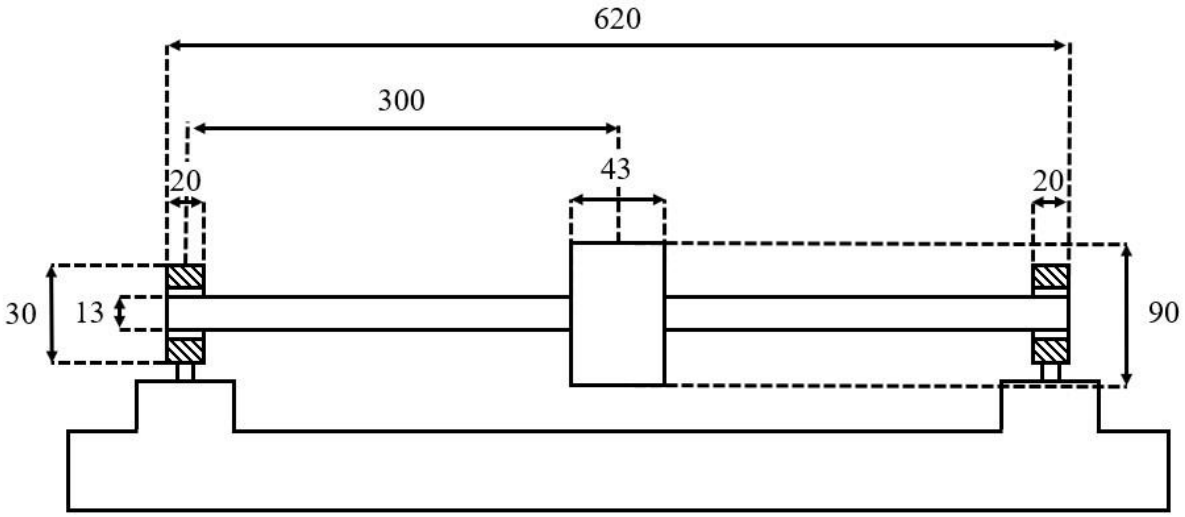

Figure 6.5 – Jeffcott rotor model used (dimensions in millimeters)

Modelling is done by finite elements to discretize the shaft and the bearings and obtain the displacements at each node. The model was divided into 13 nodes and has, therefore, 12 elements.

The shaft is made of steel, with Young's modulus E = 200 GPa, density ρ = 7860 kg / m3 and structural damping β = 2x10-4. Bearings were shaped symmetrically on nodes 2 and 12. The bearings are 30 mm in diameter and 20 mm wide, with a 90 μm radial clearance and a viscosity of 0.07 Pa.s.

Force due to the rotational imbalance was placed at node 7 and caused by a mass of 1.5 g with an eccentricity of 41 mm. The discretization of the rotor-bearing system is shown in Figure 6.6.

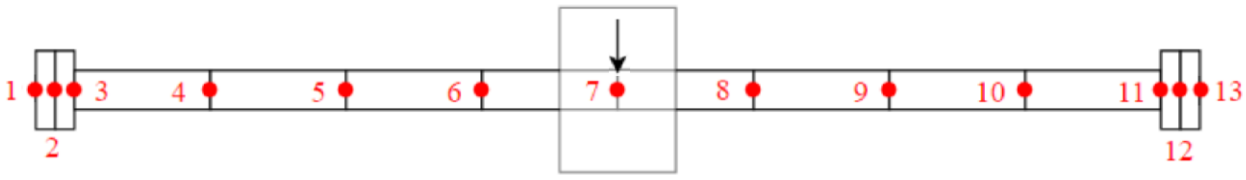

Figure 6.6 – Nodes in the rotor model used

Considering the diameter and length of the elements, there are two (2) types of elements in the model. The dimensions of each type are shown in Table 6.1.

Table 6.1 – Element dimensions

Type	Length (mm)	Diameter (mm)	Element Number
I	10	30	1, 2, 11, 12
II	72.5	13	3, 4, 5, 6, 7, 8, 9, 10

6.4 Results and discussion

First, the rotor was simulated with the rigid foundation. Figure 6.7 shows the amplitude and phase of the response for the disc node and for the bearing node.

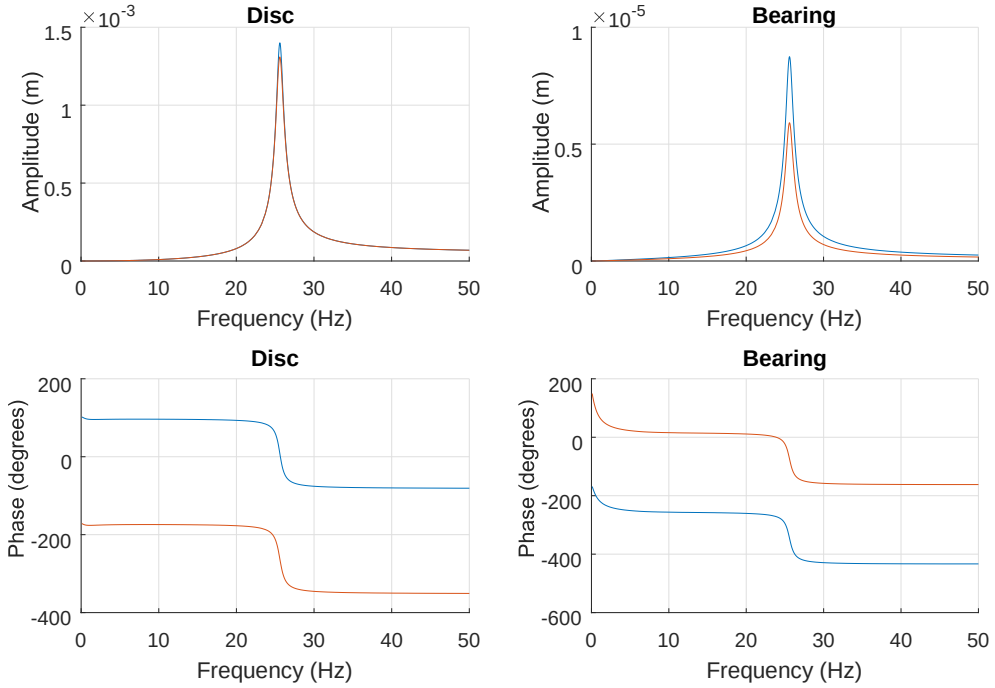

Figure 6.7 – Amplitude and phase response for rigid foundation for Y (blue) and Z (red)

The resonance frequency is approximately 25.6 Hz, as one can see in the amplitude peaks and the 180° phase shift. The Y and Z directions show very similar behavior, differing by the expected 90º of phase due to orthogonality of directions.

The next results are for a flexible foundation inserted through the method of the lumped parameters. The foundation parameters used for this simulation were: mass of

10 kg, damping of 10 Ns / m and stiffness of 100 N / m. Figure 6.8 shows the amplitude and phase results for this case.

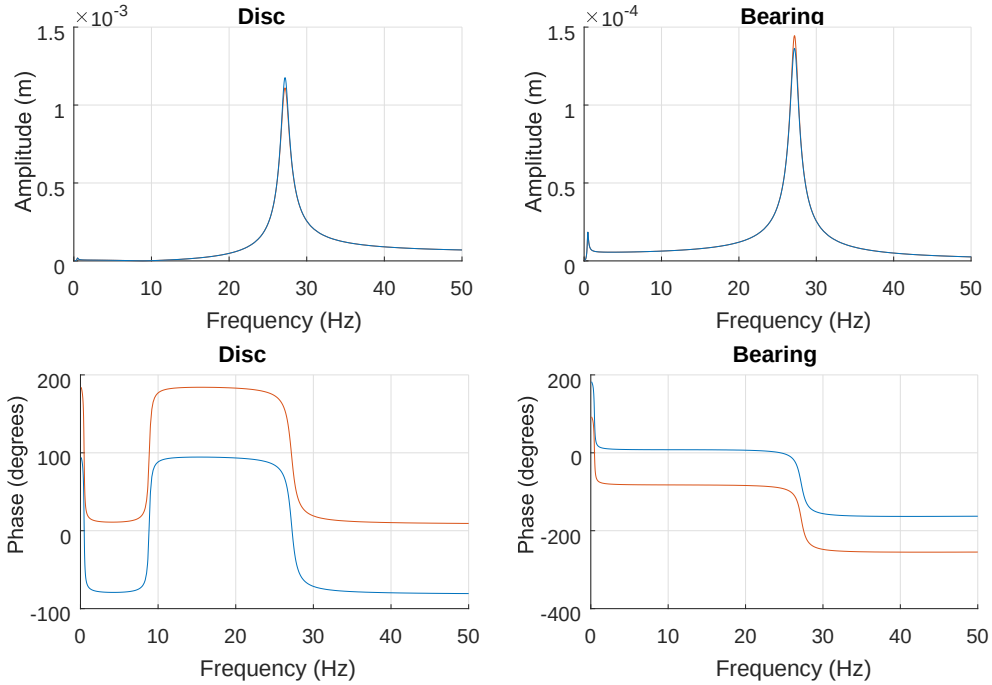

Figure 6.8 – Amplitude and phase response for flexible foundation – case 1 for Y (blue) and Z (red)

By analyzing Figure 6.8 it is possible to perceive a small amplitude peak (both on the disc and the bearing) at a low frequency. This amplitude peak depicts the influence of the natural frequency of the foundation on the response of the rotating system. The other amplitude peak is much more evident and is at a frequency of 27Hz, shortly after the first critical frequency observed in the case of the rigid rotor.

Figure 6.9 shows the amplitude and phase results for the model with the inclusion of the foundation by concentrated parameters now considering the foundation mass as 10 kg, the damping of the foundation as 10^{10} Ns / m and the stiffness of the foundation of 100 N / m.

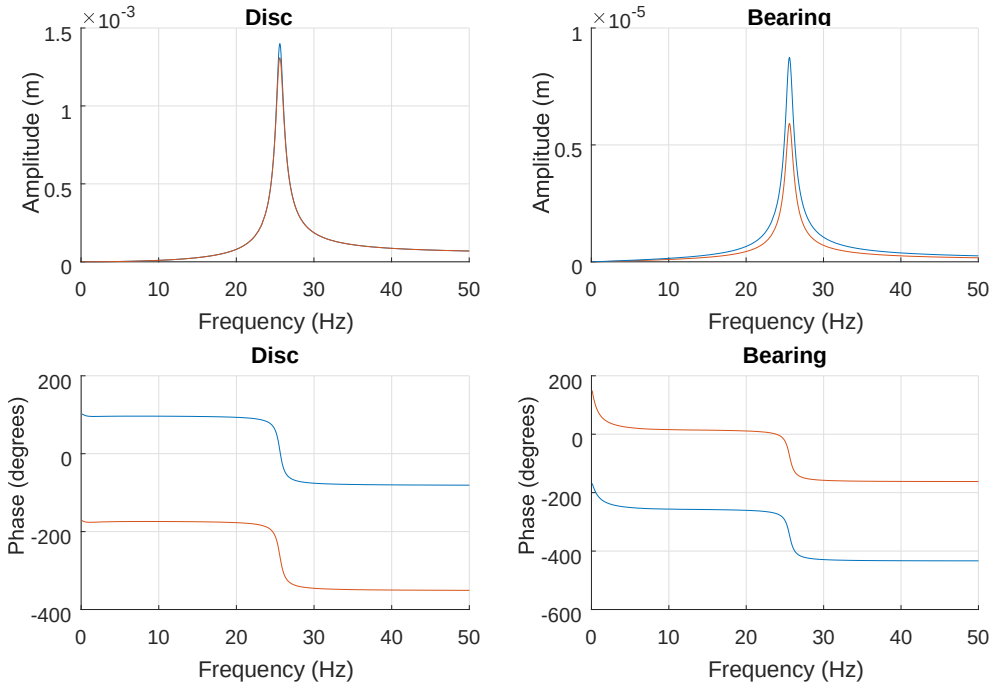

Figure 6.9 – Amplitude and phase response for flexible foundation – case 2 for Y (blue) and Z (red)

The analysis of Figure 6.9 shows that the increase in damping eliminated the first amplitude peak compared to Figure 6.8, and the resonance frequency returned to 25.6 Hz, the first critical frequency for the rigid case. A high damping prevents the influence of stiffness, leaving the results very close to the rigid case.

Figure 6.10 shows the last results simulated in the article. For this case, the mechanical impedance model is used, where the flexibility matrix is obtained from the formulation of lumped parameters (Equation 6.11). The foundation is modeled as anisotropic, with mass of 10 kg, damping of 10 Ns / m and stiffness of 100 N / m in the horizontal direction (Z) and damping of 10 Ns / m and stiffness of 10^{12} N / m in the vertical direction (Y).

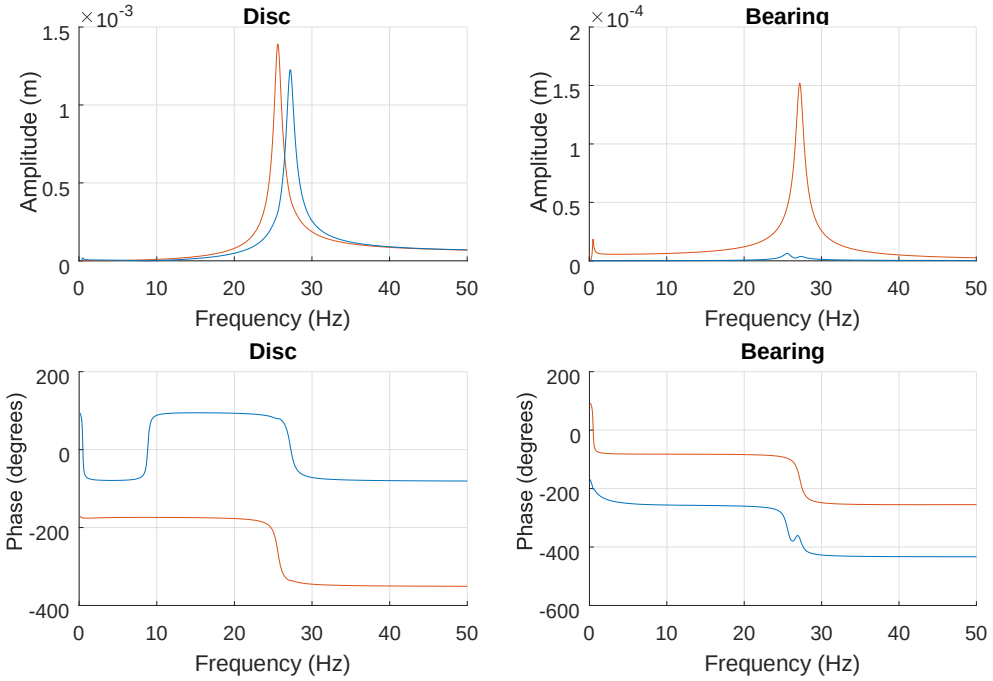

Figure 6.10 – Amplitude and phase response for flexible foundation – case 3 for Y (blue) and Z (red)

The anisotropy is evident in the behavior of amplitude and phase graphs. As expected, due to foundation parameters used in each direction, the horizontal direction presented similar behavior to case 1 while the vertical direction was similar to case 2.

6.5 Conclusion

The paper adapted in this chapter presented the frequency response of the rotating systems to elucidate the influence of the foundation in models that already include rotors and bearings.

The results indicate the influence of the flexible foundation. It is noticeable a significant change in the frequency of amplitude peaks, due to changes in overall mass, and damping. The different simulations with variation of mass, stiffness and damping resulted in near but not coincident peaks, showing that even with large parameter variations, foundation influence in response have limits.

Regarding the comparison between the modeling of lumped parameters and mechanical impedance, the results were very close, which is consistent since the mechanical impedance matrix was a result of the parameters used. As discussed, the mechanical impedance matrix can also be obtained experimentally and therefore inserted directly into the model, replacing the matrix obtained from the lumped parameters.

6.6 Acknowledgments

The author thanks CAPES, CNPq and grant # 2017/07454-8 from the São Paulo Research Foundation (FAPESP) for the financial support to this research and ABCM for licensing the use of the paper in this dissertation.

7 PAPER 4 – A COMPENSATION METHOD FOR FOUNDATION EFFECTS IN ROTATING SYSTEMS THROUGH SHAPE OPTIMIZATION

7.1 Introduction

Rotating machines have been widely used since the industrial revolution. Nowadays, rotors are found in a variety of complex configurations and different environments, such as power plants turbines and submarine pumps. Malfunction caused by excessive vibration implies in high costs and risks, then good models and optimization are reliable tools to manage this problem.

The first paper about rotordynamics, On The Centrifugal Force of Rotating Shafts, was written in 1869 by Rankine and almost 150 years later, high quality research still produces new material about different phenomena related to the topic. The interaction between rotor and foundation is explored in Feng and Hahn (1995), Kang et al (2000) and Cavalca, Cavalcante and Okabe (2005). Foundations interact with a rotor system increasing its complexity, hence creating a new series of problems and phenomena.

These new problems are aggravated by the fact that is not always viable to proper design the system for every foundation, due to the wide variances expected. Therefore, even a correctly designed and tested rotating machine can have operational problems when its foundation is changed. Modifications in machine foundation can cause increased vibrations, negatively affecting reliability.

Even when the shaft and bearings are capable to withstand the stresses from vibration, the lateral displacement of the shaft can lead to new sources of stress. Rotors and stators working with small clearances can contact each other due to vibration, leading to another source of vibration and stress (STOCKI et al, 2012).

To avoid complete redesign of machine or a costly operation of foundation adjustment, some elements in machine can be modified to restore the desired behavior, in general, through optimization techniques.

Optimization methods are based on choosing the correct objective function to minimize as well as its constraints, once it is possible to change several parameters in the computational environment. There are several optimization methods of optimization such as simulated annealing, particle swarm optimization, ant colony optimization, neural network-based optimization, and fuzzy optimization (RAO, 2009; YANG; CHOI; KIM, 2005)

When the optimization involves a complex solution domain with multiple variables, meta-heuristic methods are frequently employed because of their efficiency. This efficiency, however, comes at cost of solution's optimality, as these algorithms do not necessarily converge to an optimal solution (GEN; CHENG, 2000). Exhaustive search algorithms, on the other side, are exact algorithms and are guaranteed to find optimal solution, albeit at a higher computational cost.

In this context, this work analyzes two cases of rotors where a change in foundation results in an undesired dynamic behavior. Then, using an exhaustive search optimization algorithm, compensate for the foundation changes. Two different choices of design variable are used - shaft shape and disc placement.

The objective of optimization is to have an amplitude of vibration in operating frequency that is equal to the original one, before the changes in foundations. This way, the stop criteria will be based in FRF amplitude at this frequency and solutions will be chosen by the search method by evaluating the reduction in this amplitude compared to the previous iteration.

The first case consists in an initially stiff foundation, which is made more compliant. In the second case, foundation remains with the same damping and stiffness but is made heavier. The characteristics of the rotating system are obtained using the Finite Element Method (FEM), since it presents relative ease of implementation and has good scalability, allowing increase of algorithms computational effort according to the need of precision.

Through FEM, the rotor frequency response is obtained at the beginning of each iteration. Then, several sub-iterations analyze the influence of one specific element in

system dynamic by comparing responses before and after changes in the element. After the assessment of elements influence, the algorithm modifies the element that correlates better the desired change in response to start next iteration. The procedure can be applied to both disc and shaft elements, one at a time. Shaft optimization have the potential to achieve better results because of its effect in mass, damping and stiffness. Disc optimization influence is restricted to mass, but it is a simpler solution.

7.2 Methodology

Modelling

For a complete analysis of rotating machines, all relevant components of the system must have an adequate modeling to ensure a good representation of parts and their interaction. Therefore, shafts, bearings, discs and foundations need to be modeled discretely to allow modifications to each component without affecting the others.

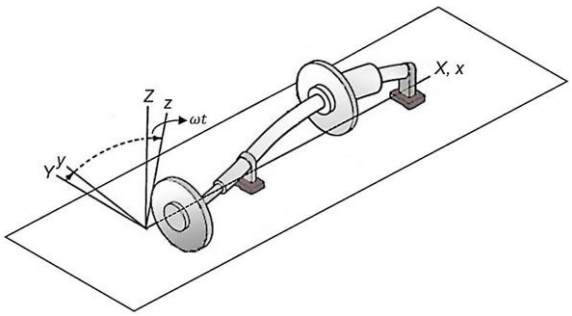

Figure 7.1 - Representative rotor system, adapted from Nelson and McVaugh (1976)

Modeling of the rotor by Finite Element Method.

The generalized model used here consists of a rotating system with discs, shaft and bearings, as illustrated in Figure 7.1, along with the coordinate systems (local and inertial). The reference system *XYZ* represent the inertial frame, where *X* is the axial axis, while *Y* and *Z* are the horizontal and vertical transverse axes, respectively. The reference system *xyz* is the rotational referential and is defined relatively to the inertial

frame by the rotation ωt around the X axis, with ω denoting the rotational speed of rotor (precession rotation).

The equation of motion of the rotating system is defined as:

$$[M]\{\ddot{q}\} + ([C] + \Omega[G])\{\dot{q}\} + [K]\{q\} = \{F\} \quad (7.1)$$

where [M], [C], [K] and [G] are the global mass, damping, stiffness and gyroscopic matrices, respectively. {F} contains the external forces, which are the unbalance forces in this study. The [C] matrix, which represents the structural damping of rotor, is considered proportional to the mass and stiffness matrices:

$$[C] = \alpha_C[M] + \beta_C[K] \quad (7.2)$$

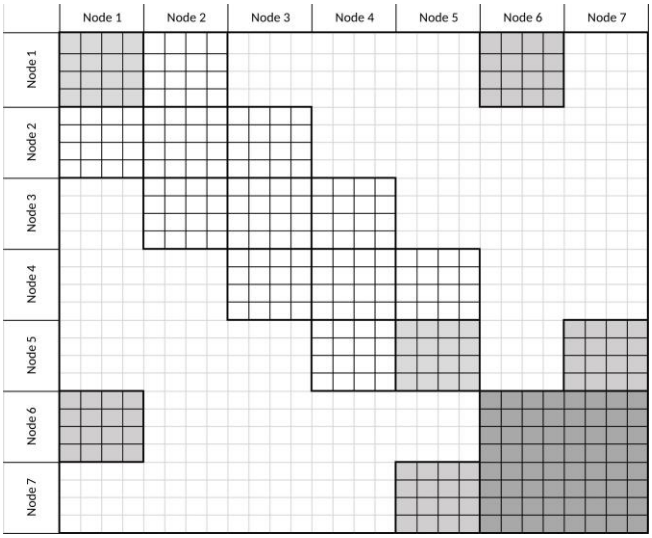

Figure 7.2 -. Construction of finite element matrices, bearings in light gray and foundation in dark gray

For a complex system comprised by a rotor and its foundation, there is no expectation for an analytical solution. The number of simplifications required to make the analytical solution feasible can result in great loss of accuracy. With this in mind, analytical solutions were discarded and a numeric approach must be chosen.

In order to numerically solve a complex problem, a discretization method is usually employed and, between the options, the Finite Element Method (FEM) is used in this paper for implementation of algorithm.

For modeling by finite element method, the continuous system is divided into a finite number of elements, which are connected to each other by nodes. Each node is

composed by 4x4 sub-matrices representing the 4 degrees of freedom per node, two translational and two rotational. Shaft elements spans two nodes, while bearings, discs and foundation effects are restricted to their respective node.

Each shaft element sub-matrix is superposed to the adjacent elements' submatrices. The systems matrices assembly can be seen in Figure 7.2. The only elements not related directly to system components are the ones outside the diagonal band. These elements are due to the bearings coupling to the foundation.

Shaft Model.

The matrices of each element (shaft and discs) are based on the ones presented by Nelson and McVaugh (1976), using Timoshenko beam theory. This type of shaft element accounts for rotational bending, shear deformation effects, elastic bending energy, translational and rotational inertia.

The shear deformation coefficients ensure that even very small length to diameter ratios elements are precisely modelled. Thereby, the shaft can be discretized into very small elements without the imprecision inherent to the common Euler-Bernoulli beam, especially for higher frequencies.

Bearing Model.

For correct operation, a rotating system need to be constrained at certain directions, usually translation and angular displacement in axis perpendicular to the shaft, at the same time the shaft must be allowed to rotate freely in its parallel axis. The bearings are responsible for both the constriction in desired directions and low friction coefficient for shaft rotation.

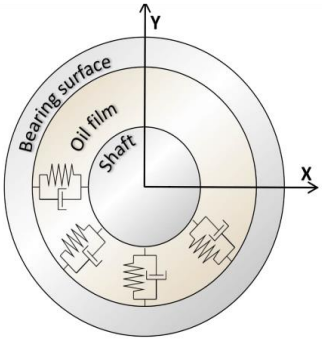

Figure 7.3 - Hydrodynamic bearing, with oil film modeled as springs and dampers, adapted from Machado and Cavalca (2009)

Among several types of bearings, hydrodynamic bearings are one of the most employed in rotors due to their simplicity, ease of assembly, low cost of production and low friction coefficient. For these reasons the system chosen for the simulations in this paper is supported by hydrodynamic bearings.

The hydrodynamic bearings are described here as short bearings and approximated by an equivalent springs and dampers system, as demonstrated by Kramer (1993). This approximation is particularly useful in an implementation of bearings by concentrated parameters, as used in this paper, due to the simplifications in system assembly and simulation. The bearings coefficients are inserted into the global matrices of system, at the bearings position, as previously discussed.

Foundation Model.

The foundation structure is responsible by connecting the rotor and the ground, it is commonly represented as rigid or flexible.

Rigid foundations are used when the focus is the response considering just rotor and bearings displacement. A flexible foundation can be represented by a mass - spring - damper system. The main approaches to include the foundation are lumped parameters, mechanical impedance and mixed coordinates.

In this paper, it is used the lumped parameters approach, as shown in Figure 7.4. Including the foundation on the model implies in more degrees of freedom to analyze, however provides a more accurate model and a more realistic situation.

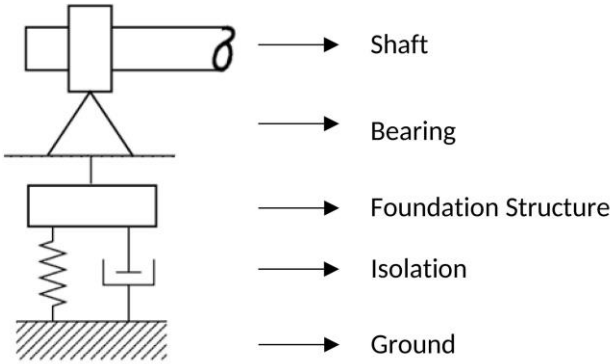

Figure 7.4 - Rotor-bearing-foundation model

Optimization Method

The optimization is based on an exhaustive search method. Search methods have been successfully employed in complex rotor optimization as shown by El-Shafei and Yakoub (2001). The main drawback of an exhaustive search is the computational effort of testing every solution at each iteration. The calculations done for each iteration must be kept to a minimum to avoid excessive execution time. On the other side, the method presents important advantages in convergence and quality of the final results.

Because of inherently performance penalty of the algorithm compared to an algorithm based on sensitivity analysis, for example, due to the much larger number of FEM and FRF computations per iteration, paralleling and GPU computing is used to improve performance, capitalizing on the ease of paralleling the simpler threads of method. Both characteristics, paralleling and simple threads, are well suited to the hardware trends in embedded low-cost controllers.

There are available methods that require less computational effort, with a trade-off in quality of solutions. Strain energy-based method, for example, uses only one FEM analysis per iteration. However, this method will ensure only the largest reduction in overall compliance at each iteration, which does not have an exact correlation to the amplitude of vibrations at a given node.

In this work, for every iteration, sub-iterations are run modeling the initial rotor with only one element modified and assessing its response. The element that correlates better with the desired response is modified. After the best modification is determined for the iteration, the result is assigned as a starting condition for the next iteration. This loop assures that the best modification is done at each iteration.

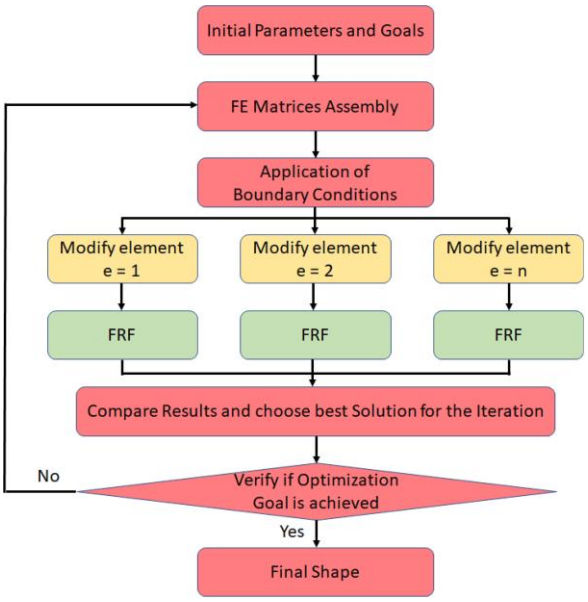

Figure 7.5 - Algorithm workflow diagram: single threaded (red blocks), block level paralleling (yellow blocks), instruction level paralleling (green)

To define the stop criteria for optimization, response in initial foundation is compared to the actual response of the system. Multiple criteria can be used to compare responses, but they need to be combined in one objective function to avoid excessive computational effort. This work uses peak amplitude of FRF around the operating range for both disc and shaft optimization as the objective function. The goal of the optimizations is to have an amplitude of vibration at operating frequency equal or less than the original one, as shown in the objective function and stop criteria of Equation 7.3.

$$\begin{aligned} &\min && FRF_{amp}(F_{op}) \\ &subject\ to && D_{Do\ max} \leq D_{Dmax} \\ & && D_{So\ min} \leq D_{Smin} \end{aligned} \tag{7.3}$$

When optimizing shaft shapes, the only restriction needed to obtain a viable shape of shaft was to not allow reductions in elements diameter. This condition was enough to obtain the shapes shown in the paper. However, when adding discs more restrictions were applied to prevent the creation of unreasonable shapes of discs. To avoid large diameters, discs were limited to the diameter of the largest disc in the original rotor and to avoid thin discs, a minimum slenderness ratio is defined.

Computational Algorithm

The simulation and optimization algorithms are written MATLAB® using a main program divided into blocks and auxiliary functions. Figure 7.5 shows the code work-flow diagram. The first three blocks are run at the start to assemble the problem matrices required to evaluate the initial response and are run in a single thread in series.

After the initial response is obtained, an iterative process starts. Each iteration is composed by several sub-iterations checking the rotor response when each element is modified. The best element to be modified is chosen by comparing the sub-iterations responses and next iteration starts. The blocks which re-assemble the problem with a modified element are run in different threads between them and the frequency sweep inside the FRF blocks is divided in one thread per frequency step. This way, the inherently high computational cost of the chosen optimization approach does not implicate in a high elapsed time for calculations.

7.3 Results and Discussion

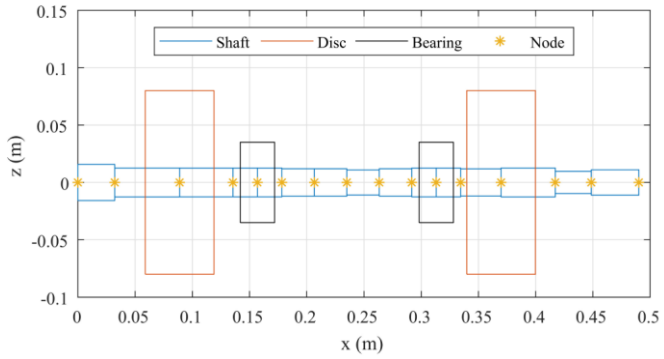

Figure 7.6 - Sketch of Rotor for Case 1

The numerical simulations use a classical rotating system, composed by a steel shaft, steel rigid discs and supported by two identical hydrodynamic bearings. For Case 1, a rotor similar to the one used by Alves, Daniel and Cavalca (2015) is modelled, for study in a more complex rotating machine. For Case 2 a decentralized disc Jeffcott

rotor is used, as shown in Figure 7.12. Although this model is a simple one, it has similar dimensions to the rotor test rig located in Laboratory of Rotary Machinery (LAMAR-FEM-UNICAMP), allowing an experimental validation of results in future.

The analyses are made using two different cases of changes in foundations and both cases are tested for the two methods: disc and shaft optimization. Both shaft and disc optimization methods are used to correct the frequency response function, that is, to return the system in a condition closer to the initial one for the rotor operating frequency.

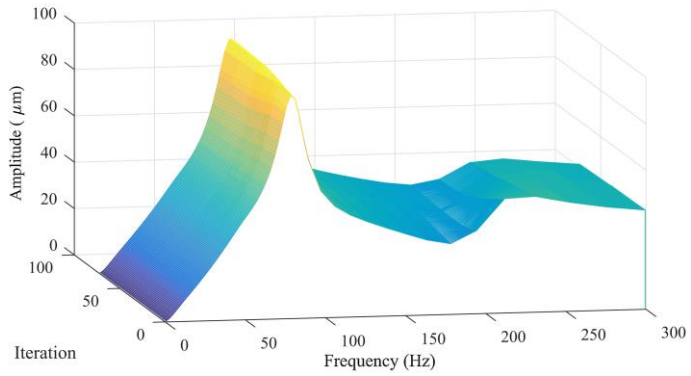

Figure 7.7 - Evolution of frequency response through iterations of shaft optimization

In Case 1, the rotor is operating at about 12900 rpm (215 Hz) in a stiff foundation and then is moved to a more compliant one. This change reduces the second natural frequency, to a value below rotor operating speed. The rotor, now operates barely above the second natural frequency and is subject to an increased amplitude vibration (see Figure 7.8, lines blue and red).

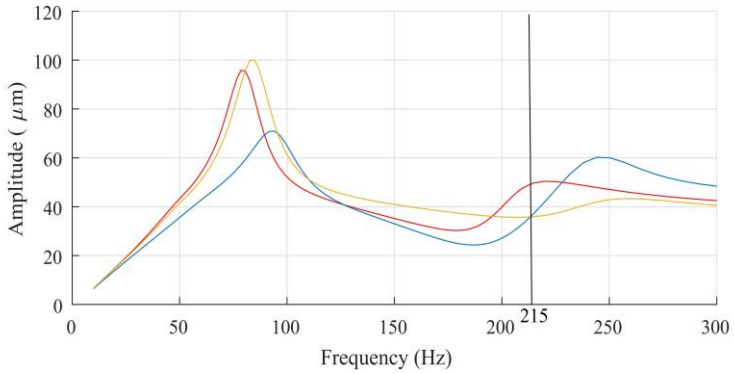

Figure 7.8 - FRF comparison between the initial response (blue) and the response in the more compliant foundation before (red) and after (yellow) the shaft optimization

The optimization aimed to restore vibration amplitude at operating frequency. Amplitude at first natural frequency is not set as an optimization parameter since it is well below operating speed. Therefore, it is crossed briefly. Ignoring this parameter will result in better solutions for the steady state. The results for each iteration of optimization are shown in Figure 7.7. It can be seen that initial iterations are affecting more the peak frequency and last iterations are almost only reducing the peak amplitude, showing smaller improvements for the given increase of shaft material.

Using the shaft optimization, a stiffer system is obtained, moving away the peak from the operating speed. The response is brought to the goal at operating speed from initial condition, as can be seen in Figure 7.8. The final rotor configuration, with optimized shaft, is shown in Figure 7.9.

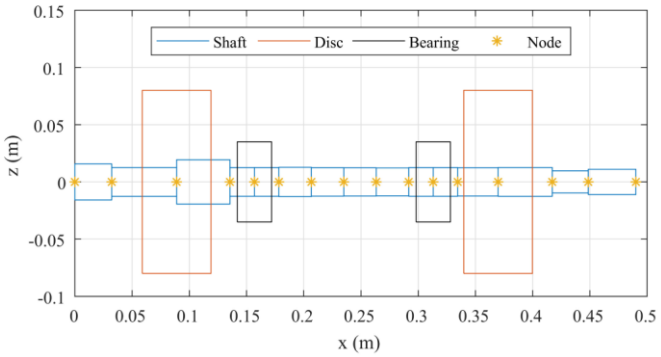

Figure 7.9 - Rotor with optimized shaft - case 1

For this same case, the disc optimization method is tested. This method is less expensive to use, but more limited due to the inability to change the stiffness of the

system. The increase of mass caused by disc placement move the amplitude peak to lower frequency, reducing amplitude at operating frequency.

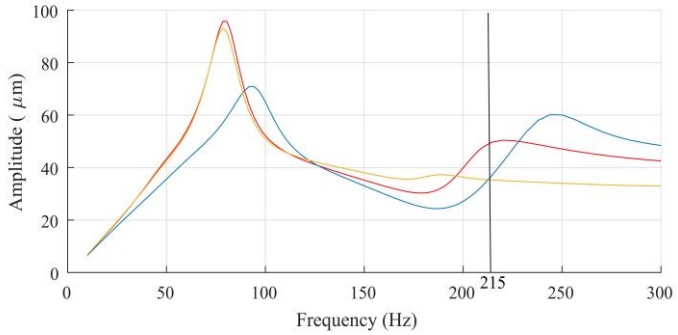

Figure 7.10 - FRF comparison between the initial response (blue) and the response in the more compliant foundation before (red) and after (yellow) the disc optimization

The desired reduction in the amplitude at operating frequency is achieved. Analysis of Figure 7.10, shows that for this case, optimization through disc placement is very efficient. Optimization goal is achieved with less computational effort and the overall response is better than the obtained through shaft optimization (see Figures 8 and 10 for comparison).

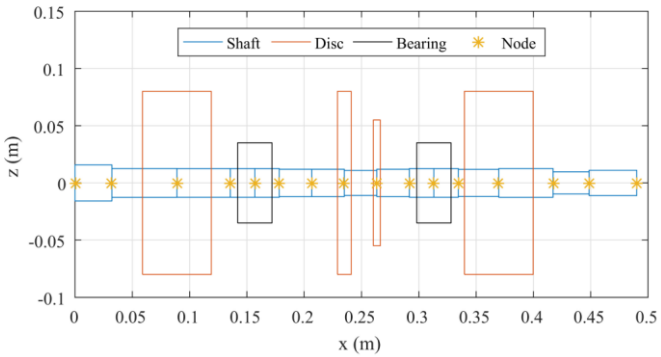

Figure 7.11 - Disc placement for Case 1

The main drawback of using disc is the inability to increase the natural frequencies. Because of that, the system will cross the second natural frequency before reaching the operating speed. In this case, however, crossing the second natural frequency is not an issue, since this peak is much attenuated by the added discs. The final rotor configuration for this optimization is shown in Figure 7.11. A small percentage of the system's initial mass was added by the means of two small discs between the bearings.

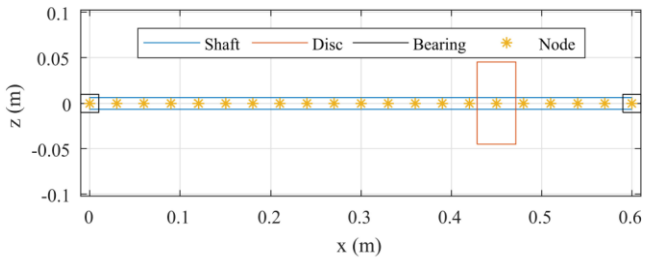

Figure 7.12 - Sketch of Rotor for Case 2

The Case 2 simulates a situation where there is an increase in the mass of foundations. The mass increase results in a lower second natural frequency and a larger peak of amplitude. The idea here is to simulate a case where a rotating system is operating at a certain rotating frequency between the first two natural frequencies, 2700 rpm (45 Hz) and, due to the change of foundation, the new operating frequency is then very close to the second natural frequency. This case presents a classical Jeffcott rotor with an offset disc.

The results for each iteration of optimization are shown in Figure 7.13. Differing from Case 1, it can be seen that the increase in the frequency of second peak maintains a steady ratio through the iterations. This steady ratio is due to the smaller change needed for Case 2, which can be done modifying only the most sensible elements in the shaft.

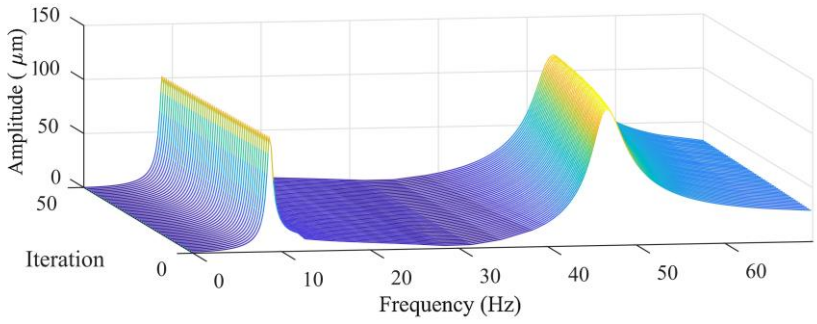

Figure 7.13 - Evolution of frequency response through iterations

The result of the shaft optimization can be seen in Figure 7.14, the operating frequency is illustrated as a black line. The final longitudinal section of the shaft shape is shown in Figure 7.15.

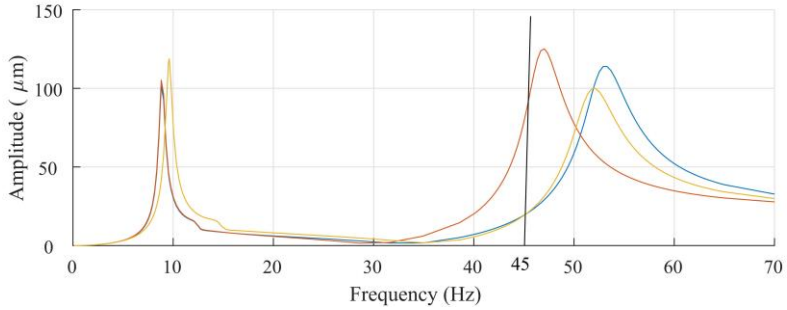

Figure 7.14 - FRF comparison between the initial response (blue) and the response in the heavier foundation before (red) and after (yellow) the shaft optimization for the second case

Finally, for the Case 2, the disc optimization method is tested. The results of change in frequency response are show in Figure 7.16 and the placement of discs is shown in Figure 7.17. The same criterion for disc optimization of Case 1 is used.

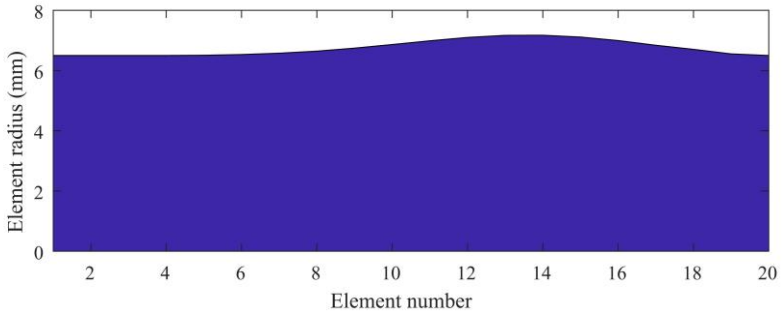

Figure 7.15 - Smoothed longitudinal shaft section after optimization for Case 2

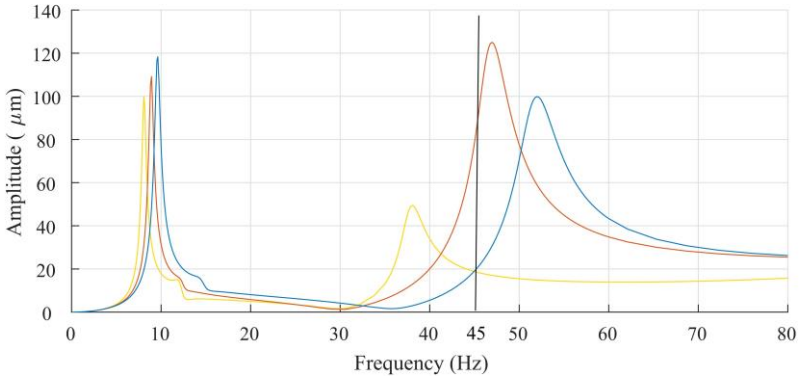

Figure 7.16 - FRF comparison between the initial response (blue) and the response in the heavier foundation before (red) and after (yellow) the disc optimization for the second case

For this second case, the placement of discs achieved amplitude levels near to the initial response in the operating frequency. However, the second critical frequency occurs before the operating speed. If the system can provide enough torque to overcome the natural frequency and the rotor can withstand the stresses while crossing the amplitude peak, the rotor with disc optimization presents the same steady-state

response of the rotor with shaft optimization, with a much lower cost inherently to this kind of modification.

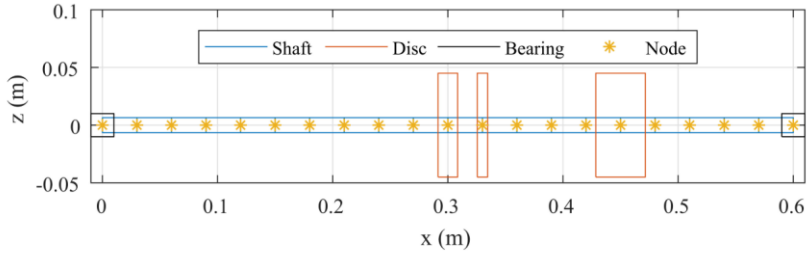

Figure 7.17 - Disc placement for Case 2

7.4 Conclusions

The simulations present in this paper show that through an algorithm, a rotor can be optimized to restore its previous response after a change in foundations. The algorithm is simple and light enough to run in inexpensive processors, making the solution viable for embedded machine analysis.

It can be noted that effects of different foundations can be counteracted by changes in rotors shaft or by the placement of discs. Modifying shafts shape present the most efficient method in terms of mass increase. A stiffer shaft can be used to increase system overall stiffness, hence moving natural frequencies out of operating range. However, shaft modifications are costly, because increases in shafts section can only be achieved through costly welding operations or milling a new shaft from a thicker bar. Disc optimization, albeit its limitation of moving the peak further into operating range, is a low-cost solution that can achieve results even better than by shaft modifications for some systems, as can be seen in Case 1.

Finally, it is interesting to comment that for the studied cases, the bearing properties, when changed inside a reasonable range, does not affect the steady state response in operating frequencies in a sensible way. Therefore, the optimization through bearing parameters manipulation is not feasible for the given examples. Case 1, which is more complex and operates at higher rotating speed is even less sensible; e.g. a tenfold increase in bearing clearance resulted in negligible changes at operating

frequency. Future works are planned to analyze which rotors are sensible to bearing parameters and optimize using their modification.

7.5 Acknowledgements

The author thanks CAPES, CNPq and grant # 2017/07454-8 from the São Paulo Research Foundation (FAPESP) for the financial support to this research and Springer for licensing the use of the paper in this dissertation.

Adapted by permission from Springer. 10th IFToMM International Conference on Rotor Dynamics, Rother, C. S.; Alencar, A. C. M. G.; Machado, T. H. A Compensation Method for Foundation Effects in Rotating Systems Through Shape Optimization, Copyright 2018.

8 CONCLUSIONS

This work presented a study on rotating machines. Starting with the introduction and importance of the theme followed by a bibliographic review on rotordynamics. After the two introductory chapters, there is a synthesis of the research followed by the articles generated and published during the master's project.

The articles covered modeling, simulation and rotor optimization, with the focus on the finite element method. Through the first article, it was possible to compare the two most commonly used shaft's models, as well as to analyze the influence of discretization on the response of the simulations.

It is perceived a small difference between the Euler and Timoshenko models for usual length and diameter ratios, which increases as the shaft becomes less slender. Even small, this difference was greater than that obtained by the increase of discretization in the cases studied. The difference between the computational cost of the two models is small, and much smaller than the one perceived when increasing discretization. In this way, it could be concluded that the use of the Timoshenko beam element for rotor simulation is advantageous and much more cost effective than increasing discretization.

The second article showed the influence of the bearings on the dynamic behavior of a rotor. There is a large difference between embedded rotors and those supported by hydrodynamic bearings for all analyzes performed - in the time, frequency and modal domains. By comparison with the bearing model used in article 1, it could be seen that most of the differences noted come from the degree of angular freedom introduced by the bearings. Therefore, the influence of the low constraining presented by the hydrodynamic bearing on the shaft's angular movements was emphasized. Bearings models that restrict angular movements will lead to considerably higher natural frequencies.

The analysis of the foundation effects performed in the third article showed the important influence of this component on the rotor dynamics. Through the various simulations it can be noted that foundations have an important role in system response. Varying parameters of foundations resulted in perceptible changes in systems'

frequency response. Phase response was particularly sensible to changes in foundations, which introduced a sudden phase shift at foundation resonant frequency.

In order to compensate for undesired effect of different foundations that can occur when operating a rotor in another foundation, optimization methods were proposed. Analyzing the optimization algorithm results of the fourth article, it is noted that the effects of foundation changes can be compensated by changes in the components of the rotating system. The elements of high polar inertia (discs) and the shafts elements are determining components in the dynamics of the system and through modifications in them, it is possible to compensate the other changes in the system.

The results of the fourth article show that both shaft modifications and disc placement were effective at modifying system frequency response characteristics. Disc placement could achieve the desired response at a fraction of the cost of shaft modifications, albeit resulting in a larger mass increase to the rotor. It was also possible to conclude from the data of the fourth article that the search algorithm presents a penalty of execution speed and should be restricted to situations in which other methods are not feasible. Although it presents fast iterations, with parallelism and possibility of execution in GPU, the search method had a considerably slower execution than other methods.

Since the amplitude of vibration at a given frequency is difficult to relate to some system parameter - the overall stiffness of the given system - the search method had to be employed. For situations in which it is possible to relate the expected behavior of the system with a property, other methods are more effective.

The induced fluid instability threshold of a rotor is more easily related to a property of the system. The frequency at which this phenomenon manifests is strongly correlated with the naturally damped frequency of the mode of vibration introduced by the bearing. Thus, the optimization of a rotor to the induced fluid instability threshold could be easily accomplished by another method.

Based on this conclusion, it was thought the next work in the field of optimization of rotating machines (a preliminary draft of the article to be proposed was presented in section 3.9). The article uses strain energy method to move the induced fluid instability threshold from the operating speed range. This method is much faster compared to

the one used in the fourth article, allowing the use of a higher element count, resulting in a more continuous shape of the resulting shaft. Both methods requiring shaft modifications resulted in a complex shaft shape, restricting the fabrication processes used to make the shaft.

References

ALENCAR, AUGUSTO; ROTHER, CÉSAR; MACHADO, TIAGO. **Estudo da Influência da Fundação na Resposta de Sistemas Rotativos**. Anais do X Congresso Nacional de Engenharia Mecânica. Rio de Janeiro/RJ: ABCM, 2018.

ALVES, D.S., DANIEL, G.B. AND CAVALCA, K.L. **Thermal effects in hydrodynamic cylindrical bearings**. Proceedings of the 9th IFToMM International Conference on Rotor Dynamics, pp. 1123–1133, 2015.

ARGYRIS, J.H., KELSEY, S. **Energy Theorems and Structural Analysis**. Butterworth, London, 1960.

CAMPBELL, W. **Protection of Steam Turbine Disc Wheels from Axial Vibration**. London: General Electric Company, 1924.

CAVALCA, K.L., CAVALCANTE, P.F. AND OKABE, E.P. **An investigation on the influence of the supporting structure on the dynamics of the rotor system**. Mechanical Systems and Signal Processing, Vol. 19, pp. 157–174, 2005.

CLOUGH, R.W. **The finite element method in plane stress analysis**. Proceedings of 2nd ASCE Conference on Electronic Computation, Pittsburg, 1960.

CRANDALL, S.H. **Rotordynamic Software: Rotating Machinery Dynamics.** Proceedings of 3rd International Symposium on Transport Phenomena and Dynamics of Rotating Machinery, Washington D.C., 1992.

D.T. POTTS. **A Companion to the Archeology of the Ancient Near East**, 2012

DANIEL, G.B, MACHADO, T.H., CAVALCA, K.L. – **Investigation on The Influence of The Cavitation Boundaries on The Dynamic Behavior of Planar Mechanical System with Hydrodynamic Bearings** – Mechanism and Machine Theory 99 p. 19-36, 2016.

DIMAROGONAS, A. **Vibration for Engineers**, 2nd ed. Englewood Cliffs, New Jersey: Prentice-Hall, 1995.

DOWSON, D. **A generalized Reynolds equation for fluid-film lubrication**. International Journal of Mechanical Sciences, 4(2), 159–170, 1965.

DUBOIS, G. B., OCVIRK, F. W.: **Analytical derivation and experimental evaluation of short-bearing approximation for full journal bearings**. Cornell Univ. Rep., 1953.

DUMITRU N., SECARA E., MIHALCICA M. Proceedings of the 1st International Conference on Manufacturing Engineering, Quality and Production Systems (Volume II) p. 396, 2009.

DURKELEY, S. **On the Whirling and Vibration of Shafts**, 1893.

EL-SHAFEI, A.A., YAKOUB, R.Y. **Optimum Design of Squeeze Film Dampers Supporting Multiple-Mode Rotors**. ASME. Turbo Expo: Power for Land, Sea, and Air, 2001

FELIPPA, C.A. **Introduction to finite element methods**. Textbook made by Department of Aerospace Engineering Sciences of the University of Colorado at Boulder, 2004.

FENG, N. AND HAHN, E.J. "**Including foundation effects on the vibration behaviour of rotating machinery**". Mechanical Systems and Signal Processing, Vol. 9, pp. 243–256, 1995.

FOOTE, W.R., PORITSKY, H., SLADE, J.J.JR. **Critical speeds of a rotor with unequal shaft flexibility**. Journal of Applied Mathematics, A 77 – A 84, 1943.

FRISWELL, M.I., MOTTERSHEAD, J.E. **Finite Element Model Updating in Structural Dynamics**. Kluwer Academic Publisher, 1996.

GEN, M., CHENG, R., **Genetic Algorithms and Engineering Optimization**, John Wiley & Sons, 2000.

GREENE, R. B. **Gyroscopic effects on the critical speeds of flexible rotors**. Journal of Applied Mechanics, Transactions of ASME 70, p. 369-376, 1948.

GUYAN, R.J. **Reduction of stiffness and mass matrices**. AIAA Journal, Vol. 3, p. 380, 1965.

HAFTKA, R.T. AND GURDAL, Z., **Elements of Structural Optimization**, 3rd edn., Kluwer Academic Publishers, Dordrecht, 1992.

HAGG, A. C., AND SANKEY, G. O., **Elastic and Damping Properties of Oil-Film Journal Bearings for Application to Unbalance Vibration Calculations**, J. Appl. Mech. 25, 141, 1958.

HOLZER, H., **Die Berechnung der Drehschwin gungen**, Julius Springer, 1921.

JEFFCOTT, H.H., "**Dynamic behavior of turbine-generator-foundation**". Philosophical Magazine, Vol. 6, p. 304, 1919a.

JEFFCOTT, H.H., **The lateral vibration of loaded shafts in the neighborhood of a whirling speed** - the effect of want of balance. Philosophical Magazine, Series 6, 37: 304, 1919b.

KANG, Y., CHANG, Y.P., TSAI, J.W., MU, L.H. AND CHANG, Y.F. "**An investigation in stiffness effects on dynamics of rotor-bearing-foundation systems**". Journal of Sound and Vibration, Vol. 231, pp. 343–374, 2000.

KAPITSA, P.L., **Stability and transition through critical speeds of high-speed rotors subject to friction**, J. Tech. Phys., IX, n°. 2, 1939.

KIMBALL, A.L**. Measurement of internal friction in a revolving deflected shaft**. General Electric Review 28, p. 554, 1925.

KRÄMER, E. **Dynamics of Rotors and Foundations**. Springer-Verlag Berlin Heidelberg GmbH, 1993.

LIU, W. AND NOVAK, M. "**Dynamic behavior of turbine-generator-foundation**". Earthquake Eng. Struct. Dyn., Vol. 24, pp. 339–360, 1995.

LUND, J. W., "**Spring and Damping Coefficients for the Tilting Pad Journal Bearing**", ASLE Trans., Vol. 7, pp. 342-352, 1964.

LUND, J.W. **Review of the concept of dynamic coefficients for fluid film journal bearings**. Journal of Tribology, Vol. 109, p. 37-41, 1987.

LUND, J.W. **Spring and damping coefficients for the tilting pad journal bearing**. ASLE Transactions, Vol. 7, p. 342-352, 1964.

LUND, J.W. **Stability and damped critical speed of a flexible rotor in fluid-film bearings**. Journal of Engineering for Industry, Vol. 96, p. 509-517, 1974

LUND, J.W., Orcutt, F.K., **Calculation and experiments on the unbalance response of a flexible rotor**. Journal of Engineering for Industry, Vol. 87, p. 785-796, 1967.

MACHADO, T. H., ALVES, D. S., & CAVALCA, K. L.. **Discussion about nonlinear boundaries for hydrodynamic forces in journal bearing**. Nonlinear Dynamics, 92(4), 2005–2022, 2018.

MACHADO, T.H**. Identificação do Desgaste em Mancais Hidrodinâmicos Através do Efeito de Anisotropia**. Tese de Doutorado, Faculdade de Engenharia Mecânica – Unicamp, 2014.

MACHADO, T.H., Cavalca, K.L. and Arima, G. "**Influence of different geometries of hydrodynamic bearing in the dynamic response of a rotating system**". SAE Technical Paper Series, 2010.

MACHADO, T.H.; Cavalca, K.L. – **Evaluation of dynamic coefficients for fluid journal bearings with different geometries**. In: 20TH INTERNATIONAL CONGRESS OF MECHANICAL ENGINEERING - COBEM 2009. Proceedings of the 20th International Congress of Mechanical Engineering. Rio de Janeiro: ABCM. v. 1. p. 1-11, 2009.

MACNEAL, R. **Finite Elements: Their Design and Performance**. CRC Press, 1993.

MARTIN, H.C., CAREY, G.F. **Introduction to Finite Element Analysis**, McGraw-Hill, New York, 1973.

MELOSH, R.J. **Structural analysis of solids**. Journal of the Structural Division, Proceedings of the American Society of Civil Engineers, p. 205-223, 1963.

MOORE, G.E. **Cramming more components onto integrated circuits**. Electronics, Vol. 38(8), p. 114-117, 1965.

MYKLESTAD, N.O. **A new method of calculating natural modes of uncoupled bending vibrations**, International Journal of Aeronautic Science, p. 153-162, 1944.

NELSON, F.C. "**Rotordynamics without equations**". International Journal of COMADEM, Vol. 10, pp. 2–10, 2007.

NELSON, F.C., McVaugh J.M. **The dynamics of rotor bearing systems using finite elements**. Journal of Engineering for Industry, Vol. 98, p. 593-600, 1976.

NELSON, H.D. “**A finite rotating shaft element using Timoshenko beam theory**”. Journal of Mechanical Design, Vol. 102, pp. 793–803, 1980.

NEWKIRK, B. L. **Shaft whipping**. General Electric Review 27, 1924.

NEWKIRK, B.L., Taylor, H.D. **Shaft whirling due to oil action in journal bearings**, General Electric Review, 28(7), p. 559-568, 1925.

PROHL, M.A., **A general method for calculating the critical speeds of flexible rotors**. Journal of Applied Mechanics, Transactions of ASME 67, A. 142 – A. 148, 1945.

RADES, M. **Dynamics of Machinery**, Universitatea Politehnica Bucuresti, 1995.

RANKINE, W.J.M. **On the centrifugal force of rotating shaft**. Engineer, Vol. 9, p. 249, 1869.

RAO, S. S., **Engineering Optimization: Theory and Practice**, John Wiley & Sons, New Jersey, 2009.

ROTHER, C. S.; ALENCAR, A. C. M. G.; MACHADO, T. H. **A Compensation Method for Foundation Effects in Rotating Systems Through Shape Optimization**. Proceedings of 10th IFToMM International Conference on Rotor Dynamics, 2018. v. 2. p. 413-427, 2018.

ROTHER, CÉSAR; ALENCAR, AUGUSTO; MACHADO, TIAGO. **Influência da Modelagem dos Elementos de Eixo na Resposta de Sistemas Rotativos**. In: X Congresso Nacional de Engenharia Mecânica, 2018, Salvador/BA. Anais do X Congresso Nacional de Engenharia Mecânica. Rio de Janeiro/RJ: ABCM, 2018.

ROTHER, CÉSAR; MACHADO, TIAGO. **Analysis of the bearings influence on the dynamic behavior of a rotating machine**. In: 24th ABCM International Congress of Mechanical Engineering, 2017, Curitiba/PR. Proceedings of the 24th ABCM International Congress of Mechanical Engineering. Rio de Janeiro/RJ: ABCM, 2017.

ROUX, VALENTINE; MIROSCHEDJI, PIERRE, **Revisiting the History of the Potter's Wheel in the Southern Levant**, 2009

RUHL, R.L., BOOKER, J.F. **A finite element model for distributed parameter turbogenerator system**. Transaction of the ASME, Journal of Engineering for Industry, Vol. 94(1), p. 128-132, 1972.

SMIL, V. **Creating the Twentieth Century: Technical Innovations of 1867-1914 and Their Lasting Impact**. Oxford University Press, 2005.

SMITH, D.M. **The motion of a rotor carried by a flexible shaft in flexible bearings**. Proceedings of the Royal Society of London, Series A, 1933.

SOBIESZCZANSKI-SOBIESKI, J. **Structural optimization: Challenges and Opportunities**. Nasa Langley Research Center, 1984

STEPHENSON, R.W. AND ROUCH, K.W. "**Generating matrices of the foundation structure of a rotor system from test data**". Journal of Sound and Vibration, Vol. 154, pp. 467–484, 1992.

STOCKI, R., SZOLC, T., TAUZOWSKI, P., KNABEL, J., **Robust design optimization of the vibrating rotor-shaft system subjected to selected dynamic constraints**, Mechanical Systems and Signal Processing, v. 29, pp. 34-44, 2012.

STODOLA, A. **Steam Turbines**. London: Archibald Constable. English translation by L.C. Loewenstein and Van Nostrand, 1905.

TIWARI, R., **Analysis and Identification in Rotor-Bearing Systems**, Curriculum Development Scheme of Quality Improvement Programme at IIT Guwahati, 2010

TUCKMANTEL, F.W.S. **Integração de sistemas rotor-mancais hidrodinâmicos estrutura de suporte para resolução numérica**. Tese de Mestrado, Universidade Estadual de Campinas, Faculdade de Engenharia Mecânica, 2010.

TURNER, M.J. **The direct stiffness method of structural analysis**, Structural and Materials Panel, AGARD Meeting, Aachen, Germany, 1959.

UHRIG, R., **Reduction of the number of unknown in the displacement method applied to kinetic problems**, Journal of Sound and Vibration, Vol. 4, p. 149-155, 1966.

VANCE, J.M., ZEIDAN F.Y., MURPHY B. **Machinery Vibration and Rotordynamics**. Hoboken, New Jersey: John Wiley and Sons, 2010.

XIE, Y. M. AND STEVEN, G. P., **Evolutionary structural optimization**, Springer, 1997

YANG, B., CHOI, S., KIM, Y., **Vibration reduction optimum design of a steam-turbine rotor-bearing system using a hybrid genetic algorithm**. Structural and Multidisciplinary Optimization 30, pp 4353, 2005.

YANG, S.H., KIM, C. AND LEE, Y.B. "**Experimental study on the characteristics of pad fluttering in a tilting pad journal bearing**". Tribology International, Vol. 39, pp. 686–694, 2006.

ZHANG, X., YIN, Z., GAO, G., & LI, Z. **Determination of stiffness coefficients of hydrodynamic water-lubricated plain journal bearings**. Tribology International, 85, 37–47, 2015.

ZHAO, S. X., ZHOU, H., MENG, G., & ZHU, J**. Experimental identification of linear oil-film coefficients using least-mean-square method in time domain**. Journal of Sound and Vibration, 287(4-5), 2005.

ZHAO, S.X., DAI, X.D. AND ZHU, J. "**An experimental study of nonlinear oil-film forces of a journal bearing**". Journal of Sound and Vibration, Vol. 287, pp. 827–843, 2005.

ZHOU, H., ZHAO, S., XU, H., & ZHU, J. **An experimental study on oil-film dynamic coefficients**. Tribology International, 37(3), 245–253, 2004.

ZIENKIEWICZ, O.C. **The Finite Element Method Set, its Basis and Fundamentals.** Butterworth-Heinemann, 2006.

APPENDIX A – LICENSING

A.1 – ABCM license for Chapters 4, 5 and 6

D E C L A R A Ç Ã O

Declaramos para fins de comprovação que os artigos listados abaixo, que foram publicados nos Anais do CONEM 2018 - X Congresso Nacional de Engenharia Mecânica, 2018, Salvador/BA e no COBEM 2017 - 24th ABCM International Congress of Mechanical Engineering, 2017, Curitiba/PR, foram autorizados pela Associação Brasileira de Engenharia e Ciências Mecânicas a serem reproduzidos na dissertação de mestrado do autor: César Rother.

Evento: CONEM 2018 - X Congresso Nacional de Engenharia Mecânica DOI: doi://10.26678/ABCM.CONEM2018.CON18-1429 Título do Artigo: Influência da Modelagem dos Elementos de Eixo na Resposta de Sistemas Rotativos Autores: César Rother, Augusto Alencar, Tiago Machado.
Evento: CONEM 2018 - X Congresso Nacional de Engenharia Mecânica DOI: doi://10.26678/ABCM.CONEM2018.CON18-0208 Título do Artigo: Estudo da Influência da Fundação na Resposta de Sistemas Rotativos Autores: Augusto Alencar, César Rother, Tiago Machado.
Evento: COBEM 2017 - 24th ABCM International Congress of Mechanical Engineering DOI: doi://10.26678/ABCM.COBEM2017.COB17-0366 Título do Artigo: Analysis of the bearings' influence on the dynamic behavior of a rotating machine Autores: Tiago Machado, César Rother

Rio de Janeiro, 28 de março de 2019.

Gherhardt Ribatski

Presidente da ABCM

ASSOCIAÇÃO BRASILEIRA DE ENGENHARIA E CIÊNCIAS MECÂNICAS
Av. Rio Branco, 124 14º andar Centro 20040-001 Rio de Janeiro RJ Brasil Tel.: 55 21 2221-0438 Fax: 55 21 2509-7128
abcm@abcm.org.br

A.2 – Springer license for Chapter 7

SPRINGER NATURE LICENSE
TERMS AND CONDITIONS

Dec 17, 2018

This Agreement between University of Campinas -- Tiago Machado ("You") and Springer Nature ("Springer Nature") consists of your license details and the terms and conditions provided by Springer Nature and Copyright Clearance Center.

License Number	4491371065325
License date	Dec 17, 2018
Licensed Content Publisher	Springer Nature
Licensed Content Publication	Springer eBook
Licensed Content Title	A Compensation Method for Foundation Effects in Rotating Systems Through Shape Optimization
Licensed Content Author	César S. Rother, Augusto C. M. G. de Alencar, Tiago H. Machado
Licensed Content Date	Jan 1, 2019
Type of Use	Thesis/Dissertation
Requestor type	academic/university or research institute
Format	print and electronic
Portion	full article/chapter
Will you be translating?	no
Circulation/distribution	<501
Author of this Springer Nature content	yes
Title	Analysis and Optimization of Rotors Supported on Hydrodynamic Bearings
Institution name	University of Campinas
Expected presentation date	Jan 2019
Requestor Location	University of Campinas Mendeleyev Street, 200 Campinas, SP 13083-860 Brazil Attn: University of Campinas
Billing Type	Invoice
Billing Address	University of Campinas Mendeleyev Street, 200 Campinas, Brazil 13083-860 Attn: University of Campinas
Total	0.00 USD
Terms and Conditions	